Casting of Halide and Fluoride Alloys for Laser Windows

Raytheon Co.

Prepared For
Air Force Cambridge Research Labs.

February 15, 1976

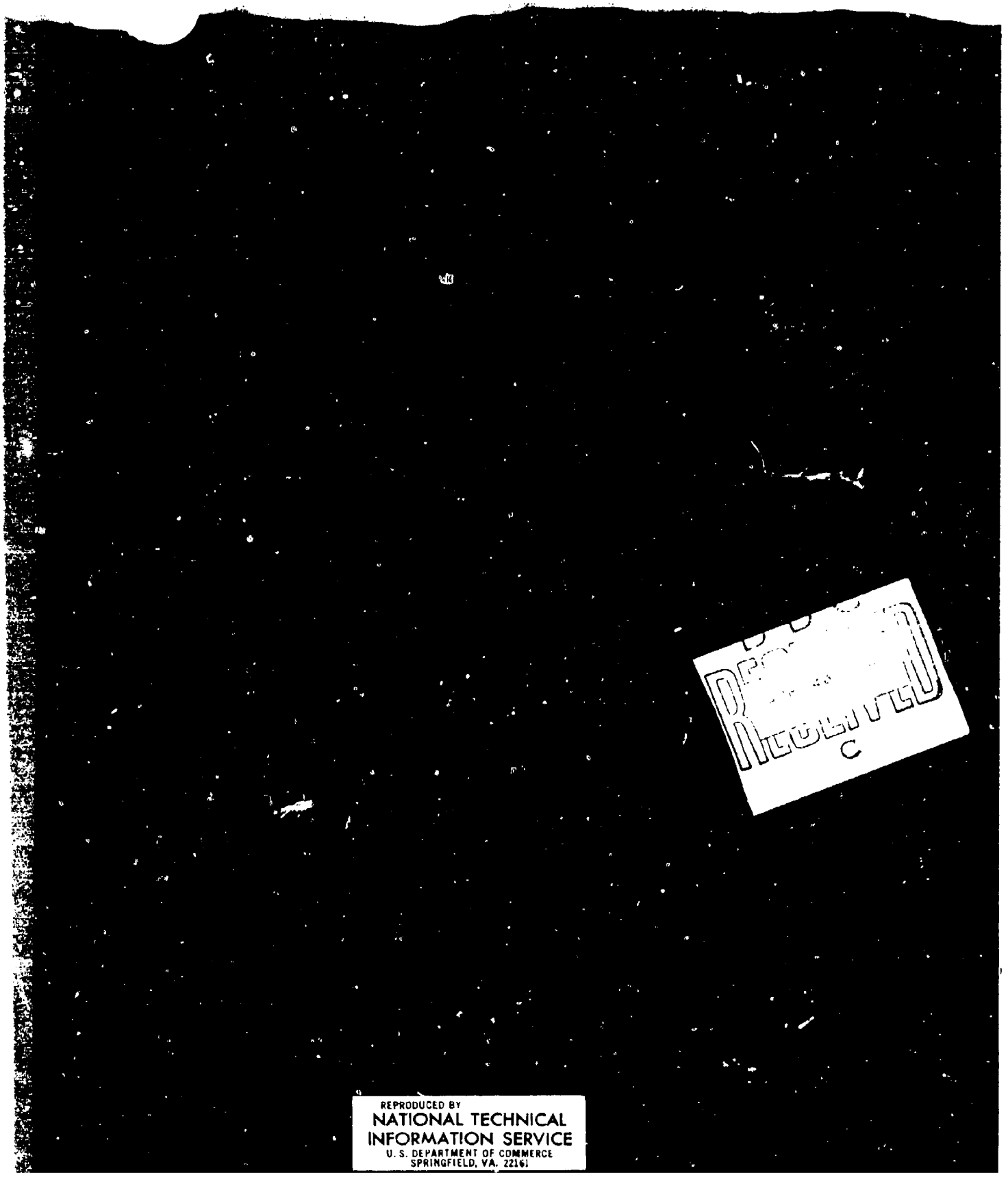

Unclassified

SECURITY CLASSIFICATION OF THIS PAGE (When Data Entered)

REPORT DOCUMENTATION PAGE		READ INSTRUCTIONS BEFORE COMPLETING FORM
1. REPORT NUMBER AFCRL-TR-76-0011	2. GOVT ACCESSION NO.	3. RECIPIENT'S CATALOG NUMBER
4. TITLE (and Subtitle) CASTING OF HALIDE AND FLUORIDE ALLOYS FOR LASER WINDOWS		5. TYPE OF REPORT & PERIOD COVERED Final Technical Report 6. PERFORMING ORG. REPORT NUMBER S-1963
7. AUTHOR(s) R. T. Newberg J. Pappis		8. CONTRACT OR GRANT NUMBER(s) F19628-74-C-0148
9. PERFORMING ORGANIZATION NAME AND ADDRESS Raytheon Company Research Division Waltham, MA. 02154		10. PROGRAM ELEMENT, PROJECT, TASK AREA & WORK UNIT NUMBERS 61101E 2669-n/a-n/a
11. CONTROLLING OFFICE NAME AND ADDRESS Air Force Cambridge Research Laboratories Hanscom Air Force Base, MA. 01731 Contract Monitor: John J. Larkin/LQP		12. REPORT DATE February 15, 1976 13. NUMBER OF PAGES 133
14. MONITORING AGENCY NAME & ADDRESS(if different from Controlling Office)		15. SECURITY CLASS. (of this report) Unclassified 15a. DECLASSIFICATION/DOWNGRADING SCHEDULE

16. DISTRIBUTION STATEMENT (of this Report)

Approved for public release; distribution unlimited

17. DISTRIBUTION STATEMENT (of the abstract entered in Block 20, if different from Report)

18. SUPPLEMENTARY NOTES

This research was sponsored by Defense Advanced Research Projects Agency. ARPA Order No. 2669.

19. KEY WORDS (Continue on reverse side if necessary and identify by block number)

Infrared Materials	Calcium Fluoride
Alkali Halides	Strontium Fluoride
Potassium Chloride	Casting
Strontium Chloride	Mechanical Properties
Alkaline Earth Fluorides	Optical Properties

20. ABSTRACT (Continue on reverse side if necessary and identify by block number)

During this program several important goals have been accomplished. The problem of residual strain in castings of alkali halides (KCl and $SrCl_2$-doped KCl) and alkaline earth fluorides (CaF_2 and SrF_2) has been overcome by the development of proper annealing and slow cooling procedures. Semi-quantitative analysis of absorption coefficients and scattering centers (produced during improper casting and annealing procedures) has shown a correlation between the two for both the halides at 10.6μm and fluorides at 3.25μm.

Consistently high quality castings of both CaF_2 and SrF_2 have been

DD FORM 1 JAN 73 1473 EDITION OF 1 NOV 65 IS OBSOLETE

Unclassified

SECURITY CLASSIFICATION OF THIS PAGE (When Data Entered)

Abstract (Cont'd.)

fabricated regardless of the starting materials. That is, either high-purity single crystal chips or pretreated (vacuum baked and RAP-reactive atmosphere processing - treated in teflon vapors) "reagent" grade powder can be used as starting material to yield equivalent castings. 5.25 μm calorimetric bulk absorption coefficients of cast CaF_2 and SrF_2 have been obtained near 4.2×10^{-4} cm^{-1} and 6.7×10^{-5} cm^{-1}, respectively regardless of the starting material, results essentially equivalent to single crystal material and near predicted intrinsic levels. Mechanical measurements (three point bending) on fusion cast CaF_2 and SrF_2 show average fracture strengths ranging from near 6000 psi to near 24,000 psi and from near 10,000 psi to near 24,000 psi, respectively, depending on the quality of polished surfaces and/ or edges and whether or not the polished test bars are vacuum-annealed prior to testing. The results are equivalent to values measured for selected single crystals. The dependence of fracture strength on both surface polish and annealing history is evidence that fracture for the fluorides is determined by surface and/ or edge flaws.

TECHNICAL PROGRAM SUMMARY

The primary objectives of this program were to complete the investigation of the properties of fusion-cast $SrCl_2$-KCl alloys and to investigate the fabrication and properties of alkaline-earth fluoride castings for high-power laser window applications. The main effort dealt with the fabrication and property evaluation of the alkaline-earth fluorides.

Time-temperature-transformation curves for precipitation and attendant hardness reduction in $SrCl_2$-KCl alloys were completed. The results indicate that for less than about 800 ppm $SrCl_2$ in solid solution, it should be possible to cool alloys from the melting point to room temperature without precipitation.

Thermal conductivity measurements taken at 93.5°C determined that there is little effect of $SrCl_2$ (up to 2 percent added to the melt) on the conductivity of KCl. Attempts were made to determine the conductivity near room temperature but were unsuccessful due to the large scatter in the data.

A serious problem with casting these materials which have large volume changes upon freezing and large thermal expansion coefficients is the residual stress in the ingots after cooling. During this program an annealing and cooling procedure was successfully developed which removes the major part of the residual stress in KCl castings.

Reactive atmosphere processing (RAP) of "reagent"-grade KCl starting material was successful in removing impurities which produced strong absorption bands in the IR. However, the broad absorption centered at about 10 μm which produces strong 10.6 μm absorption was not eliminated completely.

It was observed that many samples which do not exhibit the broad 10 micrometer absorption band still may have a high 10.6 μm absorption

coefficient. Preliminary data indicate that this high apparent absorption coefficient can be correlated with scattering center density in the bulk material.

As expected, the alkaline-earth fluorides are considerably easier to cast than the alkali halides because of their more favorable mechanical and thermal properties and smaller volume contraction on solidifying. High-quality castings up to 6 inches in diameter by about 1/2 inch thick of both CaF_2 and SrF_2 were fabricated regardless of the starting material. That is, either high-purity single-crystal chips or pretreated "reagent"-grade powder was used as starting material to yield equivalently cast ingots. Castings thicker than 1/2 inch could not be obtained without attendant problems of bubble formation and impurity precipitation.

Hot forgings of both single-crystal CaF_2 and polycrystalline cast CaF_2 were performed at temperatures near 1000° which are sufficiently high to provide ease in forging but an attendant large grain size.

Castings of CaF_2 were attempted in inert atmospheres of purified hydrogen and argon (1-50 torr). The advantage over vacuum casting is that unidirectional solidification is better accomplished because of the better heat transfer provided by the gas. The results were in general poor with castings being typically discolored.

Calorimetrically measured 5.25 μm bulk absorption coefficients for cast CaF_2 have been attained near 4.2×10^{-4} cm^{-1} regardless of the starting material. Those castings of CaF_2 fabricated in an inert atmosphere (purified argon) have 5.25 μm apparent absorption coefficients typically greater than 1×10^{-3} cm^{-1}, although one excellent casting was obtained (4.1×10^{-4} cm^{-1}).

5.25 μm calorimetric bulk absorption coefficients for cast SrF_2 have been obtained near 6.7×10^{-5} cm^{-1} regardless of the starting material. Surface absorption for the SrF_2 samples, 3.7×10^{-5} per surface, is high compared to the bulk. For CaF_2 the surface loss is not as dominant, the value being 1.4×10^{-5} per surface.

Annealing either in a poor vacuum or in an inert atmosphere at 1000°C and controlled cooling successfully removes residual stress in cast CaF_2 ingots. However, the annealing is accompanied by almost a factor of two increase in the apparent 5.3 μm absorption coefficient and a significant increase in optical scattering. These impurity scattering centers are almost certainly caused by a change in the intrinsic or impurity chemistry of the fluoride during annealing with subsequent precipitation upon cooling.

Strain-annealing of highly strained cast CaF_2 has been successful at 900°C either in a vacuum or in an inert atmosphere. Similarly strained ingots of cast CaF_2 and SrF_2 have been successfully strain-annealed at 1000°C in a high vacuum furnace and in a reactive atmosphere furnace. The reactive atmosphere is provided by the vaporization and pyrolysis of teflon. Such annealing processes do not degrade the optical properties of the ingots.

Mechanical measurements (measured in three point bending) on cast CaF_2 show average fracture strengths ranging from a minimum near 6000 psi to near 24,000 psi, depending on both the quality of polished surfaces and whether or not the polished samples are vacuum annealed prior to testing. The values are equivalent to the values obtained for single-crystal CaF_2 for which similar polishing and annealing procedures result in average fracture strengths ranging from near 7000 psi to near 26,000 psi.

Mechanical measurements (measured in three point bending) show average fracture strengths for cast SrF_2 ranging from a minimum of near 10000 psi to near 24,000 psi, depending on both the quality of polished surfaces and whether or not the polished test bars are subsequently vacuum-annealed prior to testing. This dependence of fracture strength on surface polish and annealing history provides some evidence that fracture is determined by surface and/or edge flaws. The results show that SrF_2 is equivalent in strength to CaF_2 and that polycrystalline cast material is equivalent in strength to single-crystal material.

PREFACE

This report was prepared by Raytheon Company, Research Division, Waltham, Massachusetts under Contract No. F19628-74-C-0148 entitled "Casting of Halide and Fluoride Alloys for Laser Windows." The work was supported by the Advanced Research Projects Agency and was monitored by the Air Force Cambridge Research Laboratories, Bedford, Mass.

At Raytheon Company the investigation was initially carried out in the Materials Processing Laboratory of the Research Division, under the direction of Dr. D. Readey, manager, and subsequently in the Advanced Materials Department under the direction of Dr. J. Pappis, principal investigator, and Dr. R. Newberg. Assisting with material fabrication and processing were H. Newborn, T. Wong and A. De. Optical polishing was provided by R. Cosgro; Dr. T. Kohane and T. Varitimos performed the laser calorimetry measurements. Dr. O. Guentert, W. Tye, and D. Howe provided the SEM micrographs, microprobe analyses, and X-ray diffraction analyses. P. Roman assisted with the mechanical property measurements. This report has been given an internal number of S-1963.

TABLE OF CONTENTS

TABLE OF CONTENTS (CONT'D.)

LIST OF ILLUSTRATIONS

LIST OF ILLUSTRATIONS (CONT'D)

LIST OF ILLUSTRATIONS (CONT'D)

LIST OF ILLUSTRATIONS (CONT'D)

LIST OF TABLES

1.0 INTRODUCTION

1.1 General

The continued progress in the design and realization of laser and optical systems, particularly that of high power infrared lasers operating in the 2 to 6μm wavelength regions, has created the need for improved window and lens materials suitable for use in large, high-resolution optical systems. Specifically, these materials must be strong, scatter-free, and have low absorption to satisfy optical element requirements in sizes that would often be difficult to fabricate from a common optical material such as glass. Thus, to make large, strong, high-quality optical elements from the better infrared transmitting materials such as the alkali halides and alkaline earth fluorides is indeed a formidable task.

Until recently, only pure, single-crystal and hot-pressed polycrystalline optical elements of these materials have been available. Neither the process of single-crystal growth nor that of hot pressing can be easily scaled to larger sizes. Furthermore, pure single crystals are not strong enough and hot pressed material does not have low enough scatter and absorption to allow the fabrication of large, high quality infrared optical elements.

We have been actively engaged for three and one-half years in a program whose primary goal has been to evaluate fusion casting as a fabrication technique for polycrystalline infrared window materials. Fusion casting is an attractive process in that it offers the possibility of obtaining dense, scatter-free material that can be easily scaled to larger sizes.

The initial effort on this program was directed to the alkali halides[1-3] with the objectives of investigating the effects of grain size and alloying on the mechanical and optical properties of cast material. Emphasis was placed on obtaining high yield strengths and low 10.6 μm absorption with KCl-$SrCl_2$ alloys as a function of alloy content, grain size and heat

treatment. The major achievements were the fabrication of eight-inch diameter, directionally-solidified castings with yield strengths typically around 2000 psi, and optical absorption coefficients in the mid $10^{-4}cm^{-1}$ range for these same alloys. These results were extremely encouraging, yet a major problem with high residual stress in cast halides remained.

In the present program, we addressed the residual stress problem. The characterization of KCl-$SrCl_2$ alloys was also completed, thus allowing us to demonstrate the feasibility of strengthening and casting alkali halides while maintaining their low 10.6 μm optical absorption.

The bulk of the program was directed to casting alkaline earth fluorides for optical elements in the 2 to 6 μm region. Many of the properties of the alkaline earth fluorides such as thermal conductivity, strength, thermal expansion coefficients, etc., make them far superior to the alkali halides for fabrication by casting. The experience we have had with these materials indicates that this is indeed the case. We specifically investigated the feasibility of fusion casting alkaline earth fluorides and measured the optical and mechanical properties of these materials. The effect of heat treatment on mechanical and optical properties was investigated and an optimum fabrication process was developed. The major achievements were the fabrication of up to six-inch diameter by one-half inch thick castings of both CaF_2 and SrF_2 with optical absorption coefficients at 5.25 μm near 4×10^{-4} cm^{-1} and 7×10^{-5} cm^{-1}, respectively, and with average fracture strengths near 24,000 psi for those test samples prepared with the best surface fabrication techniques investigated.

1.2 Optical Properties of Fluorides

1.2.1 Infrared absorption

The basic argument in favor of the fluorides as the materials most suitable for high-power laser windows in the 2-6μm range are already well

established, and relate directly to the predicted "failure" mechanisms of a window or lens subjected to high-power radiation. Deterioration is caused first by thermal distortion of the system elements and results in changes in focal length and aberration effects. At higher power levels, plastic flow, melting, and fracture of the optical elements will take place to give irreversible changes in the system. Uncontrolled power reflection from distorted or broken elements can then lead to damage of components not considered part of the high-power optical path itself.

The specific case of distortion and fracture of window elements has been considered in some detail, both in these laboratories[4-6] and at Rand Corporation.[7,8] The figures of merit which have been derived to characterize candidate window materials, are summarized in Table 1-1. Regardless of the mode of operation, pulsed or CW, or of the cooling configuration, the materials factor governing distortional failure is $(\beta\chi)^{-1}$ or $(\beta_s\chi)^{-1}$, and the factor governing resistance to failure by fracture is $\sigma/\alpha\beta E$ or $\sigma/\alpha\beta_s E$, for bulk loss (β) and surface loss (β_s) respectively. The alkaline earth fluorides have the double advantage of an extremely low predicted loss coefficient β, and the lowest optical distortion parameter (χ) of all the various ionic and partially covalent semiconductor compounds presently under consideration for laser windows.

The fundamental, unavoidable optical absorption mechanism operative in fluorides at wavelengths near 6μm is the excitation of lattice vibrations, primarily as a multiphonon process: that is, the simultaneous excitation of several lattice modes, together with various combinations of mode excitation and de-excitations.

In the past, quantitative analysis of multiphonon absorptions has been relatively useless in predicting the actual level of absorption. Our experiments on a number of fluorides and other halides, however, have shown that there exists a characteristic wavelength (λ) dependence for the absorption coefficient, namely

$$\beta = \beta_0 \exp - \left(\frac{\lambda_0}{\lambda}\right) = \beta_0 \exp - \left(\frac{\bar{\nu}}{\bar{\nu}_0}\right) \qquad (3.1)$$

TABLE 1-1a

Figures of Merit for Bulk Absorption Only

		Fracture		Optical Distortion at Wavelength (λ)	
cw	Edge-cooled	$\left(\frac{\sigma_c}{\alpha\beta E}\right) \cdot K$	watts	$\left(\frac{\lambda}{\beta\chi}\right) \cdot \frac{K}{R}$	watts
	Face-cooled	$\left(\frac{\sigma_c}{\alpha\beta E}\right) \cdot (K + .. h_S^* R)$	"	$\left(\frac{\lambda}{\beta\chi}\right) \cdot \left(\frac{K}{R} + .. h_S^*\right)$	"
	Pulsed	$\left(\frac{\sigma_c}{\alpha\beta E}\right) \cdot \left(\frac{CR^2}{t}\right)$	"	$\left(\frac{\lambda}{\beta\chi}\right) \cdot \left(\frac{CR}{t}\right)$	"

TABLE 1-1b

Figures of Merit for Surface Absorption Only

		Fracture		Optical Distortion	
cw	Edge-cooled	$\left(\frac{\sigma_c}{\alpha\beta_s E}\right) \cdot KR$	watts	$\left(\frac{\lambda}{\beta_s\chi}\right) \cdot K$	watts
	Face-cooled	$\left(\frac{\sigma_c}{\alpha\beta_s E}\right) \cdot KR + .. h_S^* R^2)$	"	$\left(\frac{\lambda}{\beta_s\chi}\right) \cdot (K + .. h_S^* R)$	"
	Pulsed	$\left(\frac{\sigma_c}{\alpha\beta_s E}\right) \cdot \left(\frac{CR^3}{t}\right)$	"	$\left(\frac{\lambda}{\beta_s\chi}\right) \cdot \left(\frac{CR^2}{t}\right)$	"

In this table:

σ_c is the critical failure stress

α is the expansion coefficient

β is the bulk absorption coefficient

β_s is the surface absorption coefficient

E is the Young's modulus

K is the thermal conductivity

h_S^* is the surface heat transfer coefficient

R is the window radius

C is the specific heat

t is the pulse length

χ is an optical distortion parameter

$$= \frac{dn}{dT} + (1+\nu)\alpha(n-1) + \frac{1}{2} n^3 \alpha E \langle r \rangle$$

where

n = index of refraction

ν = Poisson's ratio

$\langle r \rangle$ = an averaged stress-optic coefficient

where β_0 lies in the range 10^4 - $10^5 cm^{-1}$ and λ_0 ($= 1/\bar{\nu}_0$) is related to the free space wavelength associated with the zone center-longitudinal vibrational mode. Experimentally, the value of λ_0 is approximately 4.5 times the mode wavelength. The actual values that have been derived for a number of IR materials show that, as a group, the fluorides, in pure form, are capable of satisfying the requirements of $\beta < 10^{-4} cm^{-1}$ at the important laser wavelengths, 5.3 μm (CO), 3.8 μm (DF) and 2.8 μm (HF).

1.2.2 Optical scattering

The optical quality of an otherwise transparent material free from absorptive loss, and with perfect optical surfaces, will be determined by optical inhomogeneity produced either by built-in strain, by density changes where there are two or more components, by porosity, or by refractive-index discontinuities at the boundaries of noncubic crystallites.

A polycrystalline material with cubic crystal symmetry, such as an alkaline earth fluoride, will not scatter if it is 100 percent dense, with no pores. The crystalline boundaries, while recognized as discontinuities at X-ray wavelengths, will be essentially invisible at all wavelengths greater than 10 Å notwithstanding the size of the crystallites. Pores or inclusions smaller than 0.1 μm will produce wide-angle scatter that depends on wavelength, decreasing as the wavelength increases approximately as $1/\lambda^4$ in the visible and IR region. Larger pores or inclusions will scatter in a manner depending on their shape and orientation to a degree that will decrease as $1/\lambda^2$ in the visible and near-IR and eventually as $1/\lambda^4$ at longer wavelengths.

In practice, even single crystals show the presence of discrete scatter centers throughout the bulk. Their nature is unknown, but oxide, sulphate or carbonate precipitates are likely candidates. The likelihood of aggregation of similar impurities in polycrystalline materials implies that particular attention must be paid to prepurification of starting materials and heat treatment procedures.

1.3 Mechanical Properties and Strengthening of Fluorides

1.3.1 General

One of the primary objectives of this program was to fabricate high-strength alkaline earth fluorides using common metallurgical strengthening and fabrication techniques, keeping in mind the feasibility and cost of scale-up to the desired size. The effort on strengthening and fabrication of alkali halide materials for the 10.6 μm laser window has demonstrated the feasibility and applicability of these strengthening and fabrication techniques. In the case of the alkali halides, increases in yield and fracture strengths of well over an order of magnitude have been shown to be possible.[1-3]

On the other hand, background information, available for a large portion of the alkali halide work, is lacking for the alkaline earth fluorides. Therefore, discussion of hardening and fabrication techniques for these materials must rely on far less available experimental data. However, the alkaline earth fluorides, as pure materials, are significantly stronger than the halides, and the incremental increases in strength required for them to be useful window materials are proportionately less. In this context there are various possible strengthening techniques for the alkaline earth fluorides which include the effects of grain size and solid-solution alloying.

1.3.2 Grain size effects

The efficacy of grain size reduction in increasing the yield strength of the alkali halides is now fairly well documented. According to the Von Mises criterion, for a randomly oriented polycrystalline solid to deform plastically, it must be presumed that each grain is capable of undergoing perfectly general strain in order to conform to the distortion of its neighbors. At least five independent slip systems are required to satisfy this general requirement. Even in those materials in which five independent slip systems are operative, dislocations pile up at grain boundaries and

restrict macroscopic plasticity. It can be shown that this leads to an inverse square root ($d^{-\frac{1}{2}}$) dependence of yield strength on grain size, the so-called Hall-Petch relationship. This relationship is observed for many ductile materials and has been demonstrated to be true for polycrystalline KCl.[9]

In the fluorite structure materials CaF_2, SrF_2, and BaF_2, the most active slip system at low temperature is $\{100\}\ \langle 1\bar{1}0\rangle$ [10-12] which gives only three independent systems.[13] In fact, even this system is relatively inoperative in CaF_2 at room temperature, and both single and polycrystals of this material fail by brittle fracture with essentially no macroscopic yielding. However, above about 200°C the two $\{110\}\ \langle 1\bar{1}0\rangle$ systems become active in CaF_2 and, along with the three $\{100\}\ \langle 1\bar{1}0\rangle$ systems, give the necessary five independent systems. Thus, polycrystalline CaF_2 at elevated temperatures does deform plastically.[14] Presumably SrF_2 and BaF_2, also having the fluorite crystal structure, behave similarly at elevated temperatures. In fact, they are probably more plastic than CaF_2 because of their smaller ionic character, as indicated by their larger lattice parameters. However, little information is available on the plastic behavior of these materials except on a microscopic scale.[11, 12]

At temperatures near 300°K, most of the alkaline earth fluorides, both single and polycrystals, fail by brittle fracture. Fracture in polycrystalline materials which undergo only a small amount of plastic deformation as single crystals can be initiated by crack nuclei produced by deformation.[15-18] Analysis of this mechanism leads to an inverse square root dependence of fracture strength on grain size. Since CaF_2, SrF_2 and BaF_2 all exhibit at least microplastic behavior at room temperature, it might be expected that their fracture strength will follow a Petch relationship. Therefore, fracture strength of the alkaline earth halides should increase as the grain size decreases and should also increase

if dislocation motion is restricted by solid solution or precipitation hardening. This, of course, assumes adequate surface preparation so that surface flaws are not strength limiting.

1.3.3 Solid-solution strengthening

1.3.3.1 General

If fracture in these materials is nucleated by a dislocation pile-up mechanism, solid solution hardening will increase the fracture strength simply because it impedes dislocation motion. Therefore, as part of this program, we began preliminary investigation of solid-solution alloying as a means of increasing the strength of alkaline earth fluorides. In fact, because of the divalent alkaline earth ions, these materials offer some interesting possibilities for solid-solution effects not available in the alkali halides.

As solid solutions are made between divalent alkaline earth fluorides, the resistance to plastic flow will increase simply because of the spherical distortion of the lattice caused by ions of slightly different size impeding dislocation motion. In the alkali halides, we and others have obtained increases in yield strength of KCl-KBr alloys from 250 psi to over 2000 psi near the 50-50 composition. However, with such concentrated solid solutions, a significant decrease in thermal conductivity, coupled with the considerable decrease in plasticity, makes the material extremely thermal-shock sensitive and almost impossible to work with. Since a comparable decrease in thermal conductivity would be expected in the alkaline earth fluorides with questionable improvement in strength, the investigation of solid solutions of the divalent fluorides does not offer much promise of improved materials.

1.3.3.2 Aliovalent additions

In contrast to monovalent impurities in the alkali halides, divalent impurities produce very significant increases in yield stresses at very low concentrations. In fact, the yield strength of KCl single crystals, for example,

can be increased by a factor of over twenty by the addition of a few hundred parts per million of Sr^{2+}.[1,3] This difference in behavior between monovalent and divalent impurities in KCl has been observed for a number of different impurities.[19] Here again, virtually no information exists on the effects of aliovalent impurities on the alkaline earth fluorides. However, an increase in oxygen content of only 40 ppm in CaF_2 single crystals has been observed to decrease dislocation velocity by almost an order of magnitude.[20] Also, one of the few pieces of data on fluorides indicates that small additions of Nd^{3+} to CaF_2 can significantly decrease dislocation mobility.[21]

Several explanations of the strong hardening effect of aliovalent impurities have been proposed. Several possible mechanisms have been suggested, based on impurity-defect dipole pairs interacting with dislocation motion. One mechanism in which these dipoles can impede dislocation motion is by the tetragonal distortion produced along the dipole axis.[22] In the case of additions such as YF_3 and other rare earths in CaF_2, the extra fluorine goes into an interstitial site in the fluorite lattice.[23] The interstitial F^- coupled with the Y^{3+} on a Ca^{2+} site forms a dipole pair which produces a nonspherical lattice distortion.[24] This distortion would be expected to be as effective as divalent impurity-vacancy pairs are in the alkali halides.

The alkaline earth fluorides also offer greater flexibility than the alkali halides in that both trivalent and monovalent impurity additions may be used. The possibility exists in the alkaline earth fluorides for paired substitutions such as NaF and YF_3, together in CaF_2. In this case, no lattice defects should form and the Na^+ and Y^{3+} should produce a nearest cation neighbor pair producing the nonspherical lattice distortion and attendant hardening discussed above. Furthermore, the solubility of such a paired substitution should be much greater, permitting the possibility of greater hardening.

1.4 Fabrication Processes for Fluorides

1.4.1 Casting

One of the primary goals of this program was to investigate the feasibility of fusion casting as a fabrication technique for optical materials. As we have shown with the alkali halides, casting is advantageous because it is a conceptually simple technique which produces high-density materials with the potential of easy scale up. Of course, problems with casting do exist; a major one is the formation of voids, cracking and residual stresses brought about by the large thermal expansion coefficients, poor thermal conductivities and large volume contractions on freezing of ionic compounds.

For the alkaline earth fluorides, the situation is much more easily controlled since they have smaller expansion coefficients, higher thermal conductivities and smaller volume contractions on freezing than the alkali halides. For example, Fig. 1-1 compares the volume contraction of SrF_2 (a typical alkaline earth fluoride) with those of KCl (a typical alkali halide), aluminum and silver relative to their respective melting points, T_m. As might be expected, the volume contractions of the fluorides during freezing are considerably less than the alkali halides,yet larger than metals. On the other hand, the volume contraction for the fluoride in the solid during cooling is more similar to the alkali halides. Nevertheless, the volume contraction still strongly suggests that the alkaline earth fluorides must be directionally solidified, leaving the free liquid to absorb the volume contraction just as with the alkali halides. In any event, our experience with both the halides and fluorides indicates that the fluorides are considerably easier to fabricate by casting than the halides.

1.4.2 Hot forging

As we have done with the alkali halides, we investigated hot-forging of the fluoride alloys as a means to improve microstructure and mechanical properties. By a proper sequence of deformation and recrystallization heat treatments, it was expected that the grain size could be refined in order to obtain the full benefit of the strengthening behavior of small grain sizes.

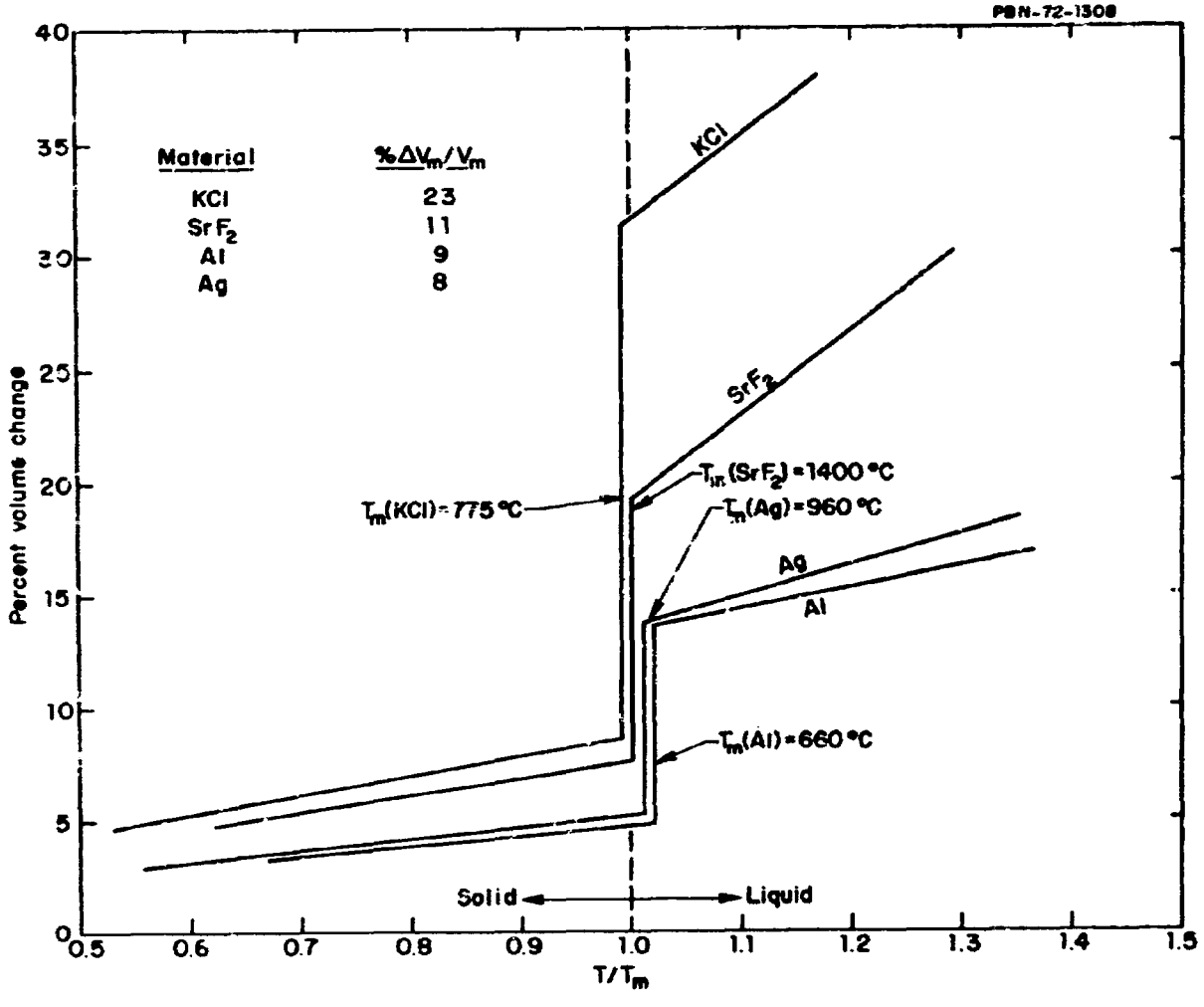

Figure 1-1 Comparison of the Volume Contraction of SrF_2 Near the Melting Point, T_m, with Those of KCl, Aluminum and Silver.

Hot forging of KCl, both in our own and other laboratories, has produced materials with uniform grain sizes below ten micrometers and yield strengths in excess of 2000 psi. One of the main difficulties with the technique is that the temperature and stress cycles must be carefully controlled to prevent secondary grain growth which may result in, at most, very large-grained material, or, at least, a material having a duplex microstructure. However, the time-temperature cycle can be properly controlled to give a uniform, fine-grain-size microstructure which produces the high yield point.

Because of their higher melting points, different slip systems, and different slip-system temperature dependencies, the hot-forging parameters for the alkaline earth fluorides are doubtlessly quite different from those of the alkali halides.

2.0 ALKALI HALIDES

2.1 Program Objectives

The program previously funded under AFCRL Contract No. F19628-72-C-0307 was originally proposed to develop stronger forms of both the alkali halides and the alkaline earth flourides and to investigate the feasibility of their fabrication by fusion casting. Because of the intense interest in the alkali halides for 10.6 μm window applications, the entire effort was devoted to the halides. All of the results of that program are presented in detail elsewhere[1-3] and will not be repeated here. In the present program, a few extensions of this work were made in order to complete the earlier results and to solve some of the remaining major problems.

The effects of in situ and prepurification of the starting materials with reactive gases such as CCl_4 was determined for cast ingots. The main goal here was to ensure that grain boundaries are not a source of absorption centers and to obtain even lower absorption coefficients than those already achieved.

Finally, to characterize the precipitation process and its effects on optical properties, the measurement of scattering as a function of wavelength for alloys of different $SrCl_2$ contents and heat treatments was completed.

2.2 Results

2.2.1 Single crystals

A number of single crystals of undoped and $SrCl_2$-doped KCl grown

during the program previously funded under AFCRL Contract No. F19628-72-C-0307 were used for these studies. Starting materials for these samples had been "reagent" grade chemicals.

2.2.1.1 Hardness and precipitation

Hardness is determined with a Vickers DPH indenter and a 10 gm load mounted on a Vickers M-55 metallograph. Determined were the effects of heat treatment time and temperature on precipitation and hardness of various $SrCl_2$ doped samples of KCl. The samples were about 1.5 × 1.5 × 0.5 cm in size. They were first solid solution annealed for 15 minutes at either 650 or 700°C followed by air quenching to room temperature. Subsequent anneals were carried out at temperatures of 200, 250, 375, 425, and 500°C for times of 1/4, 1, 4 and 16 hours. Hardness was determined for each heat treatment with at least four hardness measurements for each test.

From plots of hardness versus temperature for each time of heat treatment and for each of the three $SrCl_2$ concentrations (5000 ppm, 1 and 2 percent $SrCl_2$ nominal), the temperatures at which hardness dropped to 90 percent of the solution annealed hardness value were determined. The decrease in hardness is associated with precipitation of a second phase (presumably K_2SrCl_4) as evidenced by the turbidity developed during annealing.

These results are plotted in Fig. 2-1 as a typical TTT (time, temperature, transformation) type plot.

PRN-74-79

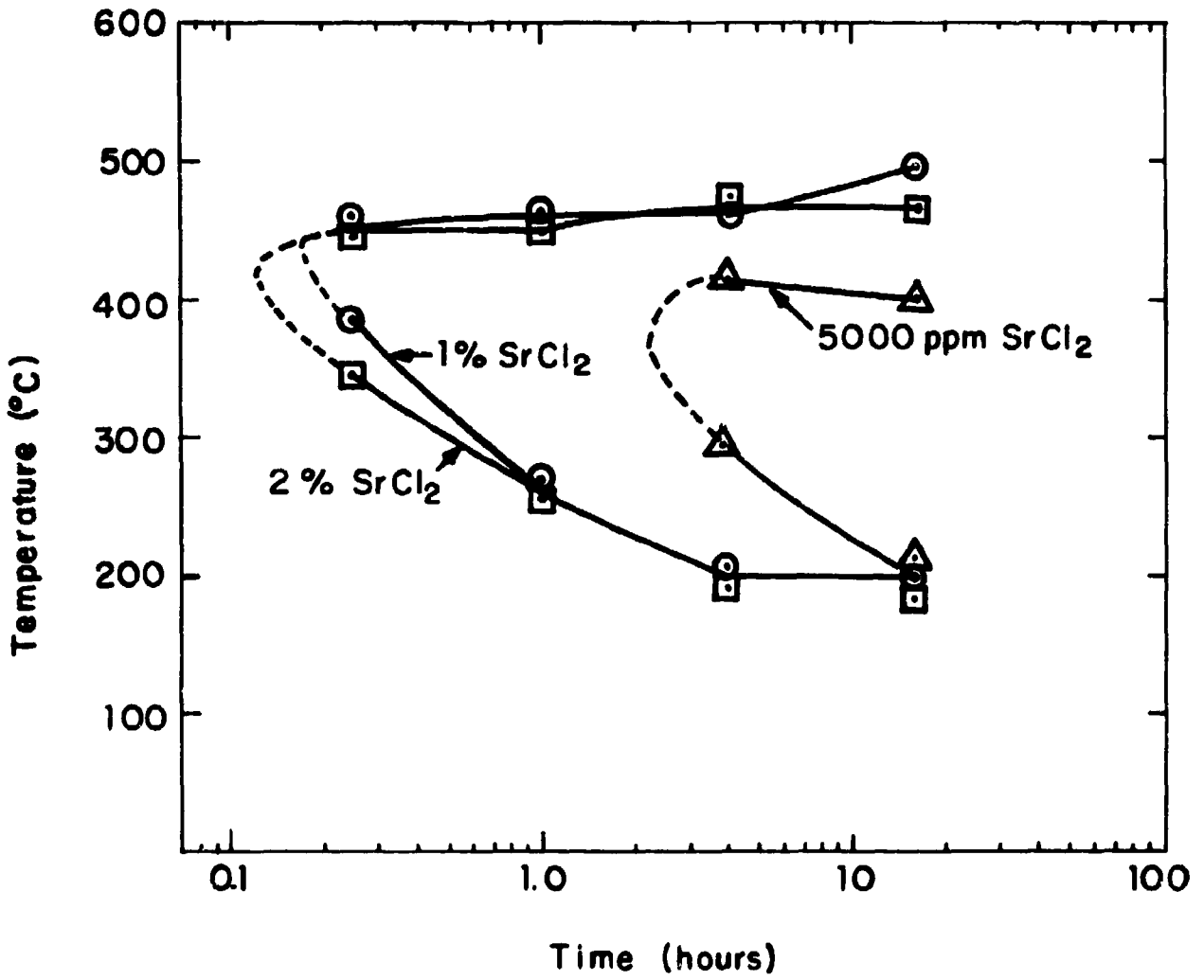

Figure 2-1 Time-Temperature-Transformation Data for Precipitation Softening in $SrCl_2$-KCl Alloys. The curves are for ten percent decrease in hardness.

The results show that a 10 percent drop in hardness as a result of precipitation occurs in a very short time between 350 and 450°C for the highest doped samples (1 and 2 percent $SrCl_2$ nominal), with very similar results for both 1 and 2 percent samples, indicating a limit has been reached. For the lower concentration (5000 ppm, $SrCl_2$ nominal), the precipitation occurs in longer times at similar temperatures, as expected. These data suggest that little difficulty should be experienced in cooling a nominal 5000 ppm (~600 ppm actual) crystal without precipitation.

2.2.1.2 Thermal conductivity

Thermal conductivity measurements were taken on samples of the variously doped $SrCl_2$-KCl samples using a Colora Thermoconductometer (Dynatech Corporation, distributor in the United States). A sample of the material to be tested is brought into contact with two boiling liquids of differing boiling points. The time is measured for a given quantity of heat, determined by the volume of liquid which evaporates from the "cold" side of the sample, to flow through the sample. If a calibrated sample with a known heat resistance is measured with a selected liquid pair, the thermal resistance values of subsequent samples can be read directly from a calibration plot. For the present measurements, the liquid pair water/trichloroethylene (boiling points of 100.0 and 87.0°C, respectively) provides a measuring temperature of 93.5°C. The lower boiling point liquid pair methylene chloride/freon 11 (41.6 and 23.8°C, respectively) providing a measuring temperature of 32.7°C produced too much scatter in the data to be of value. Cylindrical samples of about 1.0 cm diameter by 0.5 cm thick were tested. The results are shown in Table 2-1 and show that the thermal conductivity of KCl is little affected by the addition of up to two percent $SrCl_2$ (added to the melt).

2.2.2 Cast $SrCl_2$-KCl

The emphasis of casting in our two zone furnace (Figs. 2-2 and 2-3) during this program was directed toward the casting and annealing of fluorides. However, a number of 8-inch diameter KCl castings were made at the beginning of the program.

TABLE 2-1

THERMAL CONDUCTIVITY OF $SrCl_2$-KCl, 93.5°C

$SrCl_2$ Added to Melt	Thermal Conductivity (cal/ cm sec°C)
0	.0108 ± .0005 (4)
200 ppm	.0102 ± .0003 (3)
500 ppm	.0095 ± .0004 (4)
1500 ppm	.0093 ± .0004 (3)
5000 ppm	.0099 ± .0005 (5)
1 Percent	.0096 ± .0007 (4)
2 Percent	.0098 ± .0001 (3)

( ) = no. of measurements.

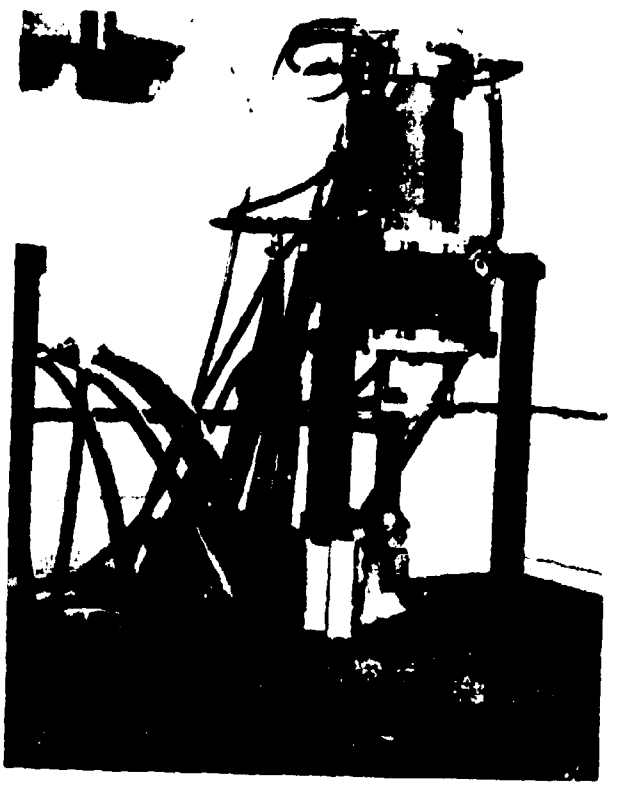

Fig. 2-2 Two Zone Casting Furnace.

Figure 2-3 Removal of a KCl Casting from the Two Zone Casting Furnace.

All castings, with the exception of two, were made from Merck "Suprapur" KCl and doped with Johnson Matthey high purity (Grade I) $SrCl_2$. The technique for casting these large pieces has been detailed previously.[1]

During this time, several high purity castings were made in a 50-ton vacuum hot press furnace (Fig. 2-4) by melting and solidifying in situ. This furnace (an all graphite system), equipped with a diffusion pump, had the capability of better vacuum than the two-zone furnace until a diffusion pump was also added to the latter. The purpose of attempting to cast in this furnace was to evaluate whether or not the better vacuum improved the optical absorption. In the hot press furnace, a 5 1~2-inch diameter ATJ graphite crucible (lined with removable grafoil) with cover was used for casting. Limitations of the system were such that uniform, unidirectional solidification was difficult to achieve. However, small samples from these castings could be analyzed for optical properties which will be discussed later.

2.2.3 Strain annealing

One of the major problems in the casting of the halides was the high residual strains produced during cooling from solidification temperatures. Handling of the cooled castings was difficult, with cracking of castings being a problem.

Internal stresses in optical materials are measured in terms of the induced birefringence, i.e., the difference in the index of refraction between light polarized in the direction of and perpendicular to the applied stress. Stress optical coefficients, in units of nanometers relative retardation per centimeter of path length per unit applied stress in pounds per square inch, for a number of optical materials are listed in Table 2-2.[4] No birefringence requirements were required for this program. However, a value of 10 nm/cm/psi was used as a goal and calculated as a figure of merit.(25) This corresponds to residual stresses in KCl (stress optical

Figure 2-4 50-Ton Vacuum Hot Press Used for Casting and Hot Forging Polycrystalline Alkaline Earth Fluorides.

TABLE 2-2

STRESS OPTICAL COEFFICIENTS OF VARIOUS OPTICAL MATERIALS[4]

(10^{-9} psi^{-1})

LiF	0.7	NaCl	7.9
CaF_2	1.7	KCl	16.0
SrF_2	5.0 (est.)	KBr	18.0
BaF_2	9.0 (est.)	Al_2O_3	1.6
MgF_2	3.0 (est.)	MgO	-2.2

coefficient equal 0.16 nm/cm/psi) of 60 psi or less per centimeter of optical path length. Note here that typical glasses have stress optical coefficients of approximately 0.2 nm/cm/psi[25], essentially equivalent to KCl.

Cast alkali halide alloys exhibit high residual stresses as shown in Fig. 2-5. These stresses are high enough to cause cracking in some cases, and have led to the development of cracking during subsequent cutting and polishing in others. These stresses are probably introduced during the cooling cycle due to temperature gradients within the ingot while some regions are more plastic than others. These temperature gradients can be decreased by decreasing the overall cooling rate. To estimate how slow a cooling rate might be necessary for KCl to attain residual stresses of less than 60 psi per centimeter of path length, we consider the case where the two surfaces of an infinite plate are cooled at a constant rate.[25] Temperature distribution through the plate is parabolic and the average temperature is between the temperatures at the surface and center of the plate. For a half thickness, $t_{1/2}$, a rate of cooling, ϕ (°C/sec), is:

$$\phi = \frac{3(1-\mu)k\sigma}{E\alpha\rho C_p t_{1/2}^2}$$

where
- μ = Poisson's ratio
- k = thermal conductivity
- σ = stress
- E = Young's modulus
- α = thermal expansion
- ρ = density
- C_p = specific heat.

If we assume $\mu = 1/3$, for residual stresses no greater than 60 psi/cm, the calculated rate of cooling for KCl is $\frac{135}{t_{1/2}}$ °C/hr. For a two-centimeter thick

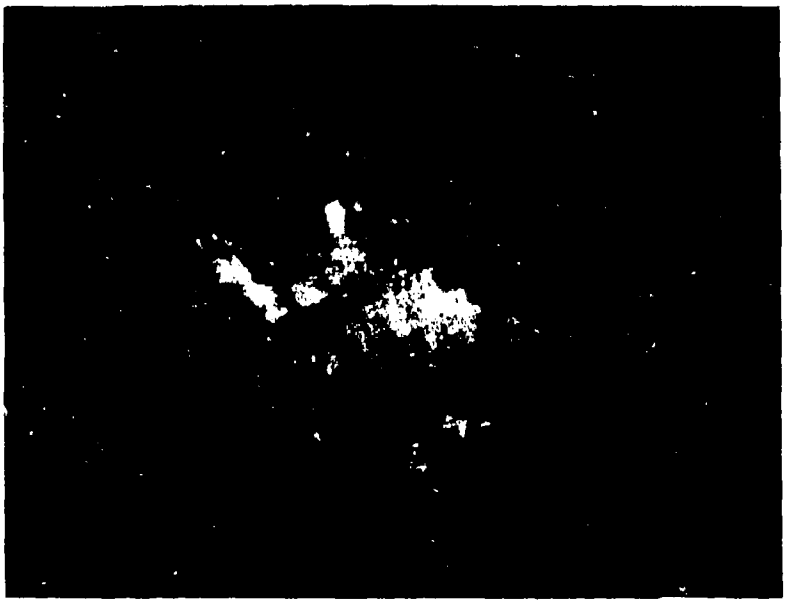

Figure 2-5 Strain Pattern of Casting NPC-15 (200 ppm nominal $SrCl_2$) as Viewed Through Crossed Polarizers. Three inch diameter sample.

casting ($t_{1/2}$ = 1 cm) the rate of cooling cannot exceed about 135°C/hr. This analysis also implies that the maximum thermal gradients may be no larger than 0.4°C/cm since:

$$T_c - T_s = \frac{\phi t^2_{1/2} \rho C_p}{2k}$$

where T_c and T_s are the center and surface temperatures, respectively.

The above analysis has assumed a uniform temperature distribution in the plane of the plate. In the present case of large cylindrical ingots (eight-inch diameter) some heat may also be extracted radially, i.e., radial cooling from the mold walls. If this is the case a radial temperature gradient could be established over a distance as large as 4 inches (10 cm) in which case the cooling rate should not exceed about 15°C/hr. Clearly, in order to prevent excessive residual stresses, the cooling rate and especially the radial temperature uniformity of the ingot must be carefully monitored and controlled. Since this may be difficult to accomplish in practice, we also investigated the effectiveness of post fabrication annealing to remove residual stresses.

Significant results were found in successful annealing runs for the halide castings. All anneals were performed in air using a large muffle furnace. To minimize thermal gradients, each sample was loosely packed in fiberfrax insulating wool and surrounded by two-inch thick firebrick.

Successful annealing is illustrated by Figs. 2-6 and 2-7 for both pure KCl and $SrCl_2$-doped KCl samples. Figures 2-6a and 2-7a show the respective samples as cast with high residual strain as viewed through crossed polarizers. Figures 2-6b and 2-7b show the same two samples after the successful annealing treatment of 10 hours at 600°C followed by cooling at 10°C per hour to room temperature.

Figure 2-6a Sample of Polycrystalline KCl As Cast. Viewed through crossed polarizers.

Figure 2-6b Same Sample After Annealing at 600°C for 10 Hours then Cooled at 10°C/hr.

Figure 2-7a Sample of Polycrystalline $SrCl_2$-KCl Alloy As Cast. Viewed through crossed polarizers.

Figure 2-7b Same After Annealing at 600°C for 10 Hours and Cooled at 10°C/hr.

As a result of the success in our strain annealing procedure, several of the large-diameter castings were similarly annealed successfully and sent out for optical polishing. However, difficulty was experienced and the specimens cracked during a grinding procedure. Upon polishing, further cracking occurred (perhaps due to strains built up during grinding). It is evident that even as annealed, the castings must be handled with great care.

2.2.4 Optical properties

2.2.4.1 Processing effects

Two castings were made using "reagent" grade KCl that had been purified in our laboratory using a reactive atmosphere processing (RAP) technique. This process consisted of pulling a quartz tube filled with KCl powder slowly through a furnace at 600°C. The purification consisted of bubbling dry argon through CCl_4 at room temperature and over the powdered KCl for 24 hours. That this treatment was not completely successful is shown by the IR transmission curve for a specimen from a casting of this "purified" KCl, NPC-47. Figure 2-8 shows the broad absorption band centered near 10 μm. Note however that NCO^- (2180 cm^{-1}), CO_3^{--} (1400-1500 cm^{-1}) or SO_4^{--} (1100-1200 cm^{-1}) absorption bands are not apparent, whereas for the unpurified "reagent" grade castings they are observed (Fig. 2-9).

Figure 2-10 gives the IR transmission curve for a specimen cut from a large casting of "superpure" material. Note that no detectable impurity bands are present, even though the sample path length is quite long. However, the measured 10.6 μm absorption coefficient for this sample is 4.8×10^{-3} cm^{-1}. This high an apparent absorption coefficient should correspond to an absorption of about 2 percent at 10.6 μm. If this apparent absorption were caused by the broad band near 10 μm, as seen in Figs. 2-8 and 2-9, then a dip in the IR spectrum in Fig. 2-10 comparable to that in Fig. 2-8 would be expected. However, none is observed. The implications of this are discussed more completely later.

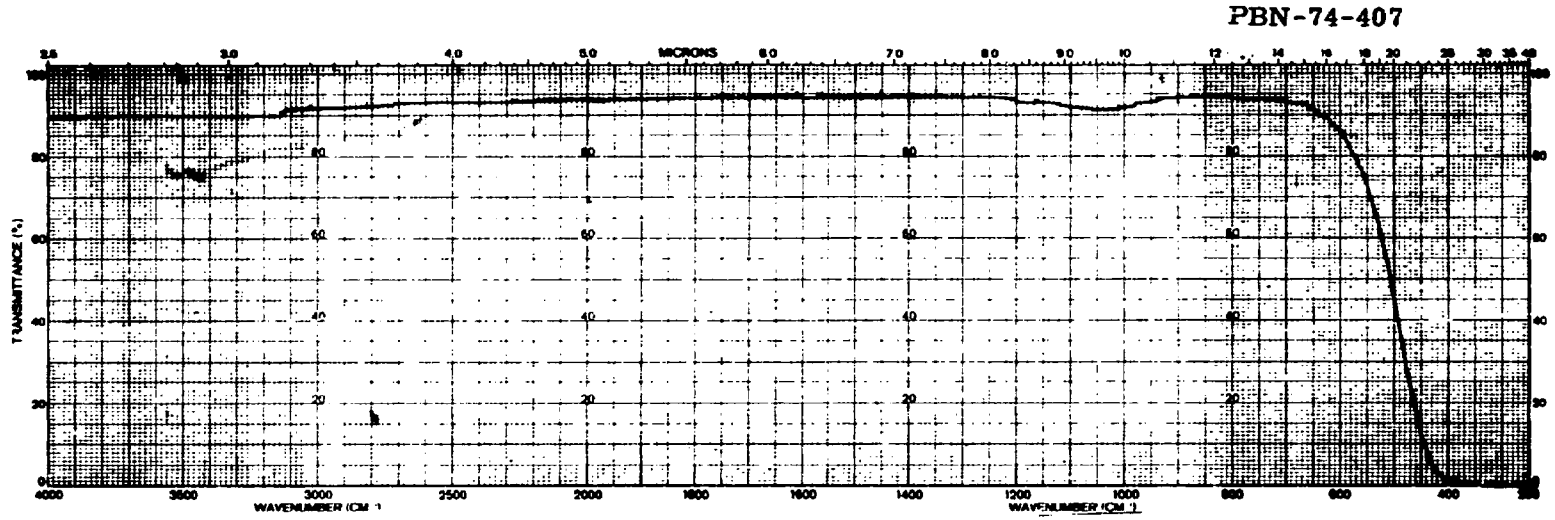

Figure 2-8 Infrared Spectrum of Sample NPC-47 (100 ppm $SrCl_2$-KCl) (Purified). 1.7 cm path length.

PBN-76-179

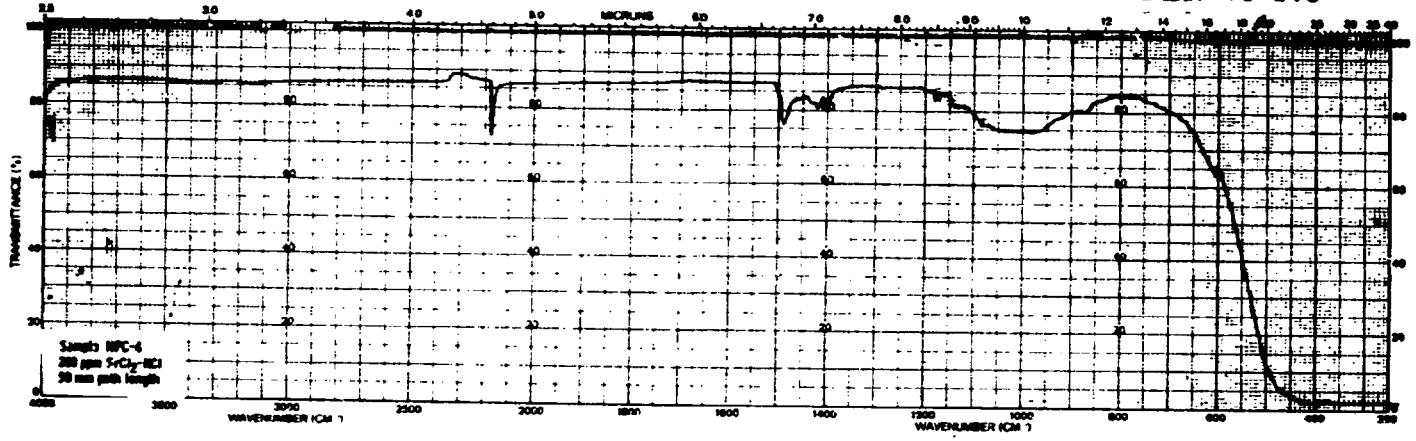

Figure 2-9 Infrared Transmission Spectrum of Casting NPC-4 (200 ppm nominal $SrCl_2$). "Reagent" grade KCl.

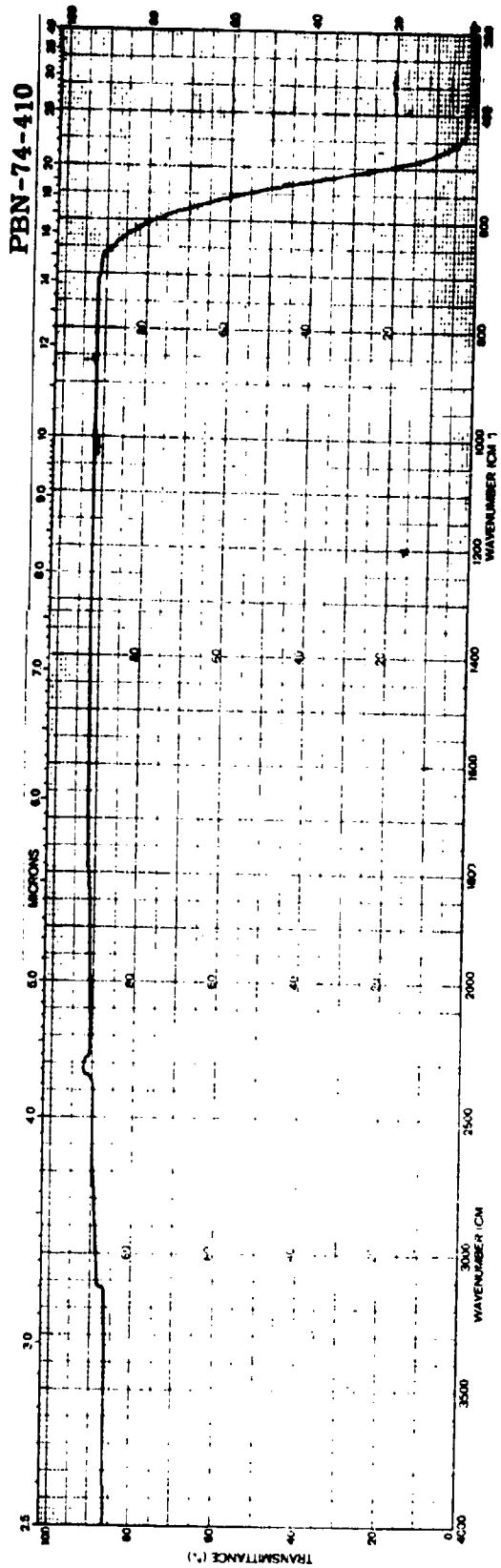

Figure 2-10 Infrared Spectrum of Sample NPC-40. (200 ppm $SrCl_2$-KCl) (Merck). 3.5 cm path length.

Figure 2-11 gives the IR transmission curve for a sample cut from a 5½-inch diameter casting produced in the vacuum hot press furnace. No impurity bands are detectable and the calorimetrically measured 10.6 μm absorption coefficient for this sample is 6.3×10^{-4} cm^{-1} (uncorrected for surface loss).

Table 2-3 gives the chemical analysis for several selected castings, as well as for the Merck "Suprapur" powder from which castings NPC-22 and 39 were produced. Casting NPC-22 was undoped while casting NPC-39 was nominally doped at 200 ppm $SrCl_2$. Casting NPC-47 is the RAP-treated one. In general, no impurity pickup was found in the casting process by either analysis (emission spectroscopy performed by Jarrell-Ash, Waltham, Mass.) or by the IR transmission results. The RAP-treated casting by analysis is as pure as the others.

2.2.4.2 Scattering centers

In order to better understand the apparent 10.6 μm absorption of various castings and single crystals such as casting NPC-40 (Fig. 2-10) which exhibits a high absorption coefficient with no evidence of a band at 10 μm, it was decided to attempt to correlate absorption and optical scatter. Qualitatively it was found that all samples with low 10.6 μm absorption coefficients scattered less in a He-Ne laser beam than did corresponding samples of high absorption coefficients.

As a result, selected samples of doped and undoped KCl (both cast and single crystal) were microscopically examined at 120× with transmitted light. Samples ranged in thickness from 10 to 22 mm and were examined by focusing from one polished surface through the sample to the opposite polished surface. All scattering centers that were microscopically visible were counted. At least four random fields of view for each sample were counted. Comparison between samples could be obtained by defining a scattering number as the total number of counted particles or voids in the total volume examined.

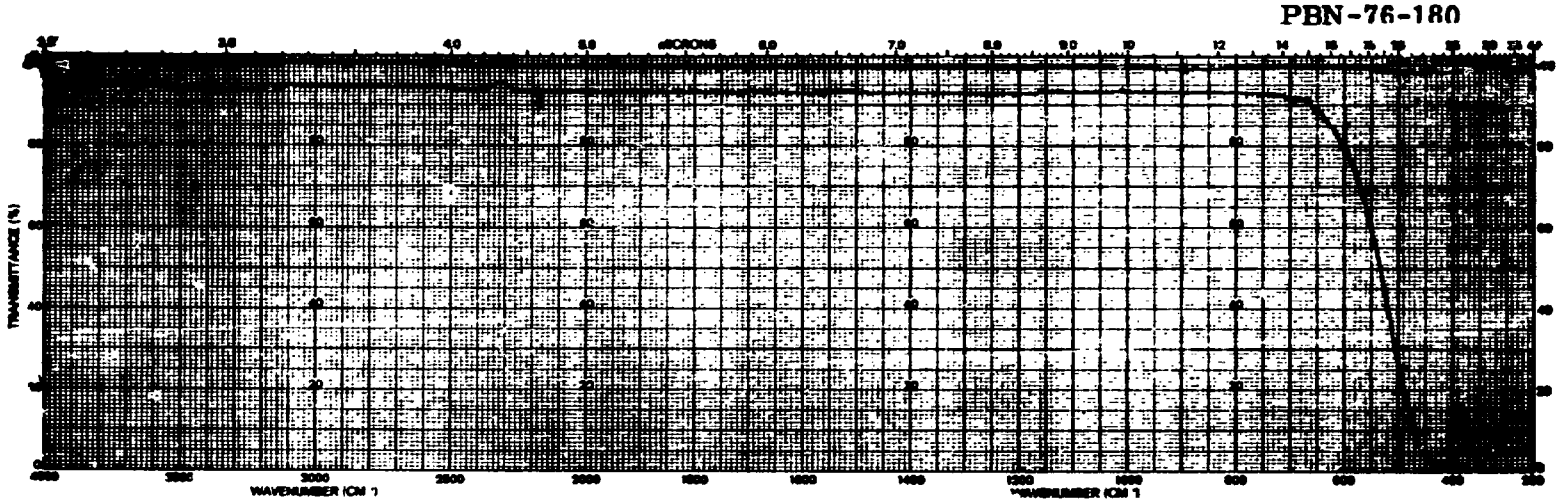

Figure 2-11 Infrared Spectrum of Sample VHP-213. (200 ppm $SrCl_2$-KCl) (Merck). 2.7 cm path length.

TABLE 2-3

ANALYSIS OF KCl CASTINGS AND MERCK "SUPRAPUR" POWDER

Detected Impurities*	Merck Powder	Casting NPC-22	Casting NPC-39	Casting NPC-47
Mg	< 1	1	0.5	1
Al	1-10	1	0.1	5
Si	ND	0.5	0.1	1
K	H	H	H	H
Ca	< 1	2	0.5	0.5
Fe	ND	0.1	ND	0.3
Cu	ND	1	0.5	0.1
Sr	ND	ND	400	300
Mo	ND	5	ND	ND
Pb	ND	.1	ND	0.5
Total Detected Impurities**	3-13	10.7	1.7	8.4

ND = not detected

H = balance

* Results in ppm; 40 additional impurities undetected

** Excluding Sr

The results summarized in Table 2-4 indicate a semiquantitative correlation between β and scatter. The lower absorption samples have very few microscopically visible inclusions, while the greater the number of inclusions, the higher the absorption coefficient. Of course, the higher absorbing samples may have an impurity band near 10 μm, but not necessarily, as has been seen. It is not evident whether the residual absorption (above the intrinsic value for KCl at 10.6 μm) for the best samples is limited by impurity absorption or by scatter.

TABLE 2-4

10.6 μm ABSORPTION AND SCATTER

Specimen	$\beta_{10.6\ \mu m}$	Sample Thickness (mm)	Center Density (cc^{-1})
73-85	$3.7 \times 10^{-4}\ cm^{-1}$	10	0
73-62	6.1×10^{-4}	15	105
VHP-213	6.3×10^{-4}	27	330
73-50	6.7×10^{-4}	20	0
73-29	7.2×10^{-4}	15	0
NPC-22	7.8×10^{-4}	14	940
73-86	1.5×10^{-3}	6	internal subgrains
72-52	2.4×10^{-3}	16	5300
73-72	3.9×10^{-3}	11	2400
TW4	3.9×10^{-3}	12	> 3900*
NPC-40	4.8×10^{-3}	11	> 3300*
72-61	5.3×10^{-3}	10	5200
TW3	6.3×10^{-3}	10	8800
NPC-31	7.4×10^{-3}	13	> 14,000*
NPC-35	1.3×10^{-2}	11	internal subgrains
NPC-39	1.7×10^{-2}	10	> 14,000*
NPC-36	1.9×10^{-2}	10	> 14,000*

* Very nonuniform from field-to-field.

3.0 ALKALINE EARTH FLUORIDES

3.1 Program Objectives

The bulk of the program was directed to the fusion casting of alkaline earth fluorides for optical elements in the 2-6 μm region. Many of the properties of the alkaline earth fluorides such as thermal conductivity, volume contraction on solidification, thermal expansion coefficient, and strength make them far superior to the alkali halides for fabrication by casting. We specifically investigated the feasibility of the purification and fusion casting of the alkaline earth fluorides - CaF_2 and SrF_2 - and measured the optical and mechanical properties of these materials. The effect of heat treatment on mechanical and optical properties was investigated and an optimum fabrication process was developed.

3.2 Results

3.2.1 Vacuum casting

3.2.1.1 General

As mentioned before, the main effort during this program was directed toward the fusion casting of the alkaline earth fluorides, CaF_2 and SrF_2. To that end, both of our large furnaces were used extensively, with most of the casting having been done in the vacuum hot press (VHP) furnace (Fig. 2-4). The two-zone furnace (Fig. 2-2) was used as a casting furnace, an annealing furnace and a purification furnace.

Figures 3-1 and 3-2 show polished windows of CaF_2 and SrF_2, respectively, cast during this program illustrating the high optical quality that can be achieved.

Ideally in the fusion casting of pure CaF_2 and SrF_2, the objectives would be to obtain a fine, uniform grain size, and to prevent gas bubbles or voids and impurity inclusions. To achieve a small, uniform grain size, rapid cooling rates are necessary, whereas slow cooling rates are required to prevent voids, inclusions, and residual stresses. However, it is possible to adjust the

Figure 3-1 Polished Windows of Cast CaF_2

PBN-75-361

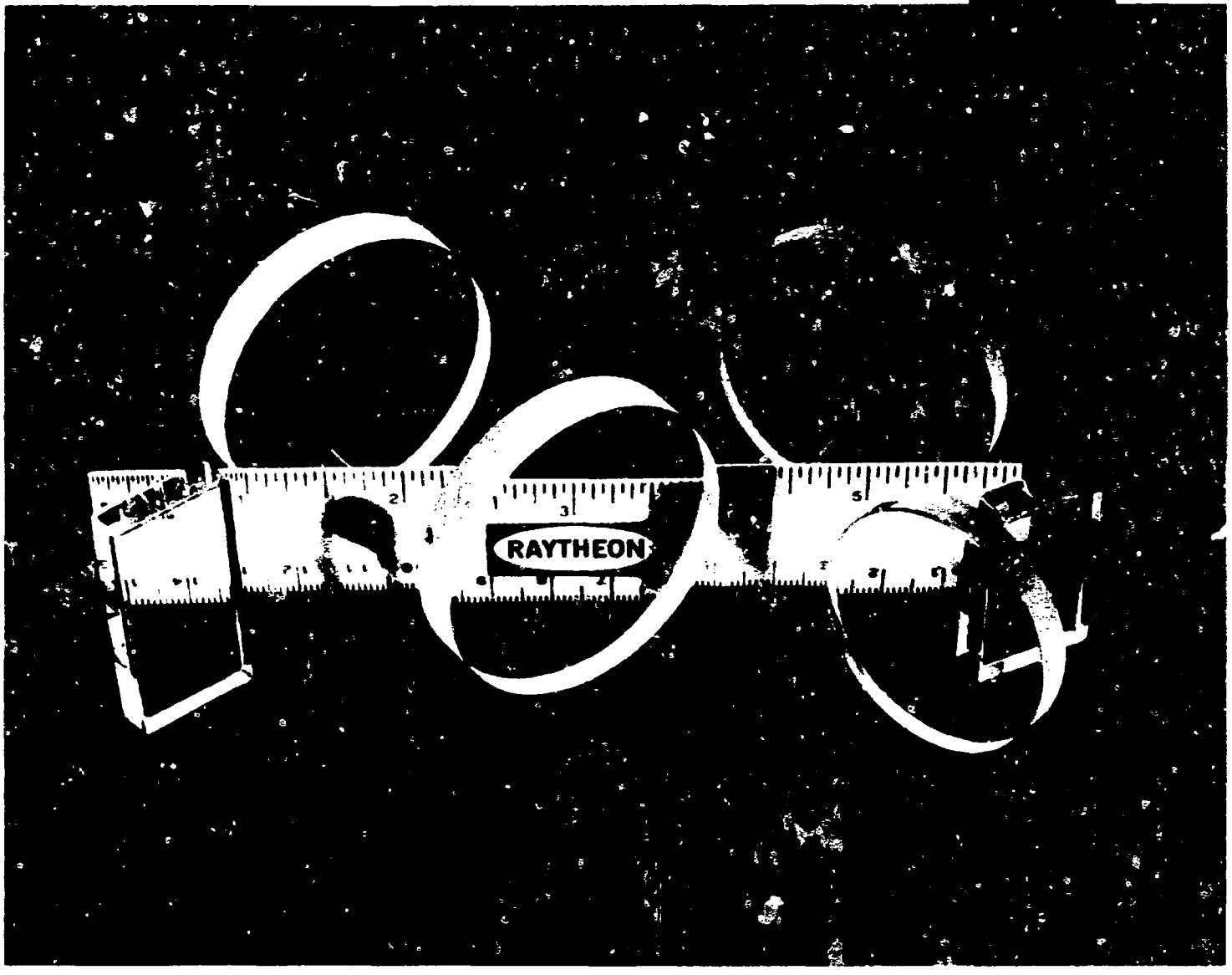

Figure 3-2 Polished Windows of Cast SrF_2

cooling rate during various parts of the casting/cooling cycle to maximize the process. For the materials we have been investigating it is difficult to obtain a fine grain size due to the slow growth rates necessary because their thermal properties, i.e., low thermal conductivity and large volume contraction of freezing, are a hindrance. The grain size of such castings is large - typically on the order of 1-2 centimeters.

In the two-zone vacuum furnace all casting is done in situ, i.e., the starting material in the mold is first melted and then to promote unidirectional solidification, the temperature of the bottom of the mold is reduced until the desired thermal gradient, $T_2 < T_1$, is established (Fig. 3-3). This is done by independently controlled power adjustments to the two heating elements (pancake-type resistance elements). After solidification is complete, the power is readjusted to minimize the thermal gradient, and the cast ingot can be cooled to room temperature at an appropriate schedule to avoid residual stresses. In the beginning, a matrix of runs was made at cooling rates of 40°C and 60°C per hour at various controlled thermal gradients established across the casting zone between the bottom and top controlling thermocouples. The two controlling thermocouples are located near the top and bottom of the crucible at a distance of three inches between the two. The best results were obtained with maximum thermal gradients.

In the vacuum hot press furnace melting is also in-situ; directional solidification is promoted by locating the crucible on a graphite pedestal which rests on the bottom water-cooled ram, thereby establishing a thermal gradient from bottom to top. However, all of these castings are quite strained due to the thermal gradient and must be subsequently strain annealed prior to further handling.

Late in the program when casting of CaF_2 ingots 2-3 centimeters thick was attempted, cooling rates as low as 2°C/hour were necessary to achieve unidirectional solidification. At such low cooling rates and by keeping the material at melting temperatures for longer periods of time (about one day) impurity pickup and visible scattering was noted, unlike the case for faster cooled centimeter-thick ingots. It is a problem to be resolved in future work.

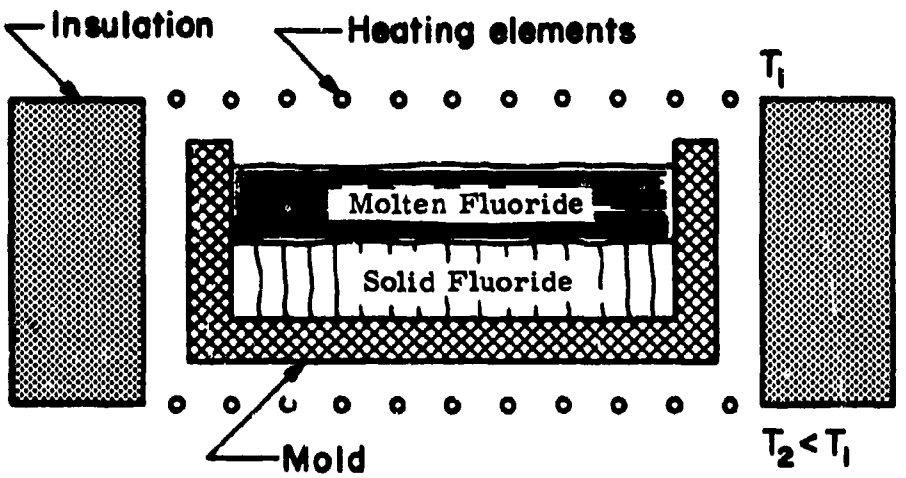

Figure 3-3 Schematic Diagram of Casting Zone of Two Zone Furnace during Solidification.

Attempts at casting strengthened CaF_2 with additions of aliovalent dopants (singly and in pairs) were made in the VHP furnace. Levels of dopants were as follows: (1) 1000, 2000 ppm NaF; (2) 200, 400, 1000 ppm LaF_3; (3) 500, 1000 ppm YF_3; and (4) 5000 ppm NaF + 5000 ppm YF_3. The results were quite dramatic due to the high residual stresses that resulted in cracking in all except the NaF-doped samples. Subsequent emission spectroscopic analysis of a NaF-doped sample indicated no detectable Na. Evidently the NaF (melting point of 990°C; boiling point of 1695°C) is volatilized during the run leaving only pure CaF_2 to be cast.

3.2.1.2 Starting materials and purification

All three types of possible impurities, dissolved anion and cation impurities and second phase particles, are more likely to occur in the alkaline earth fluorides than in the alkali halides because of the higher melting points of the fluorides. Cation impurities in commercially available starting material may not be particularly deleterious to optical properties at levels of 100 parts per million level or less if they are in solid solution as fluorides, unless, of course, the particular fluoride has an extremely high absorption coefficient. For example, magnesium would be expected to be a common impurity in CaF_2. A Mg concentration of 1000 ppm would be expected to contribute only about $\beta \cong 10^{-5}$ cm^{-1} at 5 μm wavelength since the absorption coefficient of MgF_2 is about 10^{-2} at this region. If cations dissolved as fluorides are a problem, then eliminating them by processes such as zone refining is more difficult because of the relatively high melting point of the fluorides. Impurity cation removal is probably more effectively handled by wet chemical processing of the fluorides or of their precursor chemicals. Therefore, in this program, we initially investigated the suitability of various commercially-available starting chemicals, relating cation impurity content with optical properties and attempting to determine the minimal level of purity necessary to satisfy properties.

Doubtlessly, the anion impurities are more troublesome, particularly oxygen. First, at low levels, oxygen can combine with the impurity cations to form precipitates, or impurity-oxygen pairs, or clusters which will

degrade optical properties considerably. At higher oxygen or water vapor levels, reactions typified by:

$$MF_2 + H_2O_{(g)} \rightleftharpoons MO + 2HF_{(g)} \qquad (1)$$

are thermodynamically favorable where M = Ca or Sr.

If powdered starting fluorides which have been exposed to oxygen or water-vapor-containing atmospheres are used, some pretreatment or in-process treatment must be used to remove any oxides present. There have been two common techniques by which this has been accomplished. First, small additions of lead fluoride[26] are effective if the oxide concentration is not too large, since the following reaction is favorable:

$$PbF_{2(s)} + MO \rightleftharpoons MF_2 + PbO_{(g)} \qquad (2)$$

Also, at the melting points of CaF_2 and SrF_2, the vapor pressure of PbF_2 is sufficiently high so that any excess is effectively removed by evaporation. This is a relatively simple and easily used technique.

Another somewhat more difficult purification reaction is:

$$2HF_{(g)} + MO \rightleftharpoons MF_2 + H_2O_{(g)} \ , \qquad (3)$$

since a system resistant to HF must be used. This purification reaction is most effectively carried out on powders which are then either sintered or melted to reduce surface area prior to further processing. During the initial part of this program, our efforts were concentrated on using PbF_2 and other fluorine producing scavenger materials[27] such as teflon (tetrafluoroethylene) to purify the fluoride materials, according to the following reaction:

$$2MO + C_2F_{4(g)} \rightleftharpoons 2MF_2 + 2CO_{(g)} \ . \qquad (4)$$

Initially it was decided to use high purity starting material for the castings. Consequently, Optovac single crystal (random cuttings) CaF_2 was used, as well as Harshaw single crystal SrF_2. With successful results having been achieved for high purity starting material, it was decided to initiate in-house purification of lower grade material. As a result, "reagent" grade CaF_2 (Fisher Scientific Co., Fair Lawn, New Jersey) and SrF_2 (Barium and Chemicals, Inc., Steubenville, Ohio) powders were used.

Several purification schemes were attempted. The first procedure was to vacuum bake the "reagent" grade powder at 900°C to remove as much absorbed water as possible. The partially sintered powder could then be melted in the normal way with only lead fluoride being added as an oxide scavenger according to reaction (2) with the PbO and any excess PbF_2 being removed by volatilization under vacuum at the elevated temperatures. Up to five percent PbF_2 was added to a series of CaF_2 castings. One problem with this process was that several remelts of the material were necessary with additional PbF_2 added each time for the material to be purified to the highest quality.

In the purification scheme of the SrF_2 powder, it was noticed that the as-received powder was contaminated with small black particles. The particles, being magnetic, were somewhat effectively removed by passing a magnet repeatedly through the powder. (X-ray diffraction and ion probe analyses showed the contaminants to contain Fe - probably iron oxide due to the reddish brown colored powder obtained upon grinding - plus trace amounts of Al, Si, and Ti.) After such a mechanical separation, some contamination remained because the vacuum-baked powder was discolored pink. Mixed results were obtained in casting vacuum-baked PbF_2-treated SrF_2 powder, one ingot being clear and one opaque. However, on remelting the opaque ingot with additional PbF_2 added, transparent ingots were subsequently cast as was the case for similar CaF_2.

The second procedure involved the use of the two-zone furnace and used teflon vapors at elevated temperature according to reaction (4). The teflon purification procedure used initially is as follows. The powder is slowly heated and outgassed under vacuum to 900°C until the vacuum is below 10μm. The powder to be purified is in an ATJ graphite crucible located in the lower zone of the furnace (Fig. 3-4). Teflon vapors are then introduced into the system at a partial pressure of 200 - 1000μm by independently controlling the temperature of the teflon-filled graphite crucible located in the upper zone of the furnace. The purification is run nominally for 24 hours, at which time the furnace power is turned off. Under these conditions the teflon is also pyrolyzed and the powder is contaminated with carbon. Consequently, the contaminated powder must be subsequently roasted in air for several hours at 500°C to oxidize the carbon leaving only purified powder. In the case of SrF_2, it was noted early that the carbon contamination is difficult to remove by air roasting. Castings of SrF_2 made from such powder were opaque (white precipitates), but upon subsequent remelting with additional lead fluoride added, transparent castings were obtained. Subsequent teflon vapor purifications were run at 600°C resulting in little or no pyrolysis and with no obvious graphite contamination. Nonetheless, powder from several such purification runs was roasted in air (500°C) prior to casting with mixed results. One ingot was opaque and one was clear. The former was remelted several times with PbF_2 added and was purified to transparency. It appears air roasting is detrimental to the purification process and subsequently was eliminated from the process.

Consequently, the teflon pretreatment procedure was revised as mentioned to the following. The powder is vacuum baked in the casting zone of the furnace at 300-500°C for a period of time until all outgassing from the powder is complete (noted by an improvement in the vacuum of the system). It is then heated to 600°C and held for 2 hours while teflon vapors are present, and finally the furnace is turned off. The teflon vapors may be generated by adjusting the power to the upper zone to a temperature of about 500°C. Excellent results for both CaF_2 and SrF_2 have been obtained using this procedure.

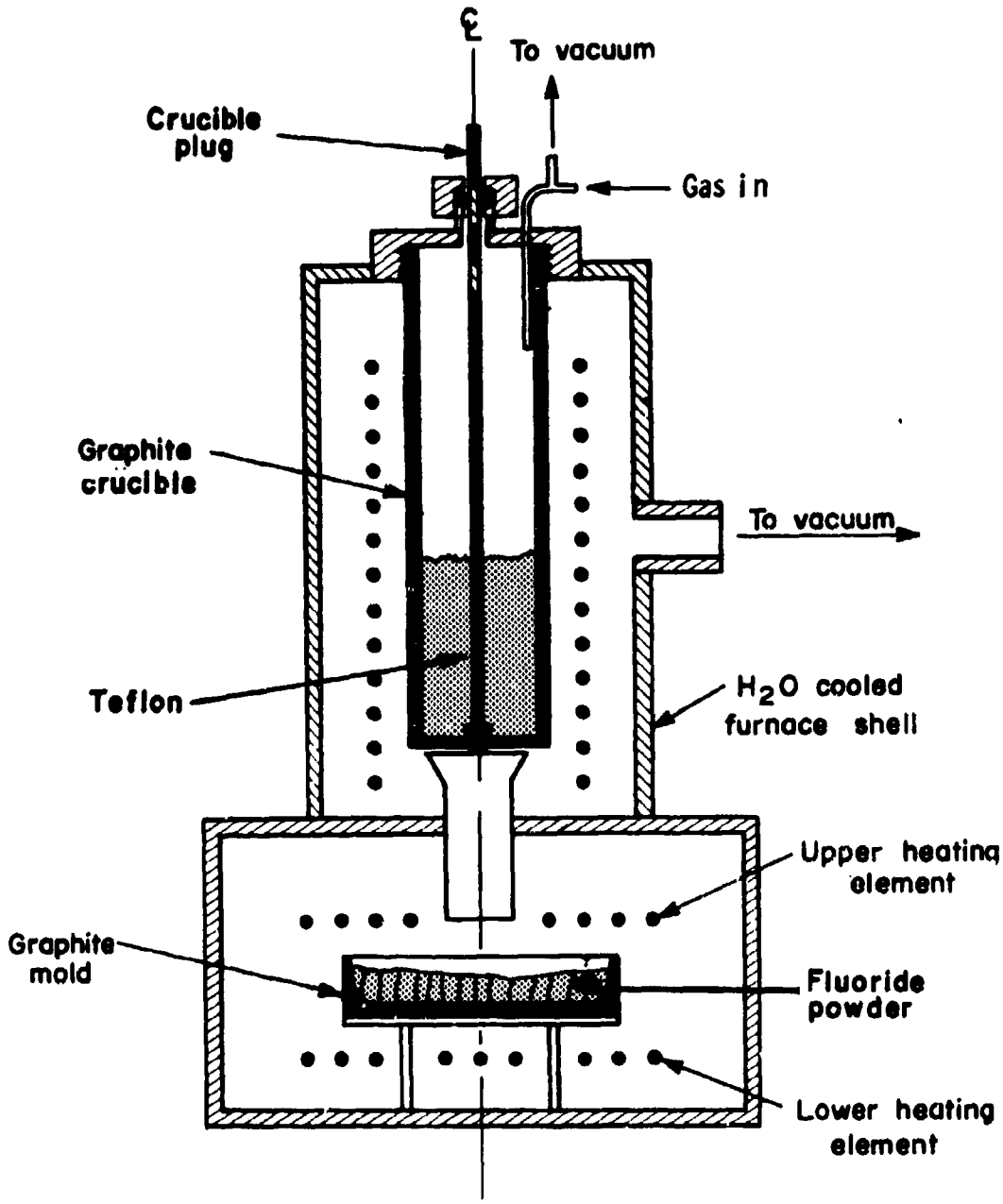

Figure 3-4 Schematic Diagram of Two-Zone Vacuum Casting Furnace.

It was at first noticed that castings produced from purified powder (both SrF_2 and CaF_2) seemed to be especially sensitive to intergranular cracking by thermal shock. It may have been due to trace residual impurities at the grain boundaries with increased sensitivity to thermal shock, as will be discussed below. The problem was alleviated by using a crucible cover with a hole - the hole presumably allowing more volatile impurities to escape more readily. Subsequently some castings cracked due to the high residual stresses developed during cooling but failure was predominantly transgranular in nature, i.e., cleavage across large grains.

Selected samples of starting materials (single crystal chips and "reagent" grade powder) and cast ingots of CaF_2 and SrF_2 were analyzed by emission spectroscopy (Jarrell-Ash, Waltham, Massachusetts). Table 3-1 gives the results of the following CaF_2 samples: (1) Optovac single crystal, (2) a casting of CaF_2 (HN-1) in the vacuum hot press furnace from single crystal ships, (3) an early casting (CF-8) produced in the two-zone furnace at the time low vacuum capabilities and alumina reactions were causing problems, (4) as-received "reagent" grade powder, (5) a casting (VHP-273) using PbF_2-treated powder, (6) a casting (VHP-272) using teflon treated powder, and (7) a casting (CF-198) produced in the two-zone furnace with its high vacuum capability. From these analyses, it is clear that casting in a high vacuum furnace does not degrade the purity of the single crystal starting material. However, in a lower vacuum (casting CF-8) an increase in cation impurities does occur, especially Fe, Cr, Ni, and Cu, probably via a corrosive attack of the stainless steel tank and water-cooled copper baffles. For purification of "reagent" grade powder it can be seen the teflon-treated material has the lowest cation impurity (0 ppm) content, containing only alkaline earth impurities (Mg, Sr, and Ba) with no Na, Al, Cr, Mn, Fe or Cu as is present in the as-received powder. The PbF_2-treated casting is somewhat improved (1.1 ppm) over the as-received powder but is not as impurity-free as teflon-treated material. The casting analyses compare (except for Mg, Sr, and Ba) with those of single crystal chips and

TABLE 3-1

ANALYSIS OF CaF_2

STARTING MATERIALS AND CASTINGS

Detected Impurities	Single Crystal	Casting HN-1	Casting CF-8	"Reagent" Powder	Casting VHP-273	Casting VHP-272	Casting CF-198
Na	ND	ND	ND	800	ND	ND	ND
Mg	0.1	0.5	0.5	10	10	5	0.1
Al	0.5	ND	0.1	0.5	1	ND	0.1
Si	0.5	0.1	0.5	ND	ND	ND	0.1
Ca	H	H	H	H	H	H	H
Cr	ND	ND	0.5	0.5	ND	ND	ND
Mn	ND	ND	0.1	2	ND	ND	ND
Fe	0.5	ND	5	5	0.1	ND	0.01
Ni	ND	ND	5	ND	ND	ND	ND
Cu	0.1	0.5	50	5	ND	ND	0.01
Sr	ND	ND	ND	400	600	400	1000
Ba	ND	ND	ND	80	100	10	10
Pb	ND	ND	0.5	ND	ND	ND	ND
Ag	ND	ND	ND	ND	ND	ND	0.1
Total impurities detected**	1.6	0.6	61.7	813	1.1	0	.32

ND = Not detected

H = Balance

* = 36 additional elements undetected, results in ppm

** = Excluding alkaline earths

castings made from such chips which have small amounts of Mg, Si, Cu and possibly Al and Fe for total analyzed cation impurity levels of 1.6 ppm and 0.6 ppm, respectively.

Table 3-2 gives the results of the following SrF_2 samples: (1) Harshaw single crystal, (2) a casting (VHP-144) using single crystal chips as starting material, (3) as-received "reagent" grade powder, (4) a casting (VHP-358) using PbF_2-treated vacuum-baked powder, (5) a casting (VHP-390) using teflon-treated air-roasted powder, and (6) a casting (VHP-394) using teflon-treated, no air-roasting powder. As can be seen from these analyses and as was the case for CaF_2, casting in a high vacuum furnace does not degrade the purity of single crystal chips. As can also be seen, the castings from both PbF_2-treated "reagent" powder and teflon-treated air-roasted powder are rich in impurities although each is progressively and substantially better than the as-received powder. However, the best purified material, as was the case for CaF_2, is the teflon-treated (no air-roast) sample which has basically only alkaline earth impurity (Ba, Ca and Mg) contamination. The single crystal material (and casting from it) has similar alkaline earth contaminants but a different level of contamination.

The above results clearly show that castings of both CaF_2 and SrF_2 can be obtained with very low cation impurity levels (with the exception of the alkaline earths) by using teflon-treated "reagent" grade powder as starting material. The teflon-treated castings are even slightly more pure than single crystal chips with the exception of alkaline earth contaminants. However, no correlation between detected cation impurities and optical properties was able to be determined quantitatively.

No anion impurity analyses have been performed on any of these materials. No effect of the present purification techniques can be quantitatively determined except, as will be discussed below, excellent optical properties are obtained regardless of the starting material. This is an indication of low levels of anion impurities in the high quality samples.

TABLE 3-2

ANALYSIS OF SrF_2

STARTING MATERIALS AND CASTINGS

Detected* Impurities	Single Crystal	Casting VHP-144	"Reagent" Powder	Casting VHP-358	Casting VHP-390	Casting VHP-394
B	ND	ND	ND	0.5	ND	ND
Na	ND	ND	1000	ND	ND	ND
Mg	2	1	0.5	0.5	1.0	0.1
Al	ND	ND	0.1	0.2	0.1	ND
Si	0.1	0.1	ND	0.1	0.1	ND
Ca	500	700	ND	ND	100	70
Cr	ND	ND	2	1	3	ND
Mn	ND	ND	0.5	0.1	0.01	ND
Fe	0.05	ND	50	20	0.1	ND
Cu	0.01	0.05	20	ND	0.01	ND
Sr	H	H	H	H	H	H
Ag	0.05	0.05	ND	ND	ND	0.01
Ba	1	ND	3000	3000	10,000	5000
Pb	ND	ND	0.5	20	ND	ND
Total impurities detected**	0.21	0.20	1073.1	41.9	3.42	0.01

ND = Not detected

H = Balance

* = 36 additional elements undetected, results in ppm

** = Excluding alkaline earths

As mentioned above, the early castings of SrF_2 and CaF_2 prepared from purified powder (and several castings prepared from single crystal chips) seemed quite susceptible to thermal shock cracking, being predominantly intergranular in nature. This behavior suggested weakened grain boundaries due to impurity precipitation and led to further investigation which solved the problem as mentioned above. Samples of two cast fluorides – SrF_2 and CaF_2 (VHP-311 and 317, respectively) that failed intergranularly were investigated by X-ray microprobe analysis of impurities and their distribution in these samples indicated a weak, uniformly distributed contamination of Al (in CaF_2) and Ca (in SrF_2). In addition, the grain boundary surfaces showed localized accumulations containing predominantly Na, S, Cl, K and occasionally also Mg, Si, Fe and Zn. These accumulations seemed to be located in surface irregularities such as holes, cracks and precipitates. To obtain a clearer correlation between surface appearance and impurity content, magnified maps of the grain boundary surfaces were produced from overlapping SEM pictures. Specific irregularities were identified and subjected to microprobe analysis, the results of which follow.

Figures 3-5 and 3-6 illustrate the example of SrF_2 (VHP-311). Figure 3-5 shows the general fracture surface area with several irregularities and a magnification of a similar irregularity, respectively. Such irregularities appear to be precipitates torn from the matrix during fracture and are clearly not contaminants from handling. Figure 3-6a is the overall X-ray spectra from microprobe analysis of both the general uniform distribution of the grain boundary surface (designated matrix) and the precipitate (designated location 1). Figure 3-6b is the stripped X-ray spectrum of the precipitate; i.e., the matrix spectrum is subtracted from the precipitate spectrum. Any differences in impurity concentrations between the two are shown as sharp peaks in the stripped spectrum. In this case the precipitate is enriched in K, Na and Cl.

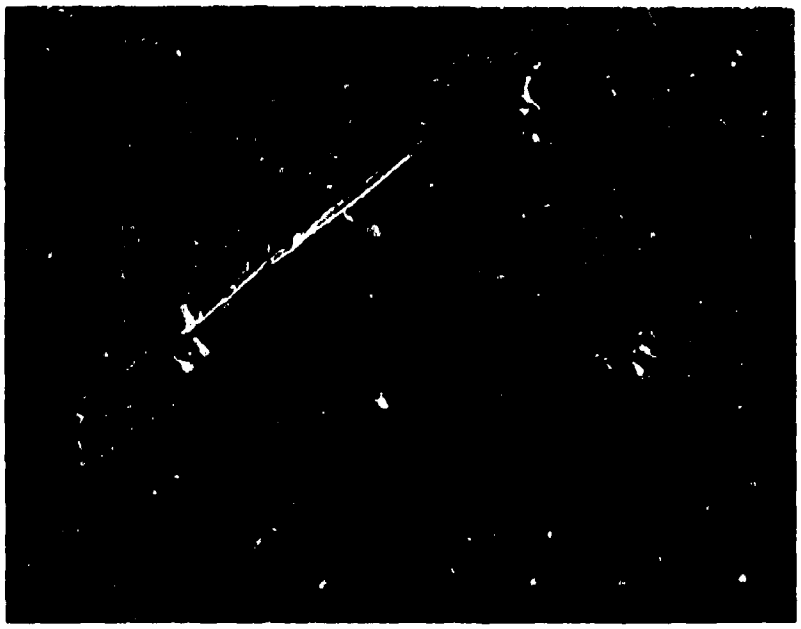

Figure 3-5a Fracture Surface of Cast SrF_2 Sample. SEM 700×

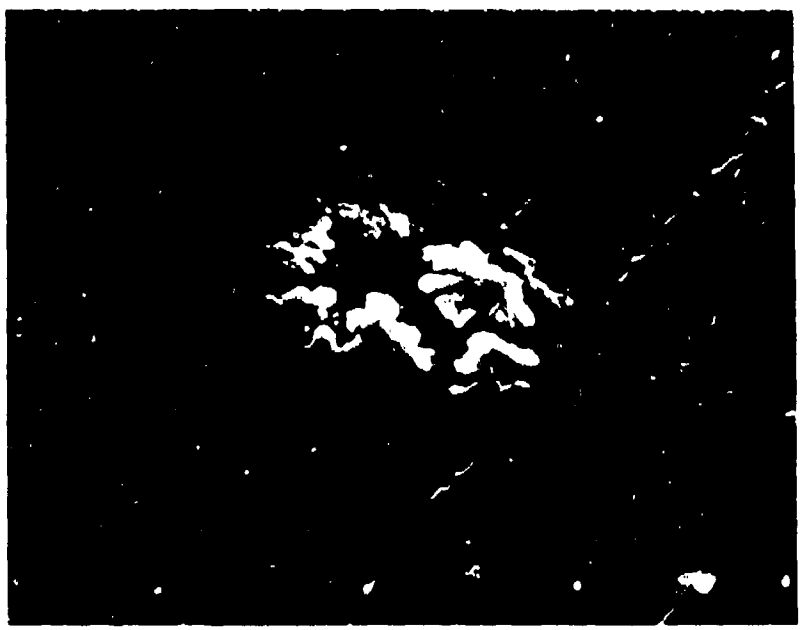

Figure 3-5b Fracture Surface of Cast SrF_2 Sample. SEM 2000×

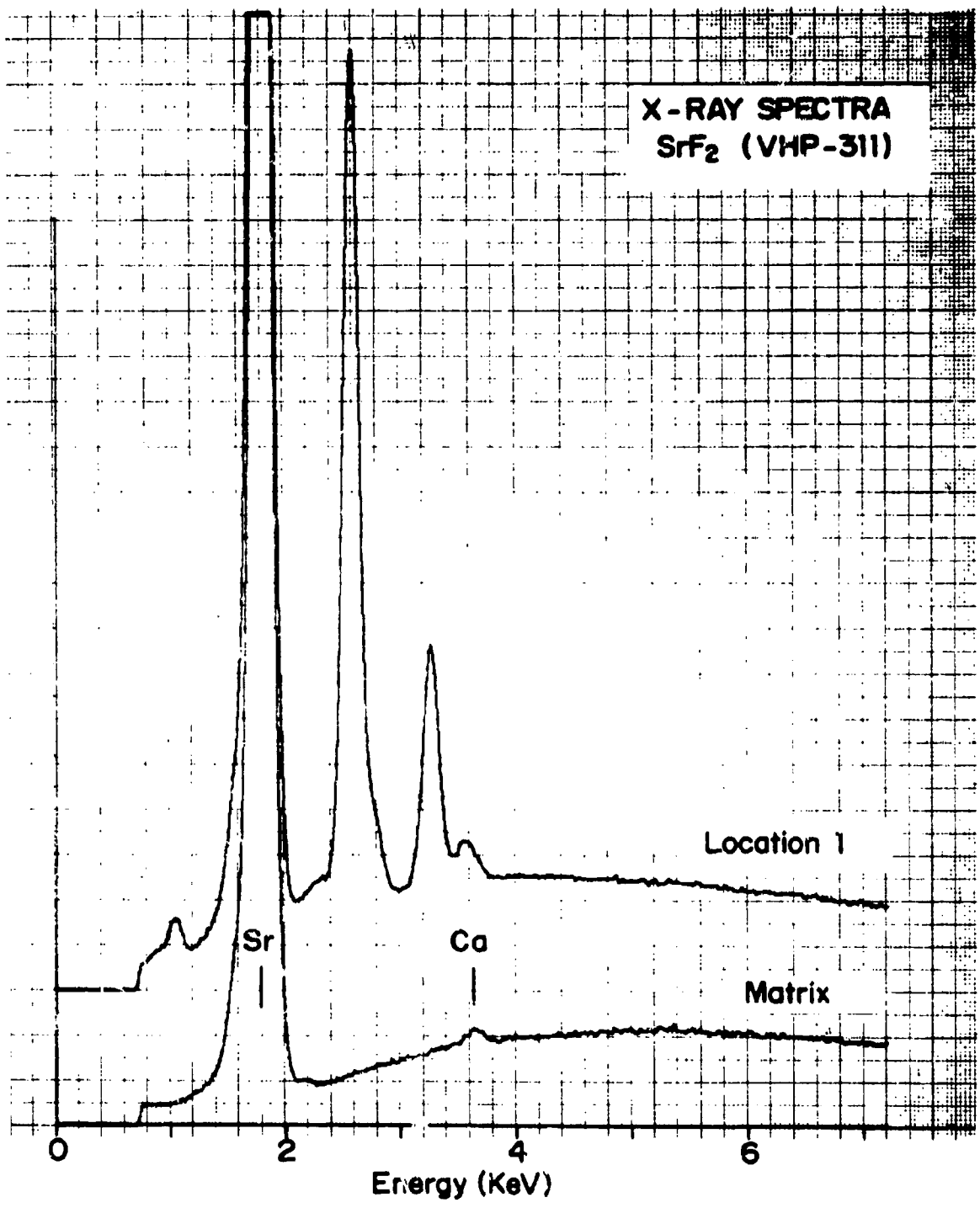

Figure 3-6a X-Ray Spectra of Cast SrF_2 Sample

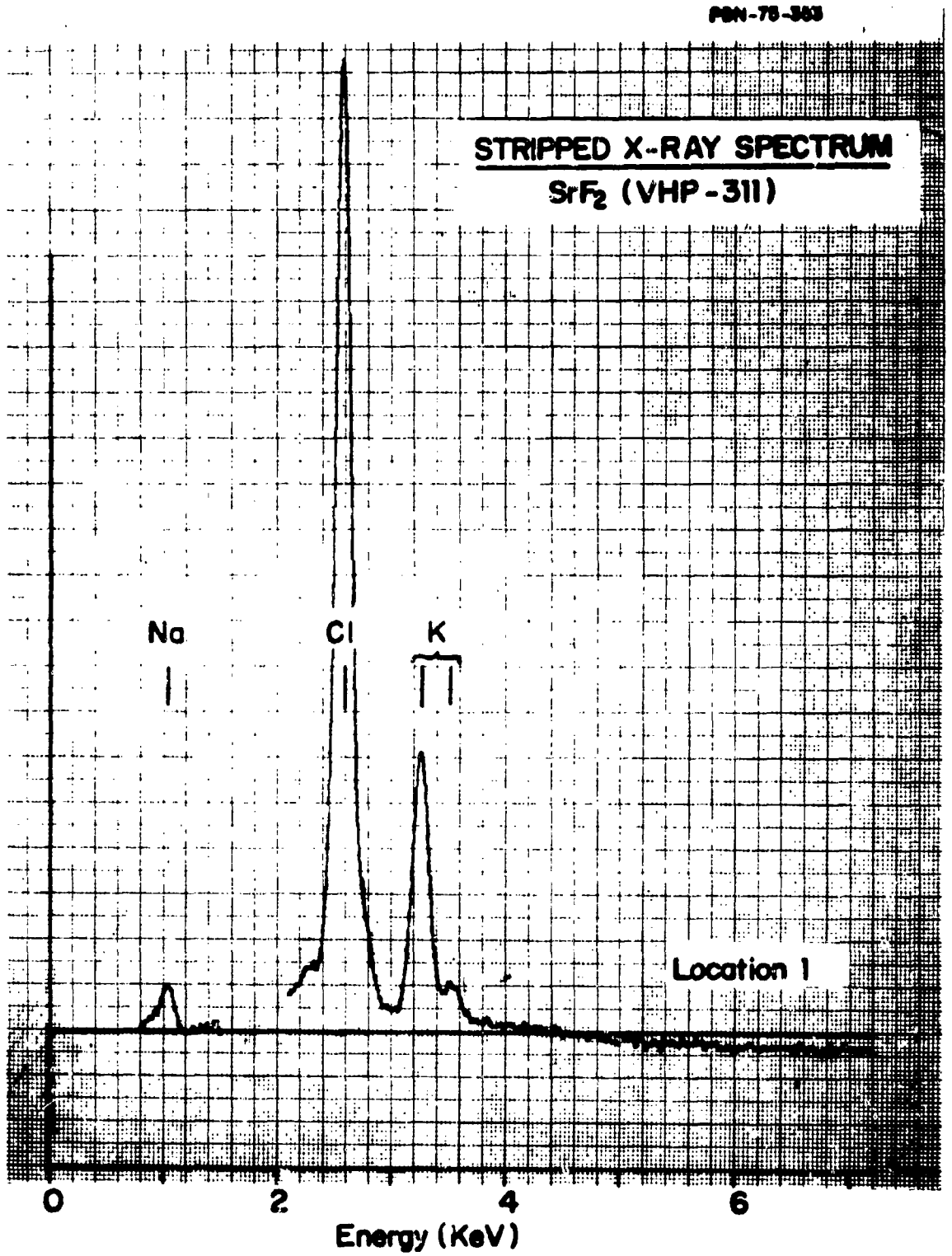

Figure 3-6b Stripped X-Ray Spectrum of Cast SrF_2 Sample

Figures 3-7a - e show similar grain boundary surfaces of cast CaF_2 (VHP-317) and three quite different surface irregularities (designated locations 1, 2, and 3 in the X-ray spectra of Figs. 3-8a and 3-8b). It can also be noted (Figs. 3-7a and 3-7b) by the ripply effect of the general surface that true intergranular failure occurred, whereas for the SrF_2, cleavage steps are also present. From the X-ray spectra of Fig. 3-8a, it can be seen that the CaF_2 matrix has few impurities. However, the irregularities are quite rich and substantially different from each other, as best seen in the stripped X-ray spectra of Fig. 3-8b. The protruding mass of location 1 is enriched mainly in Mg, Al, Si and Fe; while what appears to be a hole at location 2 is enriched in Si, S, Cl and K. Finally, the white precipitate at location 3 is enriched mainly in Na, Si, Cl and K.

The above results indicate that the bulk of the contamination may be localized in accumulations at the grain boundaries. Whether or not these impurities seriously affect the mechanical properties (such as thermal shock resistance) is not quantitatively known.

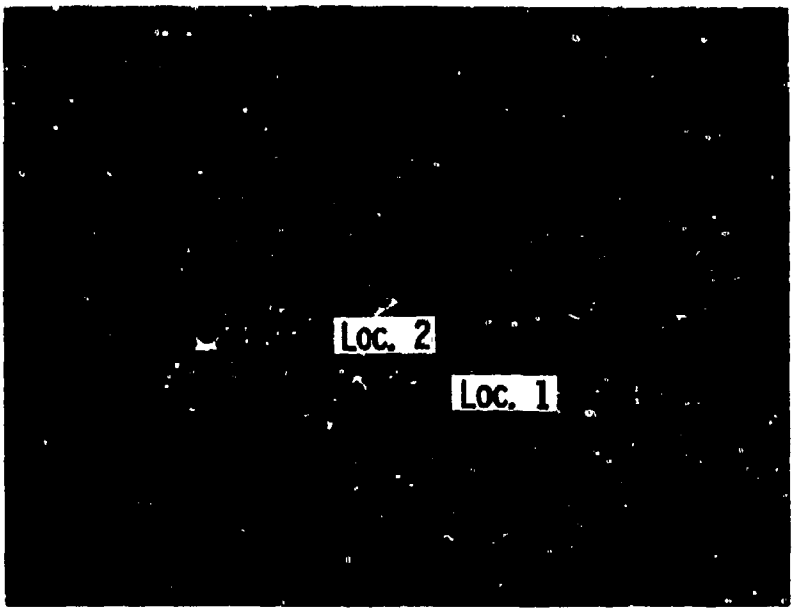

Figure 3-7a Fracture Surface of Cast CaF_2 Sample. SEM 100×

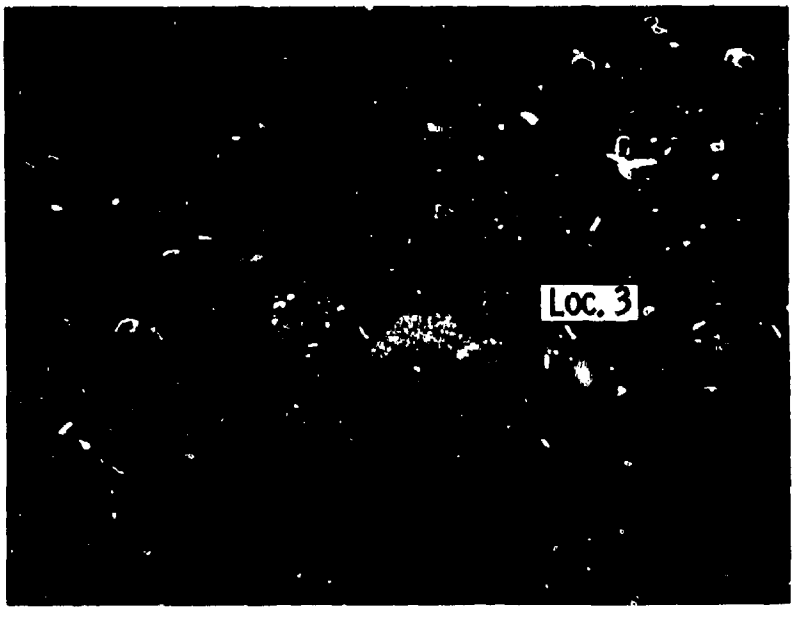

Figure 3-7b Fracture Surface of Cast CaF_2 Sample. SEM 100×

Figure 3-7c Location 1. SEM 1000 ×

Figure 3-7d Location 2. SEM 1000 ×

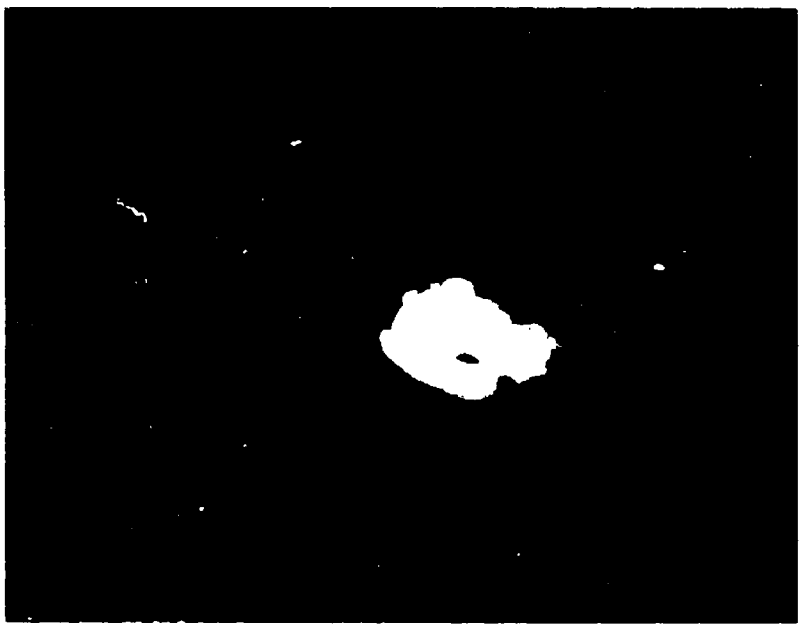

Figure 3-7e Location 3. SEM 3000 ×

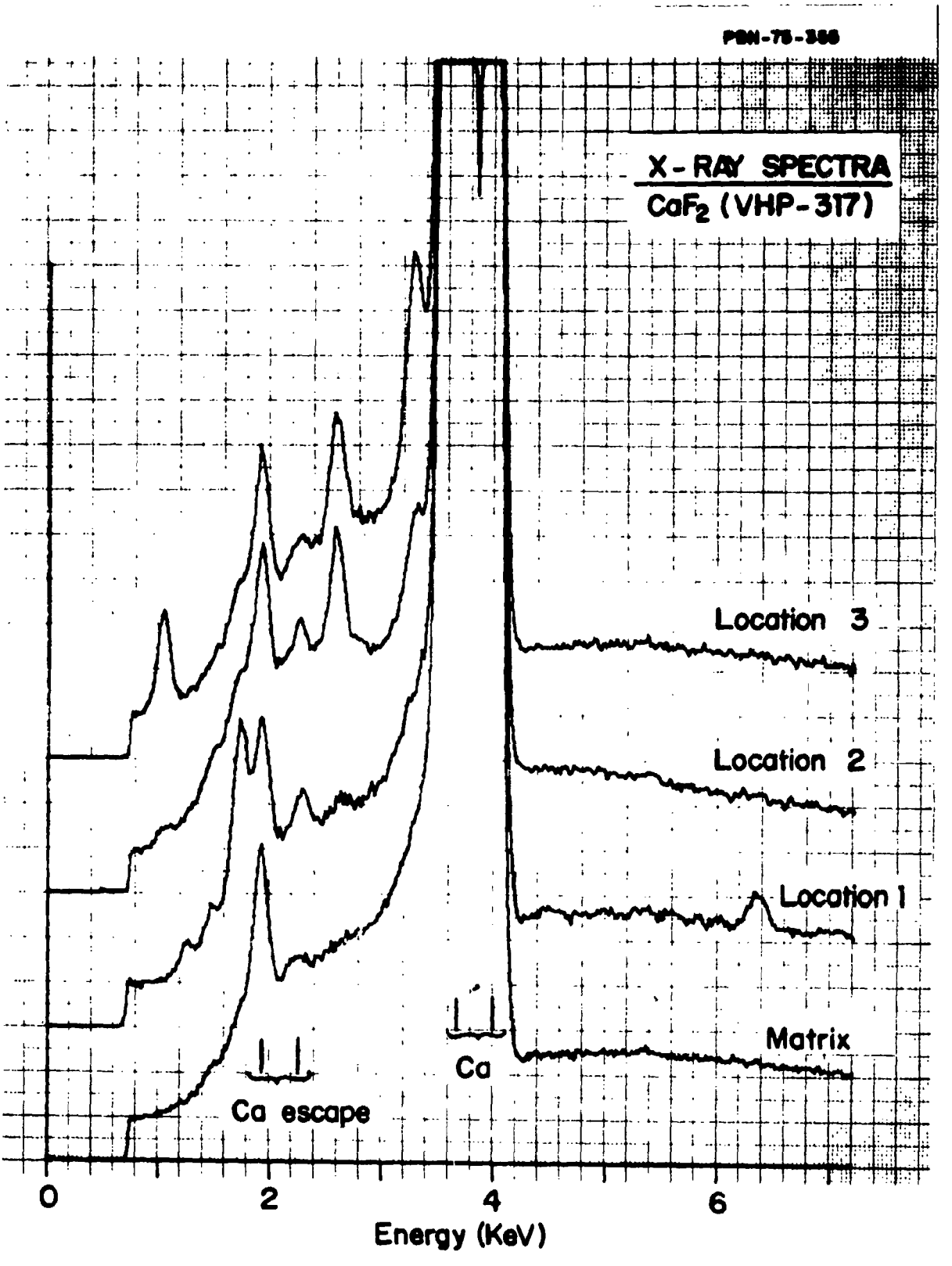

Figure 3-8a X-Ray Spectra of Cast CaF_2 Sample

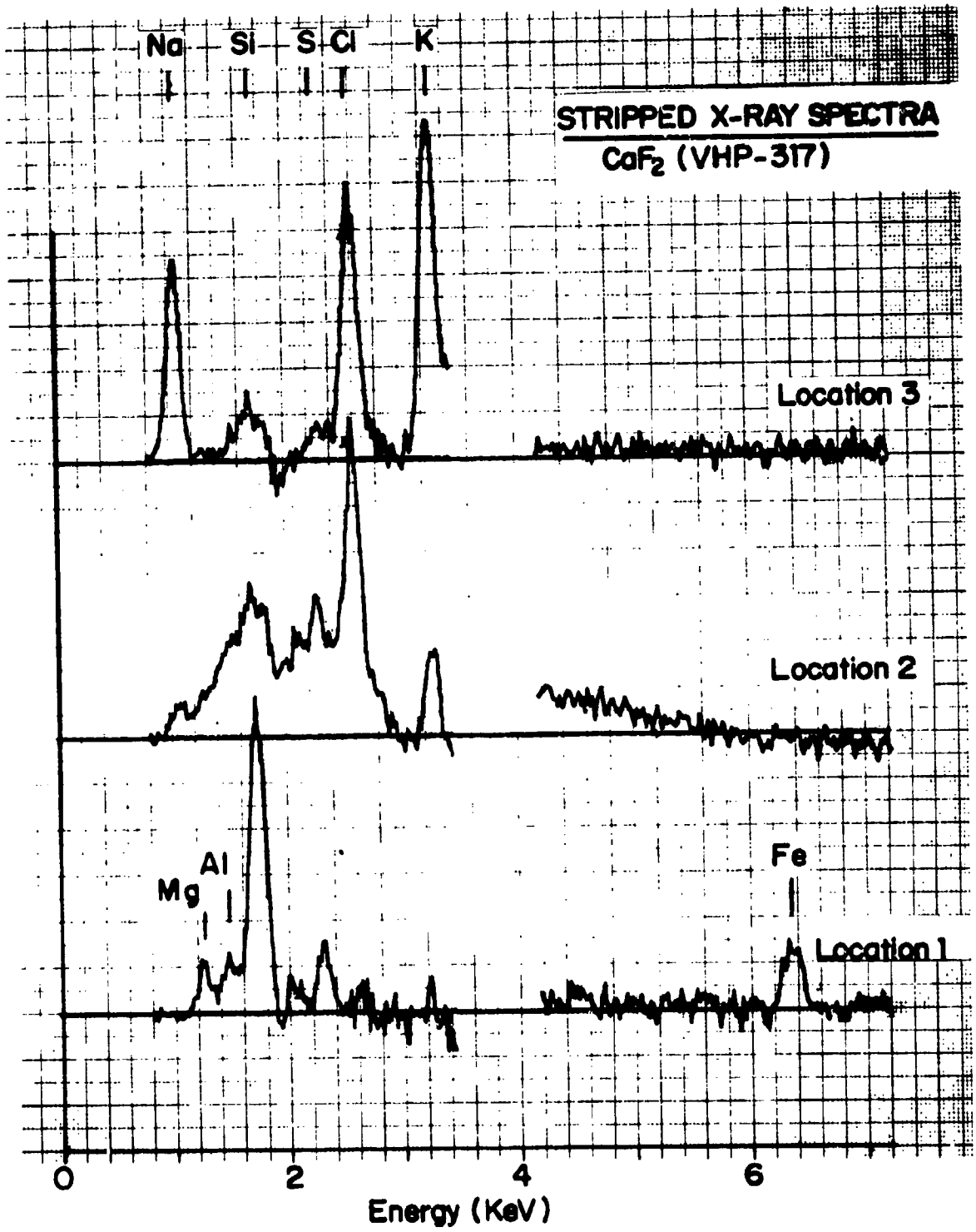

Figure 3-8b Stripped X-Ray Spectra of Cast CaF_2 Sample

3.2.2 Inert Atmosphere Casting

During the program, work was initiated to develop a casting technique in an inert atmosphere instead of the high vacuum (10^{-4} torr or better) required normally. The advantage of inert atmosphere operation is that unidirectional solidification may be better accomplished due to the better heat transfer provided by the gas. It is also desirable because, in the event of scale-up to larger sizes, an inert atmosphere may be less expensive and more convenient to provide than a high vacuum system.

A series of castings of CaF_2 were attempted in the vacuum hot press furnace using dry, high purity argon (passed over titanium chips at 800 - 900°C to remove residual H_2O and O_2) to provide partial pressures of 1, 5, 15, 25 and 50 torr. As expected, better heat transfer resulted in complete unidirectional solidification in all but two of the castings. However, except for these same two castings, as well as one other, the inert atmosphere castings were all slightly discolored (a yellowish to bluish tinge) indicating that the atmosphere was not sufficiently inert and that there was impurity pickup in the castings.

Also, casting runs of CaF_2 were attempted in the vacuum hot press furnace using a reducing atmosphere, i.e., flowing H_2 through the furnace while maintaining a vacuum of 1-25 mm Hg. There was a major problem in the corrosive attack of furnace parts, probably due to HF generated by the action of residual H_2O in the H_2 gas on the fluorides (CaF_2 + PbF_2) present. By reducing the vacuum from 25 mm to 1 mm Hg, the problem was somewhat alleviated.

None of these H_2 runs was successful in producing good, transparent material. The castings were heavily discolored dark red and obviously there was severe impurity pickup into the castings. Qualitatively, these ingots were the worst produced. However, when two of these ingots

were subsequently remelted with additional PbF_2 added in the normal manner, high quality, transparent ingots were obtained. Moreover, these transparent ingots were completely covered with a loosely adherent black film -- probably carbon. It thus appears that the impurity in these ingots was in part carbon picked up by an unknown mechanism.

3.2.3 Hot Forging

During the first half of the program only two hot forgings each of single crystal and polycrystalline cast CaF_2 were attempted. One-inch-diameter samples of each were successfully forged at 1000° C in the vacuum hot press furnace to about 80 percent reduction in thickness, as Fig. 3-9 shows. Resultant grain size was large in every case (on the order of several millimeters), as seen in Fig. 3-10 due to the high temperature of forging. No further work on hot forging was planned because of the excellent mechanical properties of the castings as will be discussed later.

3.2.4 Strain Annealing

As with the cast alkali halides, residual stresses in the cast fluorides are high enough to cause cracking during post fabrication cutting and polishing. However, by the same analysis as used for KCl, the cooling rate should not exceed 600° C/hr. for CaF_2 assuming a maximum residual stress of 600 psi/cm (stress optical coefficient equals 0.017 nm/cm/psi -- Table 2-2) for a two-centimeter-thick casting. Correspondingly, the radial temperature gradient in a cylindrical casting eight inches in diameter would require a cooling rate not to exceed 60° C/hr, with maximum thermal gradients not to exceed about 2° C/cm. Clearly, the problem is not nearly as severe as with the halides, but nonetheless the cooling rate and temperature uniformity must be controlled in order either to prevent the establishment of unwanted residual stresses during the casting process or to remove them by a post fabrication annealing procedure.

PBN-74-521

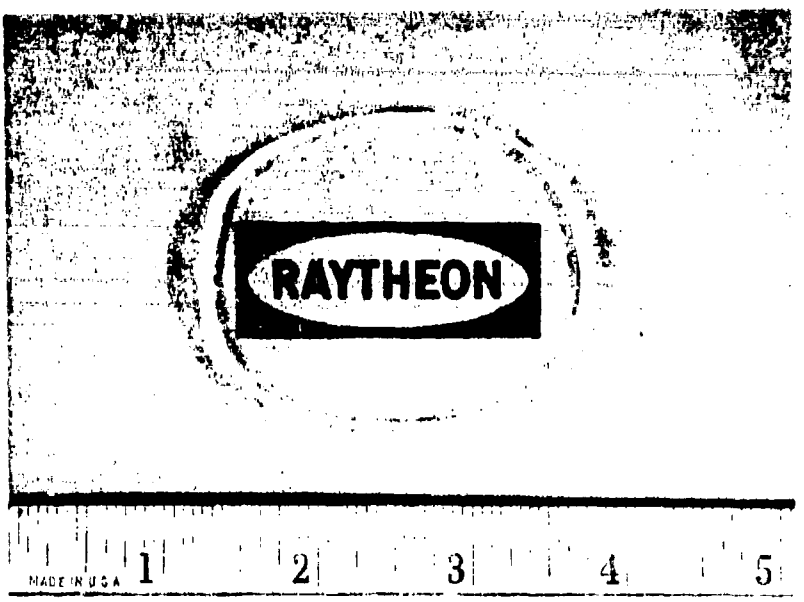

Figure 3-9 CaF_2 Single Crystal Hot Forging. Sample VHP-154. Forged at 1000°C to 79 percent reduction.

Figure 3-10 Photomicrograph of VHP-154. Hot Forged CaF_2 at 1000°C, 79 percent reduction in thickness. 25X.

3.2.4.1 Vacuum annealing

One of the major problems with the casting of the fluorides during the program was the high residual strain developed due to nonuniform cooling in the vacuum hot press furnace, and the resulting susceptibility to cracking. Early in the program, a post fabrication strain anneal process was developed. Figure 3-11 shows qualitatively the results of strain reduction (as viewed through crossed polarizers) by vacuum annealing a CaF_2 casting in the two-zone furnace equipped with only a mechanical vacuum pump and capable of a vacuum of about 10^{-2} torr. Figure 3-11a shows the highly strained as-cast sample. Figure 3-11b shows the sample vacuum annealed at 1000°C for ten hours, followed by cooling at 25°C/hr. In this case, the sample is fairly free of residual strain.

As a result of the success of these early strain anneals, several large castings of CaF_2 were similarly annealed to give strain-free samples for polishing and testing. Only later was it discovered that this particular annealing procedure degraded the optical properties (i.e., 5.25 μm absorption) by a precipitation and scatter problem. Subsequently, the interrelation between strain relief annealing and the development of scattering centers was investigated more fully and several alternative strain relief procedures were established without degrading the optical properties. Namely, vacuum annealing at 900°C, vacuum annealing at 1000°C while providing a purifying atmosphere of teflon vapor at about 50 μm of partial pressure during the run and late in the program after the addition of a new high vacuum system to the two-zone furnace, vacuum annealing at 1000°C under high vacuum (better than 10^{-4} torr) proved to be equally successful for both CaF_2 and SrF_2 as is illustrated in Fig. 3-12 for a sample of cast SrF_2. The sample is fairly strain free after vacuum annealing. As will also be discussed below, no degradation of optical properties occurs in the samples annealed by these alternative strain relief procedures.

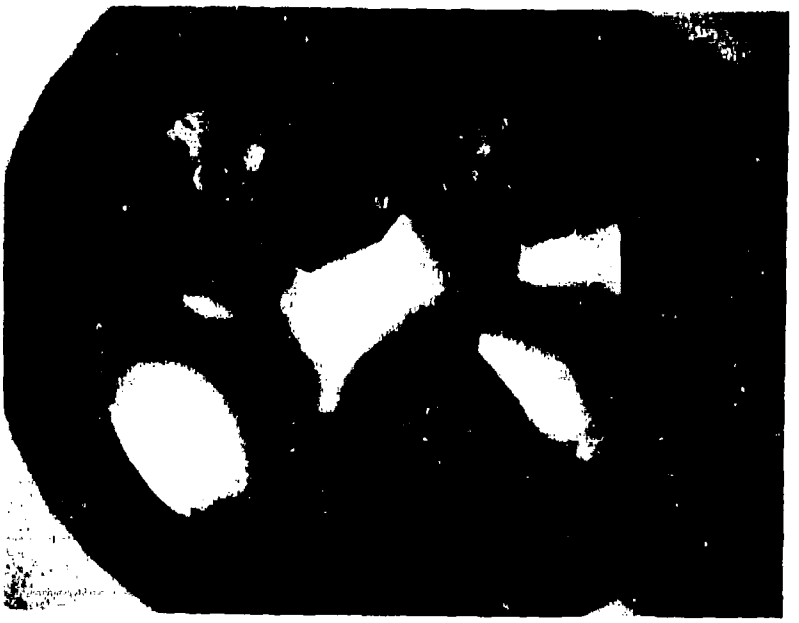

Figure 3-11a Cast CaF_2 (VHP-167), As Cast. Viewed through crossed polarizers.

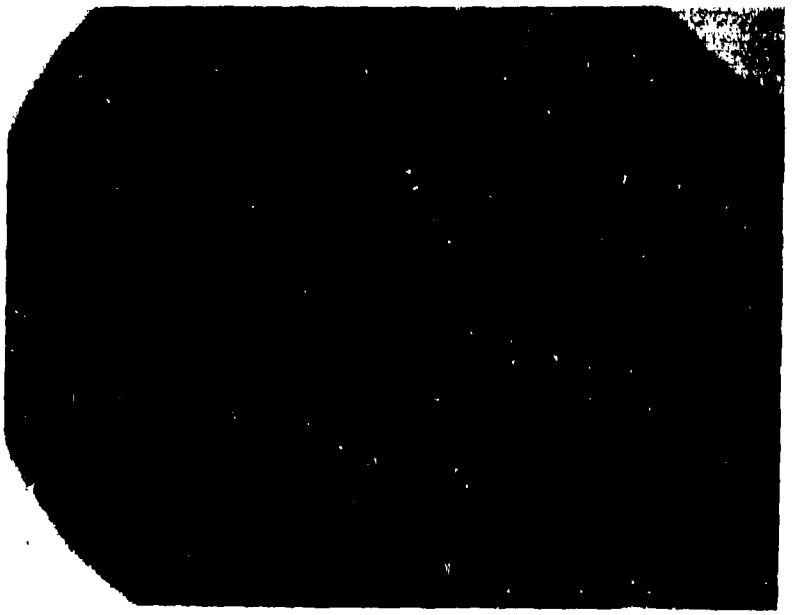

Figure 3-11b Same After 1000°C Anneal for 10 Hours and Cooled at 25°C/hr.

Figure 3-12 Cast SrF_2 (VHP-395) After 1000°C Anneal for 10 Hours and Cooled at 25°C/hr. Viewed through crossed polarizers.

3.2.4.2 Inert and reactive atmosphere annealing

During the program a large Lindberg box furnace was installed in the laboratory with heating and cooling capabilities at controlled rates of about 10 - 100°C/hr (subject to the natural heating and cooling rates of the furnace) from room temperature to 1500°C.

By using an Inconel inert atmosphere retort (approximately 10 × 10 × 12 inches inner dimensions) preliminary strain anneal runs in an inert atmosphere were attempted in this furnace. Samples were one-inch diameter single crystals of CaF_2 (Optovac). The procedure for each heat treatment was to heat the furnace at 50°C/hr to the soak temperature after purging the system as desired. The soak temperature (800, 900 or 1000°C) was held for ten hours, followed by cooling at 25°C/hr to room temperature. Table 3-3 presents the results of these runs. The samples heated in air or argon at 1000°C showed fine white precipitates distributed either uniformly throughout (opacity) or as veils. Samples heated in argon or helium without sufficient purging at 900°C also showed some opacity. However, samples annealed at 800 or 900°C and properly purged with argon were as transparent as before and showed no scattering (as viewed with a He-Ne laser beam). Annealing at 900°C in argon may be a viable alternative to vacuum annealing at 900°C.

However, since vacuum annealing was successful at 1000°C and since the above results for CaF_2 indicate a maximum useful annealing capability in argon of only 900°C without impurity pickup, an alternative was tried, i.e., reactive atmosphere annealing, and proved to be successful.

The successful procedure developed is as follows: A strained ingot to be annealed is placed in a closed graphite crucible with chunks of teflon (nominally 200 gms) added. The closed crucible is placed in the inconel retort and after the retort is purged for 24 hours with purified argon, the furnace is heated up slowly (nominally 25-50°C/hr) to 1000°C,

TABLE 3-3

EFFECT OF HEAT TREATMENT ON CaF_2 SINGLE CRYSTALS

Heat Treatment Temperature (°C)	Atmosphere	Comments
1000	Air	Sample opaque
900	Argon (unpurged)	Sample uniformly hazy
900	Helium (unpurged)	Sample uniformly hazy
1000	Argon (purged 24 hrs.)	Veils throughout
900	Argon (purged 24 hrs.)	No haziness or scatter
800	Argon (purged 24 hrs.)	No haziness or scatter

held 2 hours and slow cooled at 25°C/hr to room temperature. At elevated temperatures the teflon vaporizes and pyrolyzes to provide a "purifying" atmosphere within the closed crucible. Samples of up to about 5 1/2 inches in diameter of both CaF_2 and SrF_2 have been successfully annealed. Due to the pyrolysis of the teflon during the annealing cycle, all samples are coated lightly with a thin film of carbon which can easily be wiped or polished away.

Figure 3-13 shows a sample of cast SrF_2 cut from an ingot strain annealed using the above described procedure. The sample is viewed through crossed polarizers thus showing the marked strain reduction of the previously highly strained ingot.

Figure 3-13 Cast SrF_2 (VHP-400) After 1000° Reactive Atmosphere Anneal for Two Hours and Cooled at 25°C/hr. Viewed through crossed polarizers.

3.2.5 Optical Properties

The feasibility of casting high quality CaF_2 and SrF_2 has been demonstrated by using either high purity single crystal chips or purified "reagent" grade powder as starting materials. Figures 3-14, 3-15 and 3-16 show respectively the IR transmission spectra for an Optovac single crystal of CaF_2, a polycrystalline CaF_2 casting (VHP-167) using Optovac single crystals as starting material, and a polycrystalline CaF_2 casting (VHP-271) using purified "reagent" grade powder, with no detectable differences in the three. No impurity bands are detectable in any of the three. The 5.25 μm apparent absorption coefficients* for these three samples are $4.9 \times 10^{-4}\,cm^{-1}$, $4.8 \times 10^{-4}\,cm^{-1}$, and $4.3 \times 10^{-4}\,cm^{-1}$, respectively. These absorption coefficients were measured using a CO laser calorimeter in our laboratory.

Figures 3-17, 3-18 and 3-19 show respectively the IR transmission spectra for a Harshaw single crystal of SrF_2, an early polycrystalline SrF_2 casting (VHP-275) using Harshaw single crystals as starting material, and a polycrystalline SrF_2 casting (VHP-363) using purified "reagent" grade powder, with no detectable differences in the three. No impurity bands are detectable in any of the three. Moreover, the CO-laser-measured 5.25 μm apparent absorption coefficients are $4.0 \times 10^{-5}\,cm^{-1}$, $1.2 \times 10^{-4}\,cm^{-1}$, and $7.4 \times 10^{-5}\,cm^{-1}$, respectively.

Loss measurements as a function of length were done by laser calorimetry at 5.25 μm for cast CaF_2 and SrF_2 (both single crystal chips and purified powder used as starting materials). Figs. 3-20 and 3-21 plot total absorption versus length for the CaF_2 and SrF_2 samples, respectively. The results graphically illustrate that for both CaF_2 and SrF_2 the absorption at 5.25 μm is equivalent in each material regardless of the starting material.

---

*An apparent absorption coefficient is defined as the total absorption per unit length with no surface loss correction. The bulk absorption coefficient is defined as the total absorption per unit length less the correction for surface loss, as determined from the slop and intercept (zero length), respectively, of the absorption vs length plots.

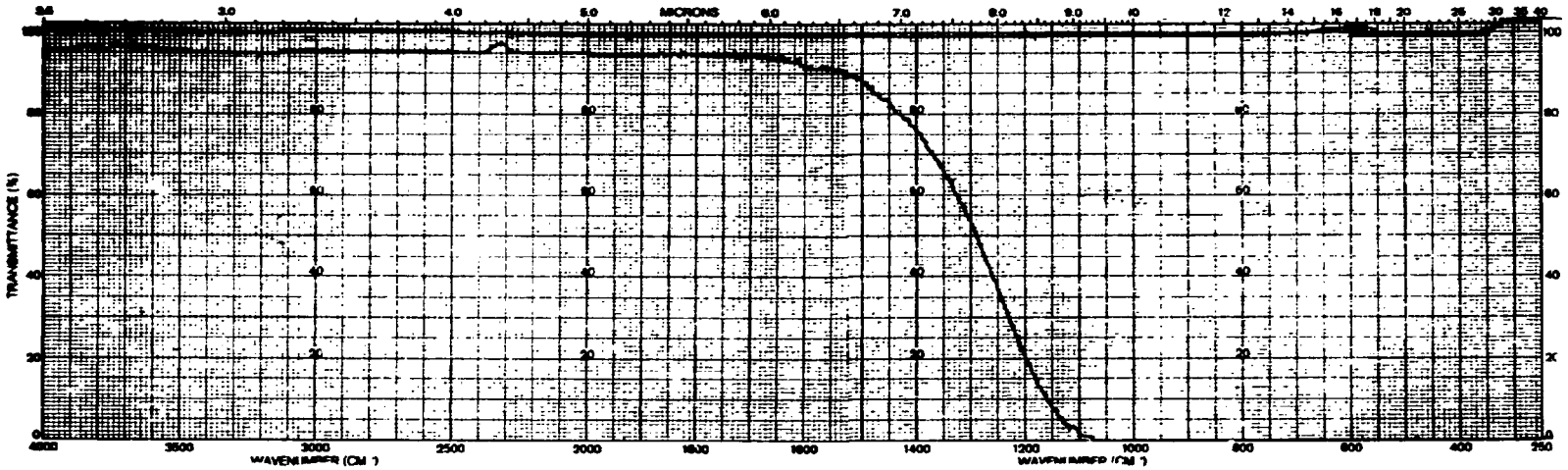

Figure 3-14 Infrared Spectrum of Sample Optovac CaF_2 Single Crystal. 5.8 cm path length.

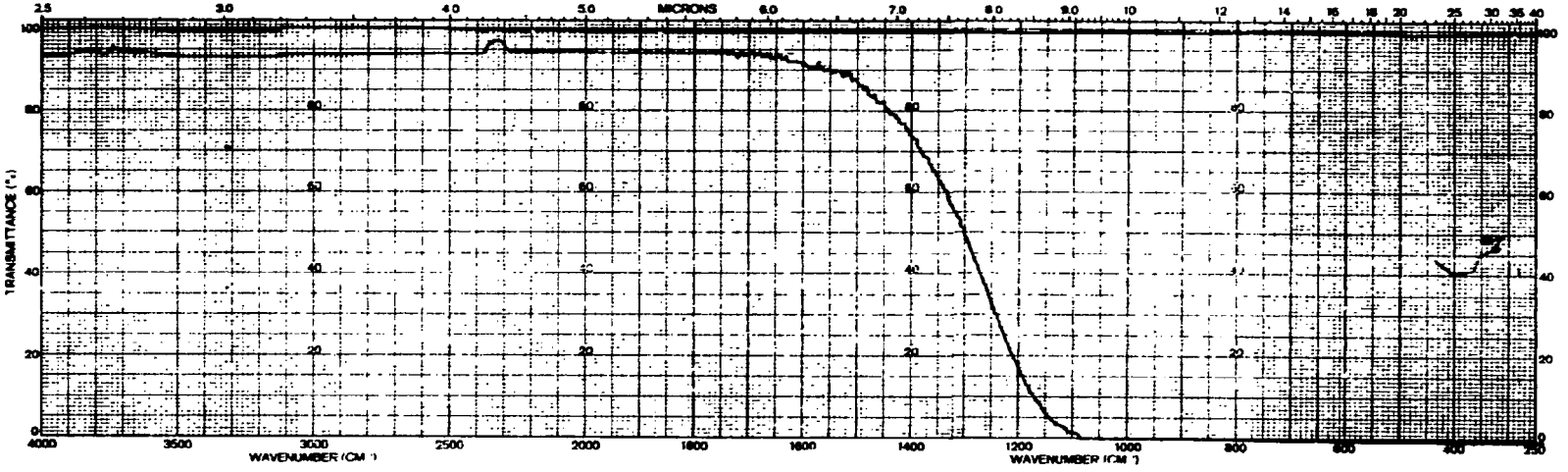

Figure 3-15 Infrared Spectrum of Sample VHP-167, Cast CaF_2. 6.5 cm path length. Optovac Single Crystal Starting Material.

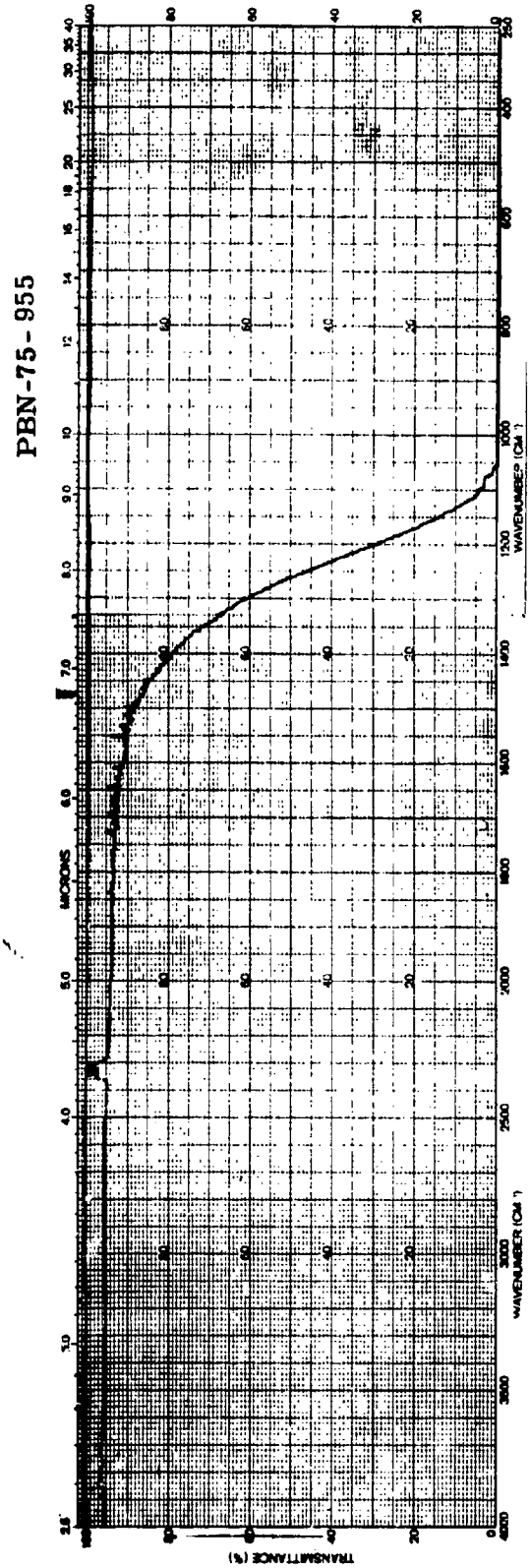

Figure 3-16 Infrared Spectrum of Sample VHP-271, Cast CaF_2. 4.4 cm path length. Purified "reagent" grade powder.

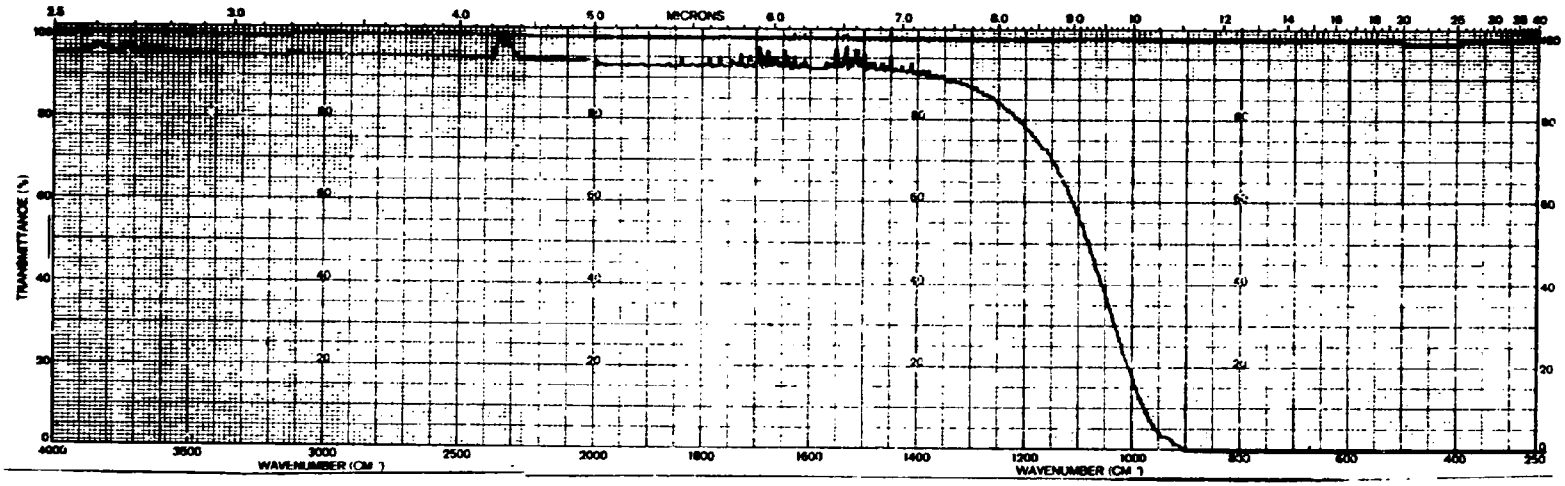

Figure 3-17 Infrared Spectrum of Sample Harshaw Single Crystal SrF_2. 5.0 cm path length.

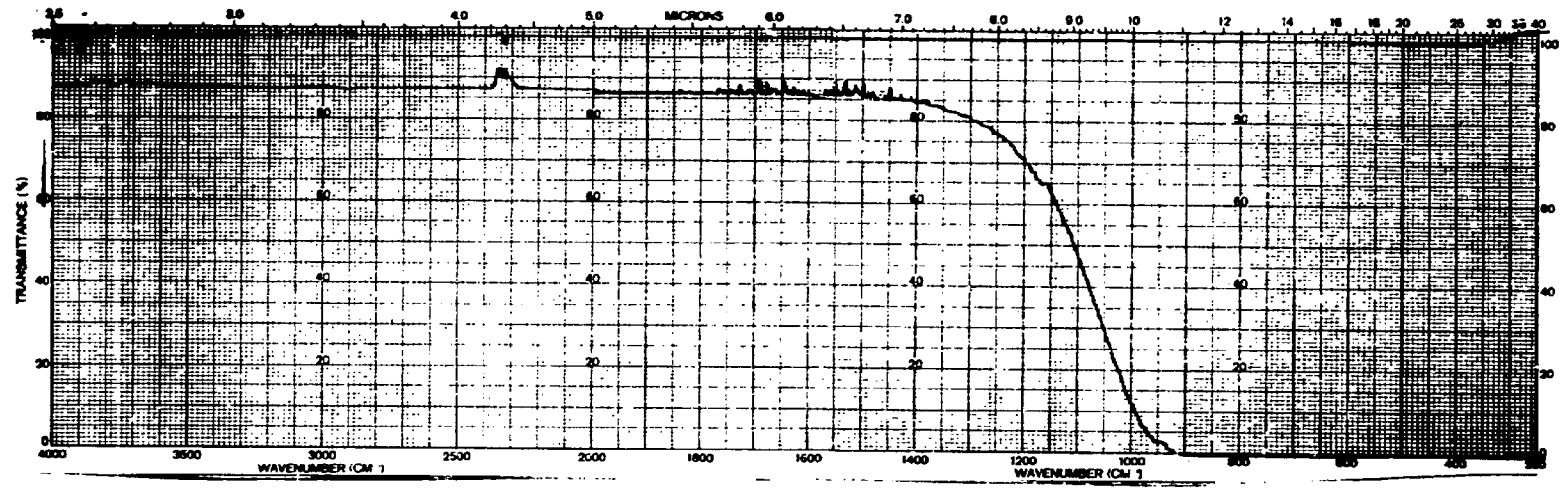

Figure 3-18 Infrared Spectrum of Sample VHP-275, Cast SrF_2. 6.0 cm path length. Harshaw Single Crystal Starting Material.

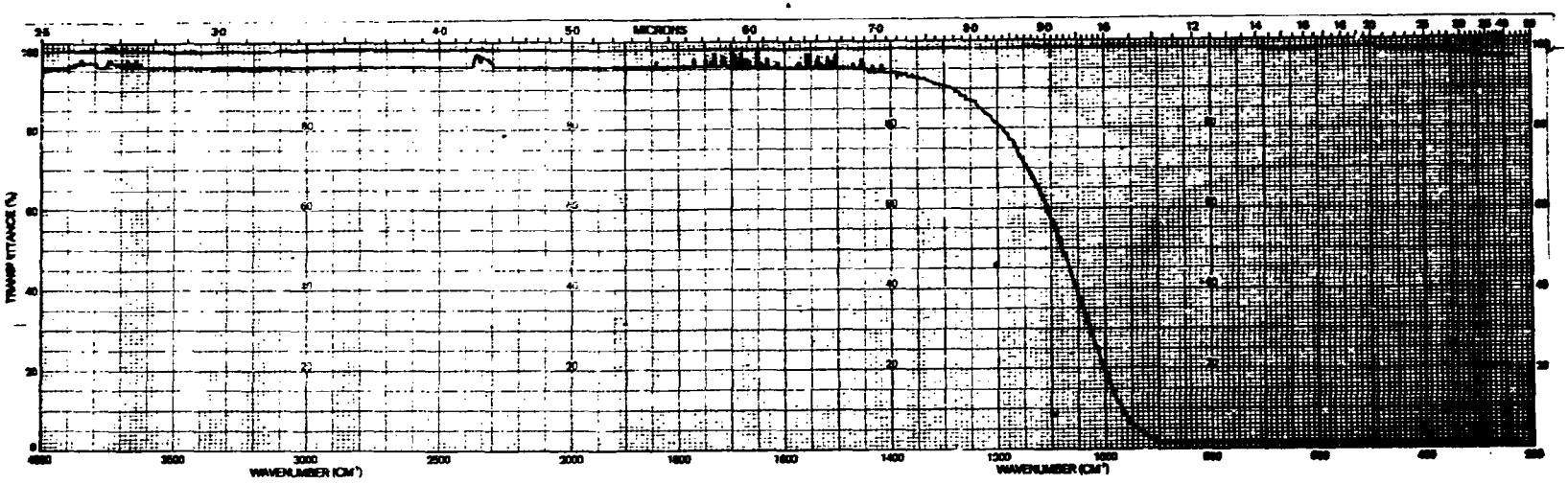

Figure 3-19 Infrared Spectrum of Sample VHP-363, Cast SrF_2, 4.5 cm path length. Purified "reagent" grade powder.

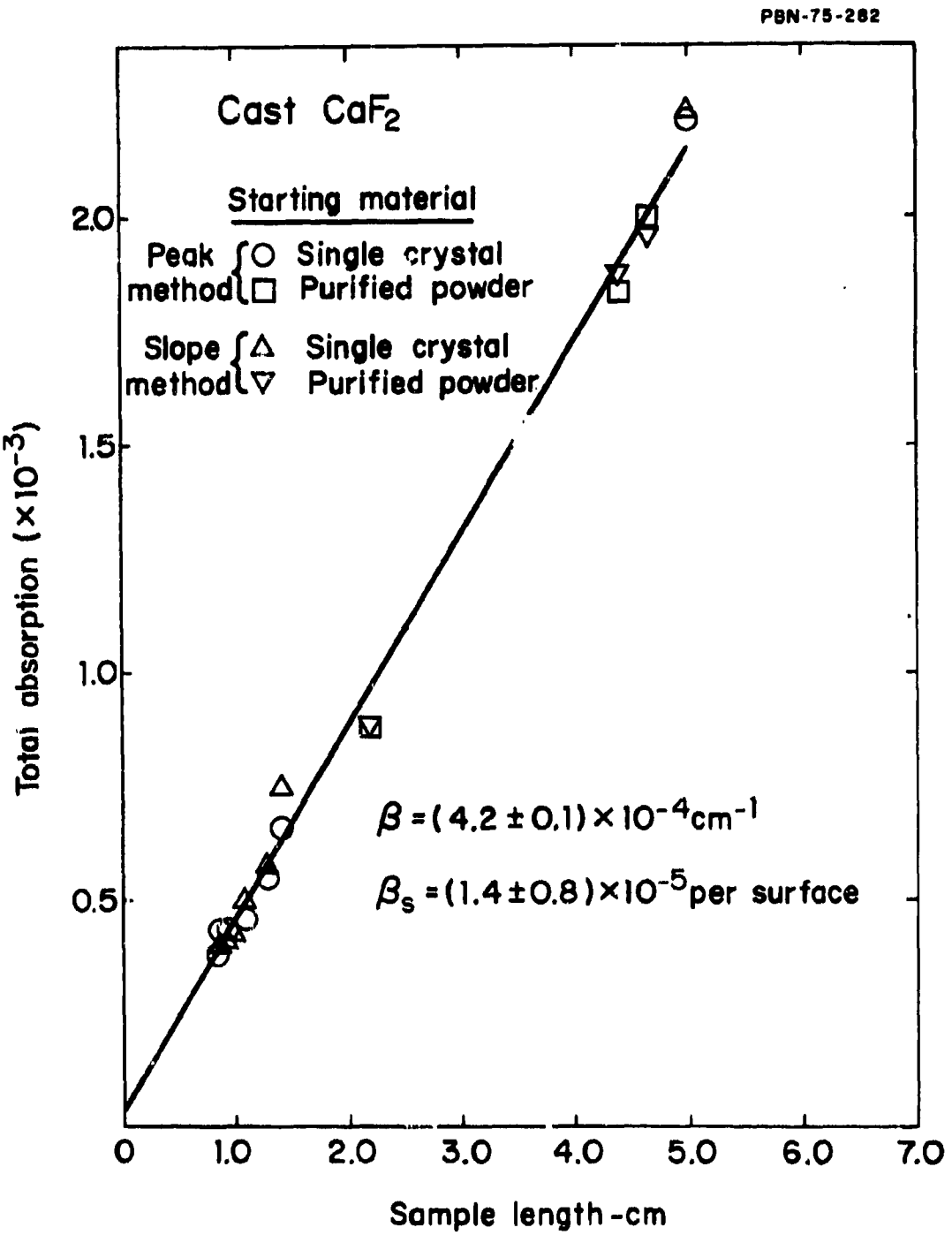

Figure 3-20 5.25 μm Optical Absorption Vs Length for Cast CaF_2

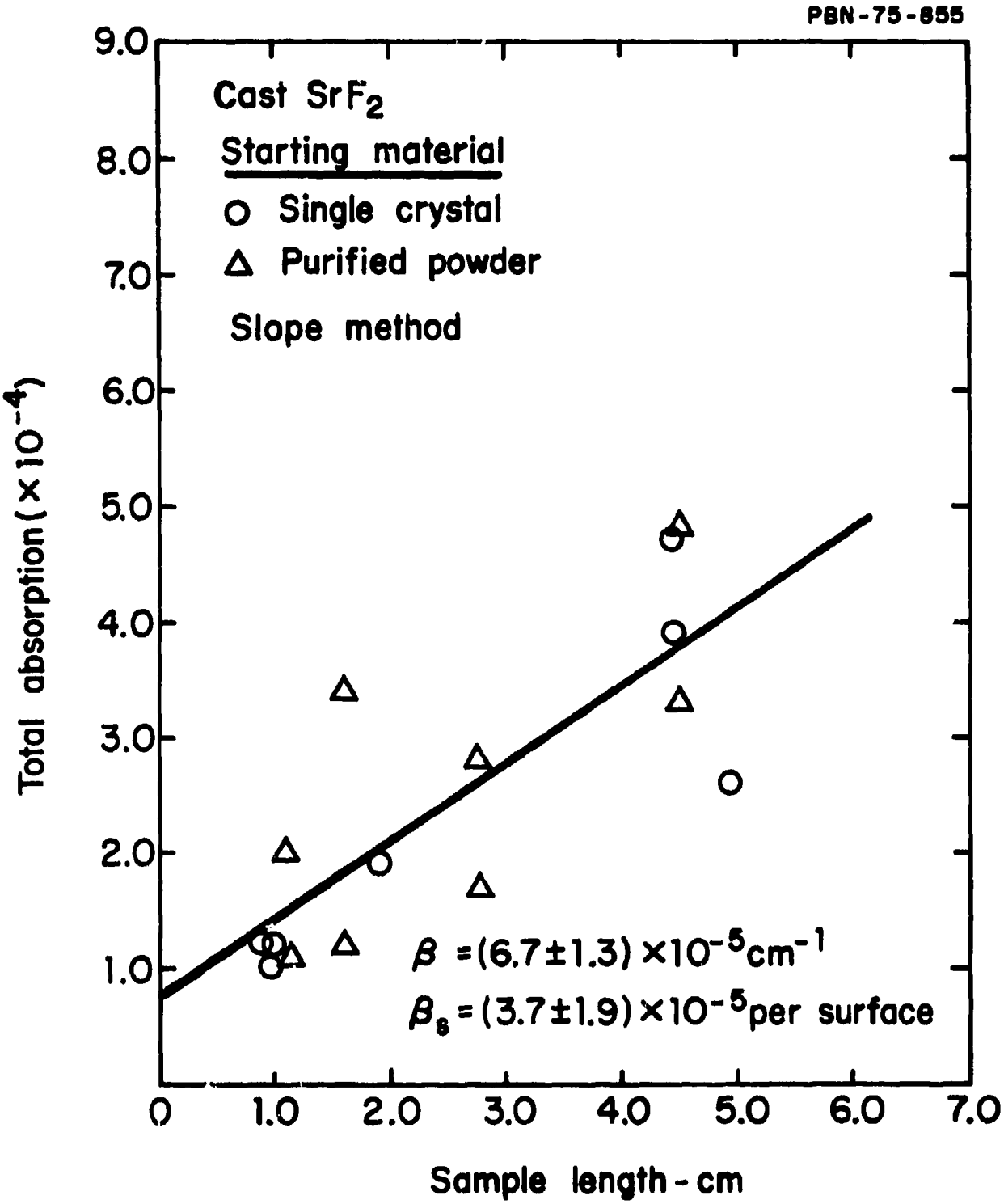

Figure 3-21 5.25 μm Optical Absorption Vs Length for Cast SrF_2.

The results are summarized in Table 3-4 for both CaF_2 and SrF_2. The average 5.25 μm bulk absorption coefficient of cast CaF_2 ingots is $(4.2 \pm 0.1) \times 10^{-4}\ cm^{-1}$, results essentially equivalent to the measured value for single crystal CaF_2 and quite near the value of $1.8 \times 10^{-4}\ cm^{-1}$ predicted[28] from the exponential law. The average bulk absorption coefficient of SrF_2 ingots is $(6.7 \pm 1.3) \times 10^{-5}\ cm^{-1}$, regardless of starting material, results essentially equivalent to the measured value for single crystal SrF_2 and near the value of $2 \times 10^{-5}\ cm^{-1}$ predicted[28] from the exponential law.

These results show quantitatively that for both SrF_2 and CaF_2, the fusion casting process does not degrade the optical properties of the high quality single crystal chips starting material. Moreover, they show that for both CaF_2 and SrF_2, the "reagent" grade powder which has been purified in-house is optically equivalent to the high purity single crystal chips when used as starting material, thus allowing substantial cost reduction in starting material. Furthermore, it is shown that the all graphite fusion casting system is capable of achieving material of the highest quality and that the polycrystalline cast material is equivalent to single crystal material.

The results, as presented in Table 3-4, also show that, at least for SrF_2 at 5.25 μm, surface absorption may be a dominant part in total absorption measurements. That is, while bulk absorption for cast SrF_2 lies near $6.7 \times 10^{-5}\ cm^{-1}$, surface absorption is in the same range, near 3.7×10^{-5} per surface. Thus, for a 1 cm sample, surface absorption would account for more than 50 percent the measured total absorption. For CaF_2 the surface absorption is not so large and may not be so damaging. That is, while the surface absorption - near 1.4×10^{-5} per surface - is nearly the same as that measured for SrF_2, the bulk absorption for CaF_2 is more than an order of magnitude larger, near $4.2 \times 10^{-4}\ cm^{-1}$, so that for a 1 cm thick sample the surface absorption may only account for less 10 percent of the total absorption value.

TABLE 3-4

SUMMARY OF FLUORIDE MEASUREMENTS

Material	Starting Material	β measured 5.25 μm	Surface Correction	β predicted Exponential Law*
Optovac CaF_2	--	$(4.7 \pm 0.3) \times 10^{-4}$ cm^{-1}	No	1.8×10^{-4} cm^{-1}
Cast CaF_2	Single crystal or purified powder	$(4.2 \pm 0.1) \times 10^{-4}$	$(1.4 \pm 0.8) \times 10^{-5}$ per surface	--
Harshaw SrF_2	--	$(4.1 \pm 0.7) \times 10^{-5}$*	$(3.9 \pm 0.9) \times 10^{-5}$*	2×10^{-5}
Cast SrF_2	Single crystal or purified powder	$(6.7 \pm 1.3) \times 10^{-5}$	$(3.7 \pm 1.9) \times 10^{-5}$	--

* From Ref. 28

Laser calorimetry measurements at 3.8 μm (DF laser) have been made by other investigators on several (near one-centimeter-thick) samples of Raytheon-cast material. An apparent absorption coefficient at 3.8 μm for cast CaF_2 was measured to lie near 3.5×10^{-4} cm^{-1} at TRW.[29] At the University of Alabama, Huntsville, 3.8 μm apparent absorption coefficients were measured near 6×10^{-4} cm^{-1} [30] and 3×10^{-4} cm^{-1} [31] for cast CaF_2 and cast SrF_2, respectively. No surface loss corrections were made on these above values, however, the values are much higher than expected due to the very low ($<10^{-6}$ cm^{-1}) predicted intrinsic values at 3.8 μm.[28]

That the teflon purification scheme best achieves high quality castings from "reagent" powder starting material and purifies the material is shown by a casting of non-teflon treated CaF_2 powder with only PbF_2 added as a scavenger. Its measured 5.25 μm apparent absorption coefficient was only 7.7×10^{-4} cm^{-1}. Similarly, a very good vacuum as is usual in the vacuum hot press (10^{-4} torr) may be necessary to achieve high quality. A casting of single crystal starting material in a 50 - 100 μm vacuum (diffusion pump turned off in the vacuum hot press) resulted in a very high 5.25 μm apparent absorption coefficient of 3.1×10^{-2} cm^{-1}.

For those samples of CaF_2 cast with a partial pressure of argon (inert atmosphere of 1 - 50 torr) present, the samples were typically discolored as mentioned previously. One sample that was discolored a faint yellow-blue had a measured 5.25 μm apparent absorption coefficient of 5.8×10^{-3} cm^{-1}; another similarly cast sample (50 torr argon) was colorless with a very good apparent absorption coefficient of 4.1×10^{-4} cm^{-1}. Clearly, the results were mixed and further work must be done to improve the process.

Late in the casting program, when thicker samples of CaF_2 (2-3 cm thick) were attempted to be cast in the two-zone furnace, an impurity pick-up again became a problem. Typical 5.25 μm apparent absorption coefficients were in the 6 - 14 $\times$ 10^{-4} cm^{-1} range, substantially higher than the highest quality samples as reported above. The impurity pick-up with visible scatter being a sympton may be similar to that developed in improper annealing techniques as will be discussed below. At this time it is an unknown impurity. Figure 3-22 shows the IR spectra of two one-centimeter samples cut from ingots of high quality and low quality (as above), respectively. No detectable impurities are evident although the poor quality sample clearly shows scatter.

Early in the casting of CaF_2, it was noticed that in random castings a bubble layer (or region) occurred about half way into the casting in a plane perpendicular to the freezing direction. It was even observed in several samples that some preferred orientation of these tiny bubbles occurred. In most cases, the bubble layer of these castings could be cut away leaving very good material in the bottom section. The reasons for the tiny bubbles is probably due to too rapid a cooling rate during casting and the entrapment of exsolved gases.

The effect of these tiny bubbles on the optical properties of the castings are shown in Table 3-5. These results indicate qualitatively the effect of impurity scatter centers on 5.25 μm absorption. Three measurements were made on a casting in which there was a region of bubbles. In the region with no bubbles and least scatter, a 5.25 μm apparent absorption coefficient of 5.7 $\times$ 10^{-4} cm^{-1} was measured. Nearer the bubbly region, a slightly higher absorption occurred, while directly through the bubbly region (high scatter), a high apparent absorption coefficient of 2.3 $\times$ 10^{-3} cm^{-1} was measured.

PBN-75-957

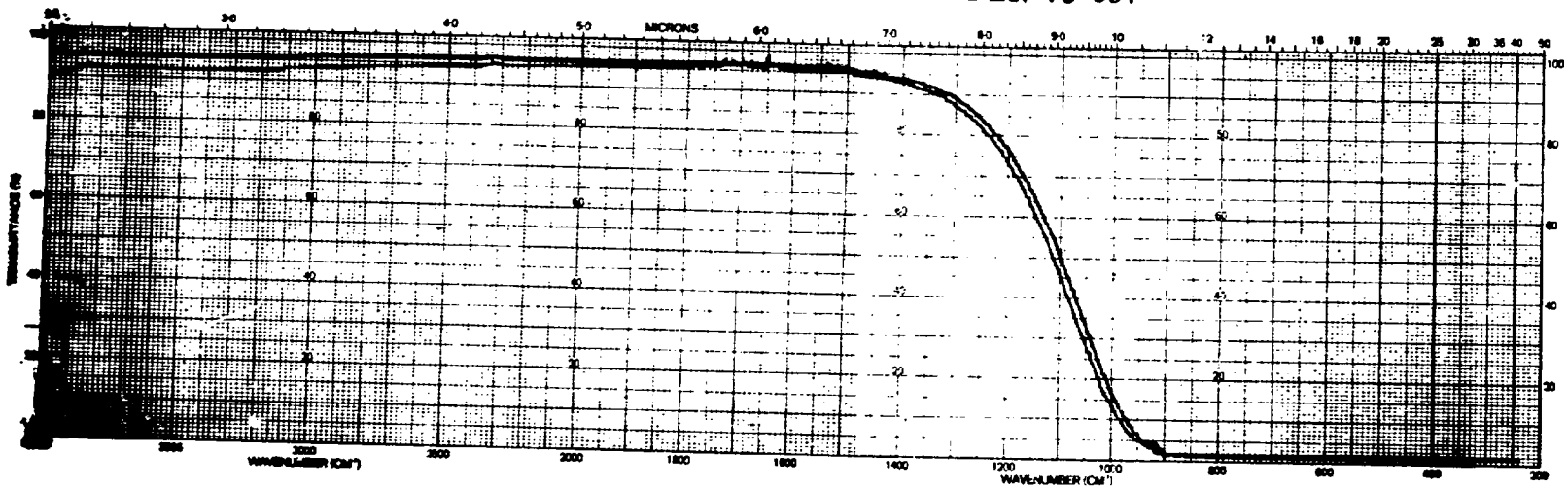

Figure 3-22 Infrared Spectra of Cast CaF_2.
Upper trace: High Quality CaF_2, 1 cm path length.
Lower trace: Poor Quality CaF_2, 1 cm path length.

The impurity scatter results can also be graphically seen in Fig. 3-23. This figure shows two CaF_2 castings, one with (VHP-194) and one without (VHP-167) scattering as viewed with a He-Ne laser beam. The specimen with scattering had a measured 5.25 μm apparent absorption coefficient of 2.0×10^{-3} cm^{-1} (average of 3 samples from one large casting), while the scatter free sample had an apparent absorption coefficient of 4.8×10^{-4} cm^{-1}.

TABLE 3-5

APPARENT ABSO[illegible]ON COEFFICIENTS AND SCATTERING

CaF_2 CASTING HN 1

5.25 μm Absorption Coefficient	Location in Sample
5.7×10^{-4} cm^{-1}	through clear area
6.6×10^{-4} cm^{-1}	near bubbles
2.3×10^{-3} cm^{-1}	through bubbles

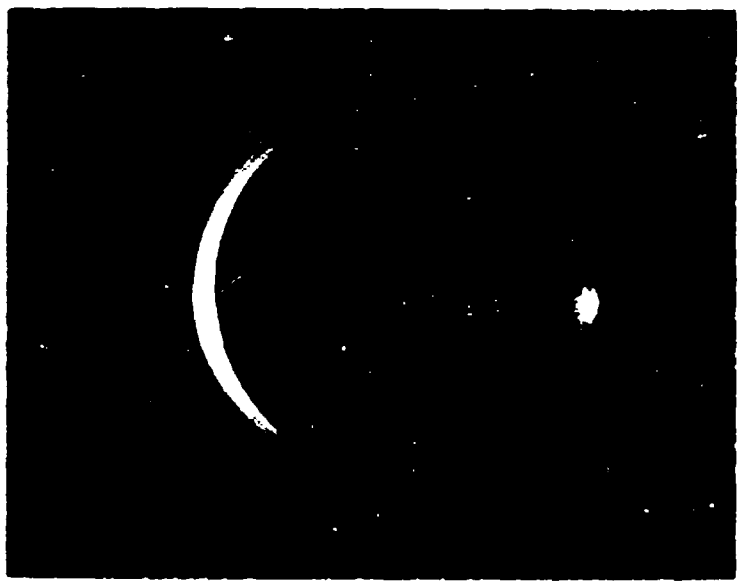

CaF_2 Casting with Scattering

CaF_2 Casting without Scattering

Fig. 3-23 Left. Sample of cast CaF_2 (VHP-194) showing scatter.
Right. Sample of cast CaF_2 (VHP-167) showing no scatter.

Impurity scattering was clearly a serious problem and its possible development during early strain annealing experiments required further investigation. The effect of annealing at 1000° C in a poor vacuum (10^{-2} torr) is shown in Fig. 3-24 and Table 3-6. Figure 3-24 shows the formerly impurity scatter-free casting (Fig. 3-23) after such an anneal at 1000°C for seven hours followed by cooling at 25°C/hr. Again a He-Ne laser beam is directed through the interior of the sample. Fig. 3-24a shows the high degree of impurity scatter now in the sample produced during the anneal. The two figures together show the nature of preferred orientation of the scattering centers. Fig. 3-24b shows the same sample but with the specimen rotated by about 20°. Much less scatter is apparent.

The impurity scatter also degraded the optical properties of the annealed (1000°C) castings (Table 3-6). For this sample (VHP-167), as annealed and with scatter, the 5.25μm absorption coefficient was 8.0×10^{-4} cm^{-1}, an increase of about 70 percent over its scatter-free (and unannealed) absorption coefficient. Similarly, another sample (HN1 of Table 3-5) was annealed and the resultant absorption degradation noted, an increase of about 90 percent to 1.1×10^{-3} cm^{-1} from 5.7×10^{-4} cm^{-1}. Specimens VHP-194, 196, and 203 also similarly annealed show high absorption coefficients (Table 3-6).

Fig. 3-25 shows graphically some of scattering centers produced in VHP-167 after annealing at 1000°C. The micrograph was taken in transmitted light and focussed in the interior of the sample; it shows the preferred orientation of these scattering centers which are about 100 μm long. It has not yet been established what the scattering centers are, but there is some evidence that they are platelets (viewed on edge). Fig. 3-26 shows types of scattering centers present in another annealed sample (VHP-194). These were found in a more random nature, and show an elongated bubble as well as faceted inclusions. Fig. 3-27a clearly shows two of these faceted inclusions just beneath a { 111 } cleavage plane of

Fig. 3-24a Scattering in Cast CaF_2 (VHP-167) After Annealing.

Fig. 3-24b Same Only Rotated About 20°.

TABLE 3-6

5.3 μm ABSORPTION AND HEAT TREATMENT

CaF_2 CASTINGS

Specimen	Heat Treatment	$\beta_{5.3\,\mu m}$
VHP-194	1000°C*	$20.2 \pm .4 \times 10^{-4} cm^{-1}$ (3)
VHP-196	1000°C*	$36.6 \pm 2.0 \times 10^{-4}$ (3)
VHP-203	1000°C*	$9.4 \pm 1.8 \times 10^{-4}$ (5)
VHP-167	As Cast	4.8×10^{-4}
-CF-17	1000°C*	$8.0 \pm .1 \times 10^{-4}$ (2)
-CF-17-52	1000°C; 1000°C + teflon*	6.1×10^{-4}
VHP-268	As Cast	4.8×10^{-4}
VHP-264	As Cast	4.8×10^{-4}
-CF66	900°C*	4.9×10^{-4}
VHP-271-P1	As Cast	4.3×10^{-4}
VHP-272-P2	As Cast	4.2×10^{-4}

( ) = number of measurements.

* Vacuum annealed in low vacuum -- 10^{-2} torr.

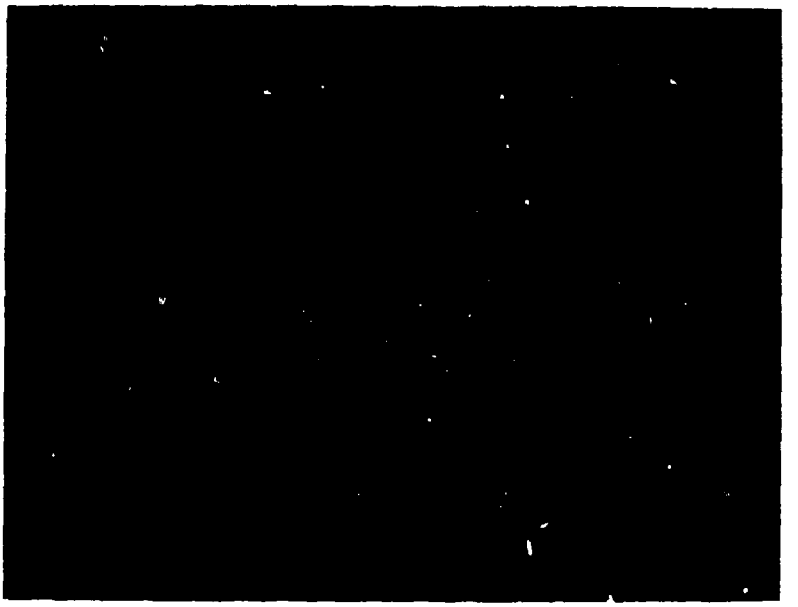

Fig. 3-25 Scattering Centers in Cast CaF_2 (VHP-167) After Annealing. Transmitted light. 100X

PBN-74-412

Bubbles in CaF_2 Casting

50μ

Figure 3-26 Scattering Centers in Cast CaF_2.

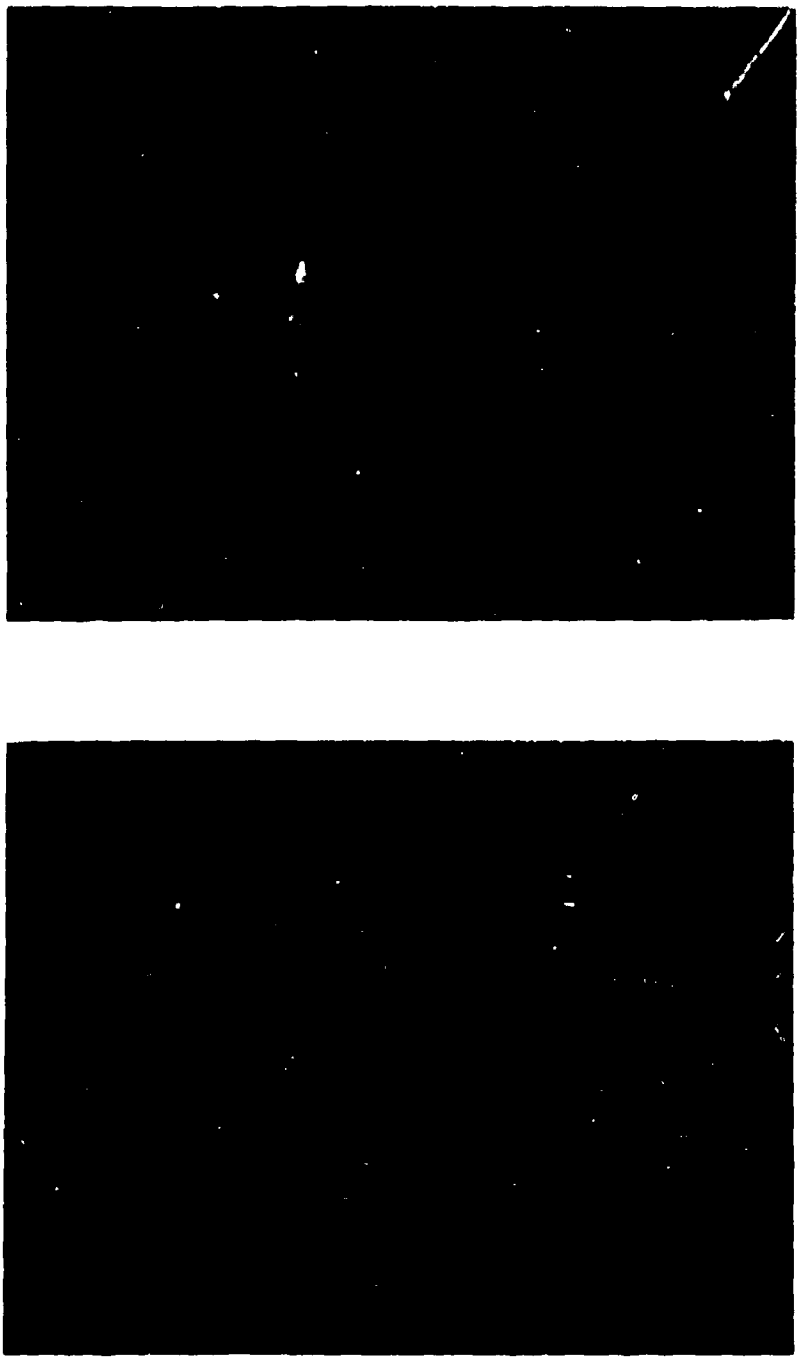

Figure 3-27a Scattering Centers (arrows) Just Below Cleavage Surface in Cast CaF_2. Top: incident illumination. Bottom: transmitted illumination. 300×.

CaF_2. The three-fold symmetry strongly suggests that these may be "negative" crystals. Fig. 3-27b shows the inclusion (lower arrow) of Fig. 3-27a at higher magnification. Fig. 3-27c shows the other inclusion (upper arrow) of Fig. 3-27a that was farther below the surface. It has now been brought to the surface (the lower inclusion now having been removed) by careful polishing. This micrograph now shows the inclusion as the inverted triangular shape of its pre-polished state and indicates that it is the opposite face of a perfect octahedron, and that it also was almost completely polished away. Fig. 3-27d shows the same inclusion at 5000 × (SEM) and clearly proves that it is a void and not a particle and that it was faceted. Furthermore, ion probe analysis showed no impurities either in or near the inclusion.

The problem of increasing of impurity scatter centers and optical degradation during stress relief can be overcome by proper stress relief annealing as shown in Tables 3-6 and 3-7. Table 3-7 lists a series of Optovac single crystals variously vacuum annealed for ten hours and slow cooled at 25°C/hr (except for VHP-225). Note that by vacuum annealing (10^{-2} torr) below 1000°C (CF-58 and CF-60), no increase in absorption coefficient (or impurity scatter) occurred. At 1000°C an increase did occur (CF-33 and CF-59) as it did in similarly annealed castings, as discussed previously. However, the increase at 1000°C was overcome by either annealing in a better vacuum (10^{-4} torr compared to about 10^{-2} torr normally) or by vacuum annealing in a teflon vapor atmosphere (partial pressure of about 50 μm) as shown by VHP-225 and CF-52-2, respectively. Specimen CF-52-1 seems to indicate that the damage may be reversible, i.e., a sample vacuum annealed with the degrading 1000°C procedure and subsequently reannealed at 1000°C with teflon vapors present showed some improvement in optical quality. Similarly, a post anneal at 1000°C with teflon vapors present improved the previously degraded casting VHP-167 (Table 3-6). Note from Table 3-6 that castings (VHP-264-CF-66) as well as single crystals may be vacuum annealed at 900°C at low vacuum with no increase in absorption coefficient or impurity scatter centers.

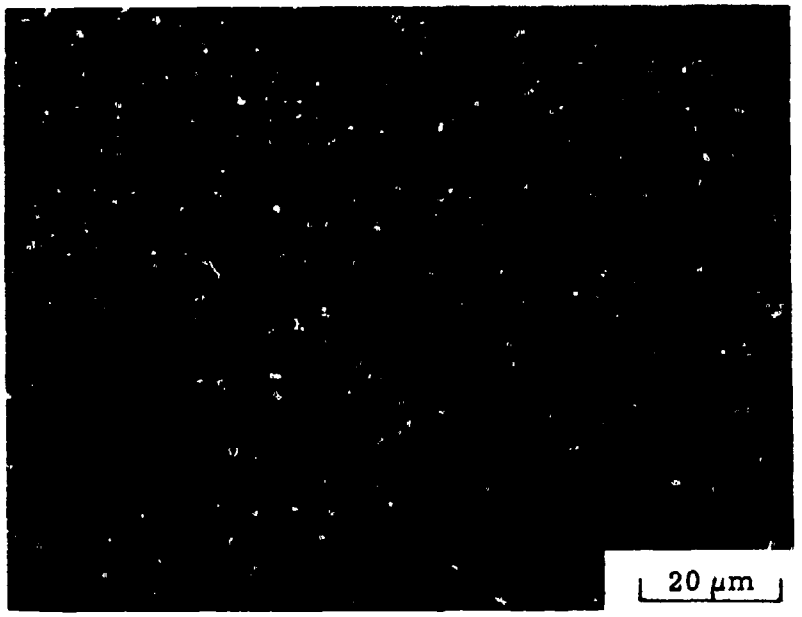

Figure 3-27b Scattering Center just Below Cleavage Surface in Cast CaF_2. 1000×.

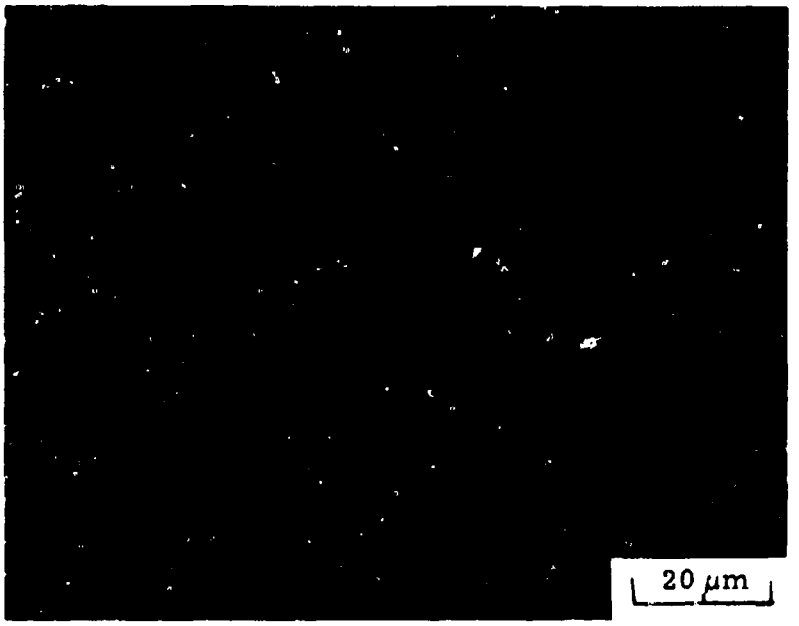

Figure 3-27c Scattering Center after Polishing Sample to Bring it to the Surface in Cast CaF_2. 1000×.

Fig. 3-27d Scattering Center at Surface in Cast CaF_2. SEM 5000X.

TABLE 3-7

5.3 μm ABSORPTION AND HEAT TREATMENT
SINGLE CRYSTAL CaF_2

Specimen	Heat Treatment	β5.3 μm
Optovac Single Crystal	As Received	$5.0 \pm .1 \times 10^{-4} cm^{-1}$ (2)
CF-58	800°C*	5.0×10^{-4}
CF-60	900°C*	4.7×10^{-4}
CF-59	1000°C*	9.6×10^{-4}
CF-33	1000°C*	$6.6 \pm .5 \times 10^{-4}$ (5)
CF-52-1	1000°C; 1000°C+ teflon *	$6.2 \pm .2 \times 10^{-4}$ (2)
CF-52-2	1000°C+ teflon *	5.0×10^{-4}
VHP-225	1000°C **	4.5×10^{-4}

( ) = no. of measurements

* Vacuum annealed in low vacuum -- 10^{-2} torr.

** Vacuum annealed in high vacuum -- 10^{-4} torr.

Since both high purity single crystals and castings behave similarly in the vacuum annealing runs, there is evidence that the problem at 1000°C is one of impurity pickup and/or precipitation of excess vacancies during the annealing process. However, the problem can be overcome by vacuum annealing at a lower temperature or by annealing in a purifying atmosphere or in a better vacuum.

For the samples of CaF_2 single crystals heat treated in the Lindberg box furnace, the results were as follows: For the samples annealed in purified argon at either 800 or 900°C (sufficiently purged), no increase in the 5.25 μm apparent absorption coefficient ($4.7 \pm 0.3 \times 10^{-4}\ cm^{-1}$) was measured as compared to unannealed single crystal CaF_2. At 1000°C (in argon) an increase was observed ($1.2 \times 10^{-3} cm^{-1}$) with a corresponding increase in scattering (as viewed with a He-Ne laser). These results correlate with those reported above on vacuum (10^{-2} torr) annealing at 800, 900 and 1000°C. In both cases it seems clear that the systems are not sufficiently O_2-free, but that the damaging reactions occur only above 900°C, at least within the time period of these runs (10 hours) and with the low but unknown impurity concentration present.

These results are important because it has been shown that the high quality castings produced in the vacuum hot press, although severely strained, can be annealed for strain relief with no resultant degradation of the optical properties.

3.2.6 Mechanical Properties

3.2.6.1 Fracture Strength

Mechanical property measurements have been obtained for CaF_2 and SrF_2. Fracture strength as a function of surface preparation was determined for single crystal CaF_2 and SrF_2 and for polycrystalline cast CaF_2 and SrF_2. The stress strain curves were determined in three-point

bending on an Instron universal testing machine. The sample span was one inch and the cross-head speed was 0.05 cm/min. Nominal sample cross sections were 3/16 × 3/16 in. Selected samples were also tested in four-point bending with an inner span of one inch and an outer span of two inches. Test bars were obtained from annealed ingots by cutting and polishing and were tested immediately or were either chemically polished in concentrated H_2SO_4 or were vacuum annealed at either 900°C or 1000°C followed by slow cooling prior to testing. For a number of samples extra attention was given to polishing the edge bevels, as will be noted. Sample dimensions were measured after testing to prevent surface damage. Grain size for the polycrystalline cast samples is generally on the order of one cm. In all cases fracture occurred with no apparent yielding.

The results as presented in Tables 3-8 and 3-9 show the effects of polishing and annealing on the fracture strength of CaF_2, and indicate qualitatively the large effect surface preparation has. By going from a rough polish (wet 600 grit grinding paper - Fig. 3-28) to a normal in-house laboratory polish (Fig. 3-29) or to an optical polish (polished on a pitch lap by an optician) as shown in Fig. 3-30, the strength of cast CaF_2 is raised from 6100 psi to 16,000 psi and 13,300 psi, respectively. Note that for the samples on which extra attention was paid to polishing the edge bevels, the fracture strength is not significantly changed for the lab and optical polishes.

For single crystal CaF_2, the polishing results are similar, i.e., going from a rough polish to lab and optical polishes, the fracture strength is increased from 7200 psi to 25,000 psi and 18,400 psi, respectively, values essentially equivalent to the cast material and not unexpected due to the large grain size of the castings.

These polishing results (and the large scatter in the data) for both cast and single crystal material indicate that strength is limited by surface and edge flaws. Damaging flaws may be removed in part by more careful mechanical polishing.

TABLE 3-8

FRACTURE STRENGTH OF CAST CaF_2

As-Polished			As-Annealed		
Rough (psi)	Lab (psi)	Optical (psi)	Rough (psi)	Lab (psi)	Optical (psi)
(24000)	24100*	19500	17000	27000*	(53800)
8500	22800	18600	15300	26400*	33500*
7700	20800	17600*	13800	24100	28600
6900	20700	15400	11700	22000	26000
6400	19800*	14900	9600	20600	24500*
6200	19700*	14500	8900	20500*	24200
5700	19100	13300		19600	23900*
5000	18100*	13300*		18600	22200
2000	14700	11900*		17500	21900
	13800*	11900		16800*	21600*
	12300*	11400*		16100*	20700
	9500	11000		11500	18800*
	8300	10800		10900	17900*
	7900	8200*		6700*	
	7800	7600*		5400	
6100	16000	13300	12700	17600	23600
±1800	±5500	±3400	±2900	±6300	±4100

*Extra attention to polishing the edge bevels.

() Sample not included in average value.

TABLE 3-9

FRACTURE STRENGTH OF SINGLE CRYSTAL CaF_2

As-Polished			As-Annealed		
Rough (psi)	Lab (psi)	Optical (psi)	Rough (psi)	Lab (psi)	Optical (psi)
14200	30800	28500	27500	36800	33000
11400	26600	20600	22800	25200	30100
9700	23200	17500	22500	22500	28800
8100	22000	15700	17000	20400	28400
5700	21800	15400	16700	10700	25000
3000	(7800)	12500	13200	10600	23500
2900			7600		16600
2600			4800		
			3400		
7200	25000	18400	15100	21000	26500
±4100	±3400	±5100	±7900	±9000	±5000

( ) Sample not included in average value.

Figure 3-28 Surface of CaF_2 Sample After Rough Polish (600 grit SiC Paper) 187 ×

PBN-75-359

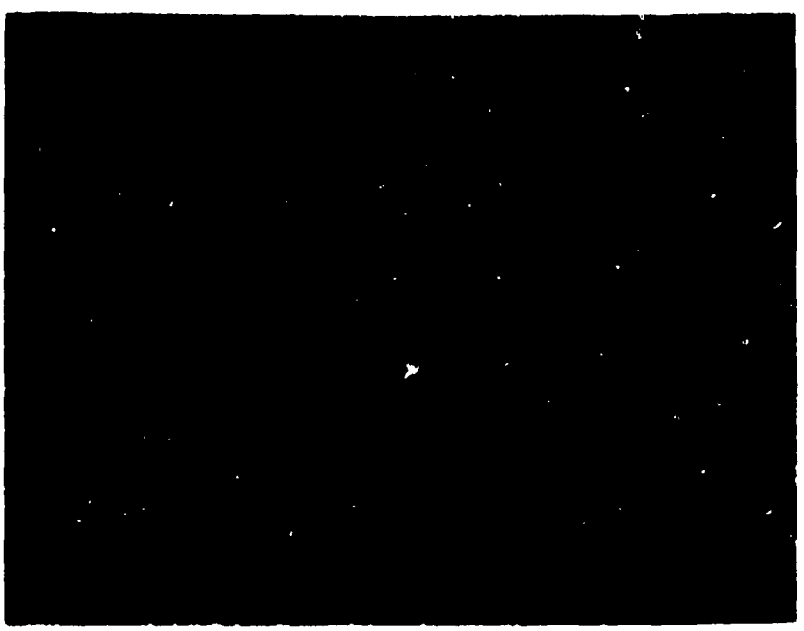

Figure 3-29 Surface of CaF_2 Sample After Laboratory Polish. 187×

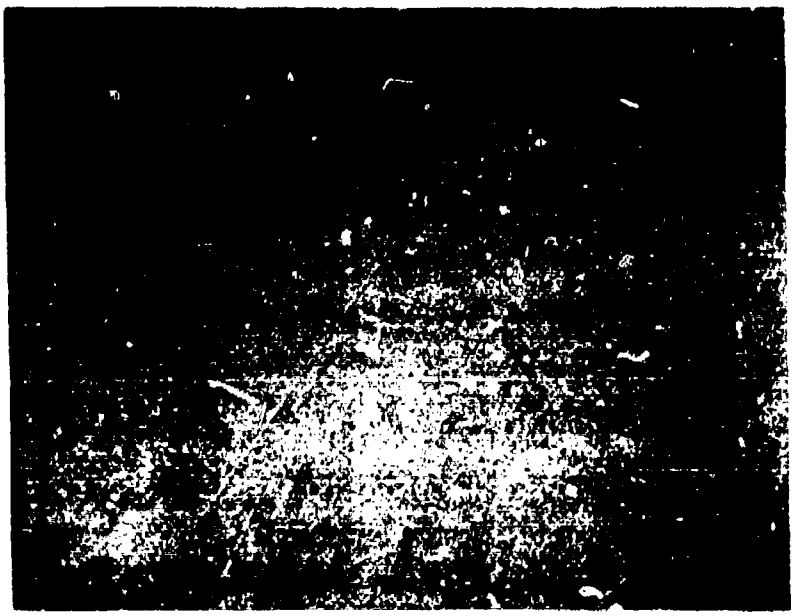

Figure 3-30 Surface of CaF_2 Sample After Optical Polish (Pitch Lap). 187 ×

Further evidence is seen in the effect of annealing individual test bars prior to testing as also indicated in Tables 3-8 and 3-9. Annealing significantly increases the fracture strength of both cast and single crystal specimens. Samples similarly polished as above - rough, lab, and optical polishes - and annealed prior to testing show increased fracture strengths of 12, 700, 17, 600 and 23, 600 psi, respectively, for cast CaF_2 and 15, 100, 21, 000 and 26, 500 psi, respectively, for single crystal CaF_2. As was the case for as-polished cast samples, those as-annealed test bars on which extra attention was paid to polishing the edge bevels, the fracture strength is not significantly changed.

Evidently by annealing the test bars, some surface damage is either reduced or removed, a further indication that the fracture strength of CaF_2 is limited by surface flaws. This assumes that bulk strain in all the bars are the same, supported qualitatively by viewing each specimen between crossed polarizers before testing and noting no differences. That is, all test bars appear macroscopically strain-free, whether they are to be tested as-polished or as-annealed (polished then subsequently annealed).

In all the above cases, fracture was predominantly transgranular in nature (i.e., cleavage). However, in the cases of samples of cast CaF_2 which were taken from castings annealed in the degrading anneal procedure (1000°C in poor vacuum of 10^{-2} torr) fracture was totally intergranular in nature and strengths were markedly reduced to 4700 ± 600 psi (lab polished samples) from 16, 000 psi. However, even in this instance, surface damage is somewhat limiting, since similar samples which were subsequently chemically polished showed an increased strength to 6500 ± 1300 psi. It appears that particular annealing procedure not only degrades the optical properties but also significantly affects the mechanical properties. Since fracture is intergranular, it suggests grain boundary weakening as a result of an impurity precipitation problem as previously discussed.

Fracture results for single crystal and cast SrF_2 samples as listed in Table 3-10 show a similar surface damage dependence although not as marked as for CaF_2. For cast SrF_2 the as-polished samples (rough, lab and optical polishes) show average fracture strengths of 9, 900, 12, 100 and 23, 700 psi, respectively. Similarly polished samples annealed prior to testing show an increased strength to 15, 000, 16, 100 and 21, 900, respectively. To those samples to which extra care was taken in polishing the edge bevels, no significant changes are seen. Note that for SrF_2, annealing does not have much effect on the optically polished samples unlike the case for rough and lab polished samples. If the annealing process heals damaging surface flaws, as was suggested by the CaF_2 results, then for optically polished SrF_2 samples at least such flaws may either not exist prior to annealing or may not be healed by annealing.

Single crystal SrF_2 shows an equivalent fracture strength compared to cast samples, i.e., the values for lab polished single crystal SrF_2 are 11, 300 psi and 16, 400 psi for as-polished and as-annealed samples, respectively.

For samples of cast material tested in four-point bending the measured values of fracture strength are lower than for similar samples tested in three-point bending. For optically polished samples of cast CaF_2 the average measured fracture strength (four-point bending) is 12, 300 $\pm$ 1500 psi, only slightly lower than the value measured in three-point loading, 13, 300 $\pm$ 3400 psi. Other investigators to whom samples were sent have measured the average fracture strength of annealed optically polished cast CaF_2 to be 13, 000 $\pm$ 4600 psi[32] (four-point bending), significantly lower than the value of 23, 600 psi measured in three-point bending (Table 6-11). For annealed optically polished samples of cast SrF_2 the measured value is 14, 200 $\pm$ 4500 psi, significantly lower than the comparable value reported above for three-point bending tests; for

TABLE 3-10

FRACTURE STRENGTH OF SrF_2

As-Polished				As-Annealed			
Cast SrF_2			S.C. SrF_2	Cast SrF_2			S.C. SrF_2
Rough (psi)	Lab (psi)	Optical (psi)	Lab (psi)	Rough (psi)	Lab (psi)	Optical (psi)	Lab (psi)
11400	24400*	29600	16100	17100	25600*	26200	23400
11100	22900*	27500	12500	14300	25400	24300	18900
10900	19500	25700	11800	13600	21200	24100	15700
10300	17700	23400	4800		20900	22600	7700
10200	17700*	23200			19900	21400	
10200	15300*	20700			18000*	20200	
9800	14800*	15500			16700	19700	
9200	14600	(5700)			15100*	17000	
8900	12200	(5300)			14900*	(7900)	
6600	11400*	(4500)			14500	(4200)	
	11300*				14100*		
	9100*				11300		
	8300				9400*		
	8300*				9400		
	7900				5000		
	7500						
	6800*						
	6500						
	6209*						
	5800*						
9900	12100	23700	11300	15000	16100	21900	16400
±1300	±5600	±4300	±4100	±1500	±5700	±2800	±5700

*Extra attention to polishing the edge bevels.

( ) Sample not included in average value.

optically polished samples of cast SrF_2 the measured value is 14, 200 $\pm$ 1100 psi. Note that, as was the case for values measured in three-point bending tests, the fracture strength of these optically polished samples of SrF_2 is not significantly affected by annealing.

The present results are somewhat ambiguous in assessing the relative strengths of SrF_2 and CaF_2. Annealed optically polished CaF_2 samples seem to be equivalent to similar SrF_2 samples, in three-point bending tests. Note, however, the large scatter of values (Table 3-10) measured for optically polished samples of SrF_2 of 4500 - 29, 600 psi and 4200 - 26, 200 psi for as-polished and as-annealed samples, respectively. Nearly 20-30 percent of the samples fracture at loads less than 15, 000 psi. By comparison, all samples fractured at loads greater than 20, 000 psi for annealed optically polished CaF_2 samples (Table 3-8). Also, note that in four-point bending tests the optically polished samples of CaF_2 and SrF_2 are nearly equivalent in strength. Overall, it appears that CaF_2 and SrF_2 are equivalent although SrF_2 may be more susceptible to post fabrication damage and resultant wider scatter of strength values.

The above results indicate that the strength of these fluorides may be limited by surface damage, both since there is such a wide scatter in the data and since there seems to be a dependence of strength on surface finish and annealing history. Selected fractured samples were examined microscopically in order to determine possible points of fracture initiation. In general, many samples at both high and low measured values appeared to fail from points at or near the surface. Several examples of such damage are illustrated in the following figures. The surface in compression is marked with an arrow. Figure 3-31a shows a fracture surface at low magnification (optical microscope) of a CaF_2 sample that failed at 53,800 psi. Figure 3-31b shows the same surface at higher magnification in a scanning electron microscope. These fractographs show that

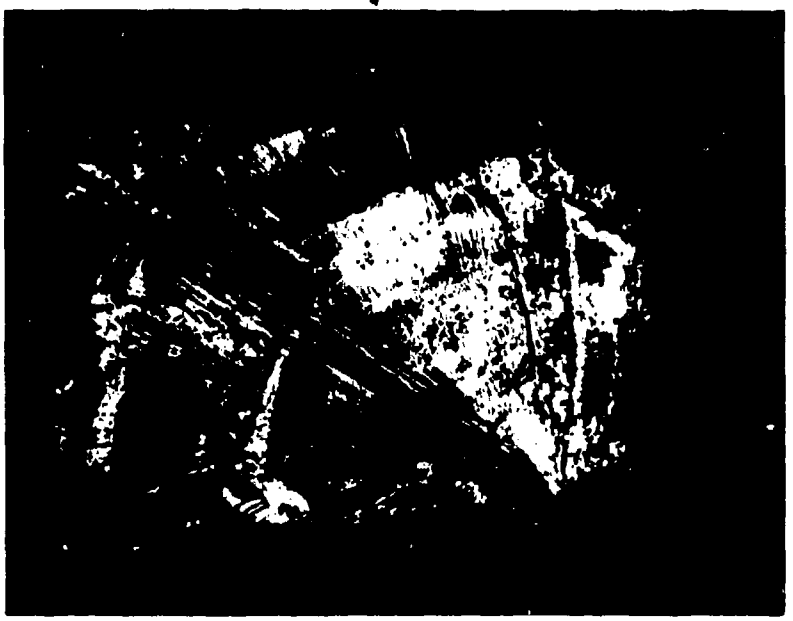

Figure 3-31a Fracture Surface of CaF_2 Sample That Failed at 53, 800 psi

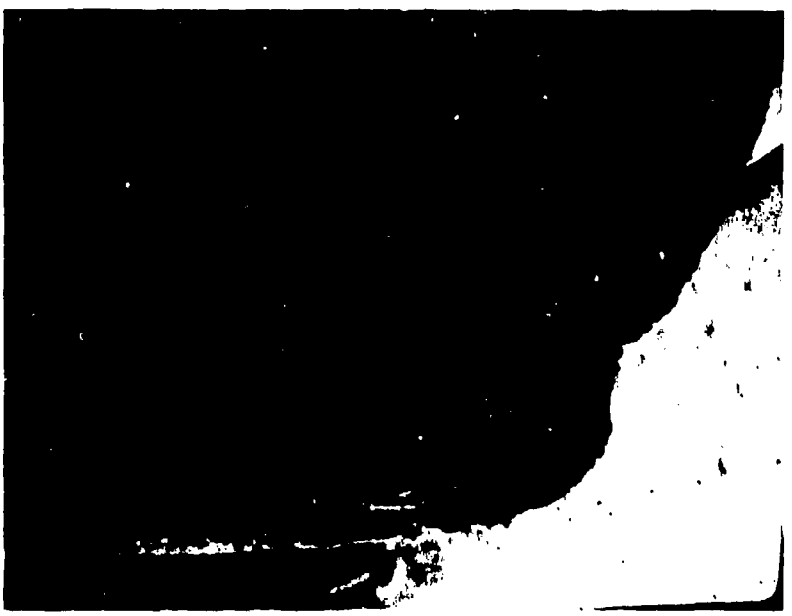

Figure 3-31b Same. SEM, 30X

fracture initiated at or near the edge bevel. Figures 3-32a-c show a similar fracture surface for a CaF_2 sample that failed at only 5100 psi. Again it shows that fracture initiated at or near the edge bevel.

Similar observations were also found for SrF_2. Figures 3-33a-c show the fracture surface of a sample that failed at 29, 600 psi and indicate an initiation point at the surface. Figure 3-34 shows the surface of a sample that failed at only 4500 psi, indicating an initiation point near the edge bevel.

Clearly, the above results show that fracture in both high and low strength samples of both CaF_2 and SrF_2 may initiate at or near the surface and/or edge. Although it appears that surface flaws are strength limiting in these materials, the exact nature of the flaws is not known.

3.2.6.2 Hardness

Hardness measurements were also taken on samples of CaF_2 and SrF_2. Hardness is determined with a Vickers DPH indenter and a 50 gm load mounted on a Vickers M-55 metallograph. The results that appear in Table 3-11 show that there is no difference in hardness in single crystal or cast material for either SrF_2 or CaF_2 and that CaF_2 is slightly harder than SrF_2.

TABLE 3-11

VICKERS HARDNESS* OF CaF_2 AND SrF_2

	SrF_2	CaF_2
Single Crystal	171 $\pm$ 2	191 $\pm$ 2
Polycrystalline Cast	173 $\pm$ 1	194 $\pm$ 2

* Vickers Hardness Number, 50 gram load; average of four measurements.

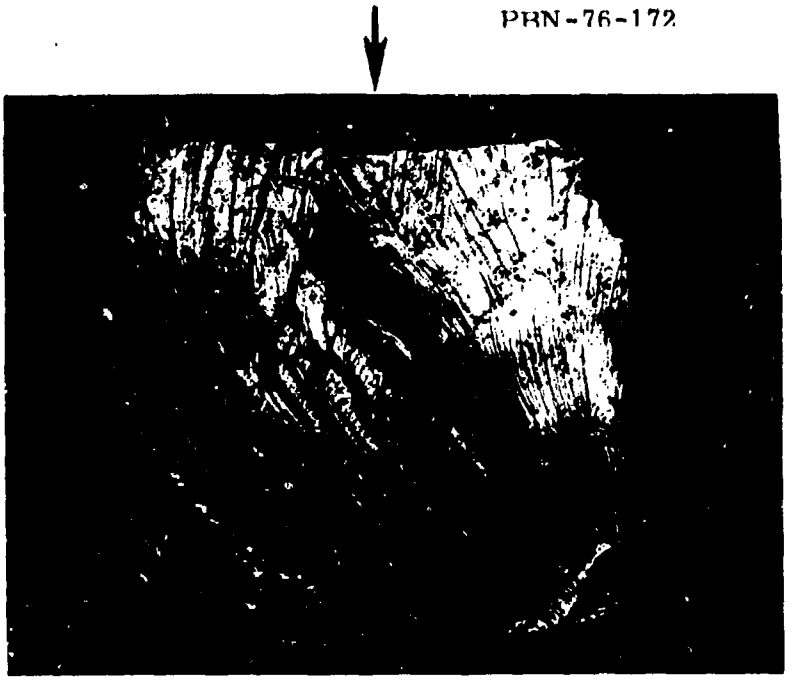

Figure 3-32a Fracture Surface of CaF_2 Sample That Failed at 5400 psi. 15X

Figure 3-32b Same. SEM, 30X

Figure 3-32c Same as Fig. 3-32a. SEM, 100X

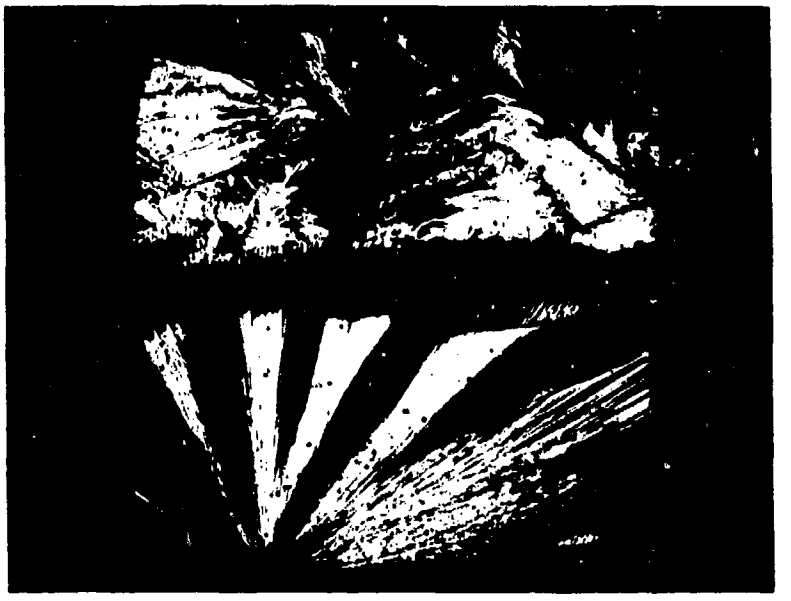

Figure 3-33a Fracture Surface of SrF_2 Sample That Failed at 29, 600 psi

Figure 3-33b Same. SEM, 100X

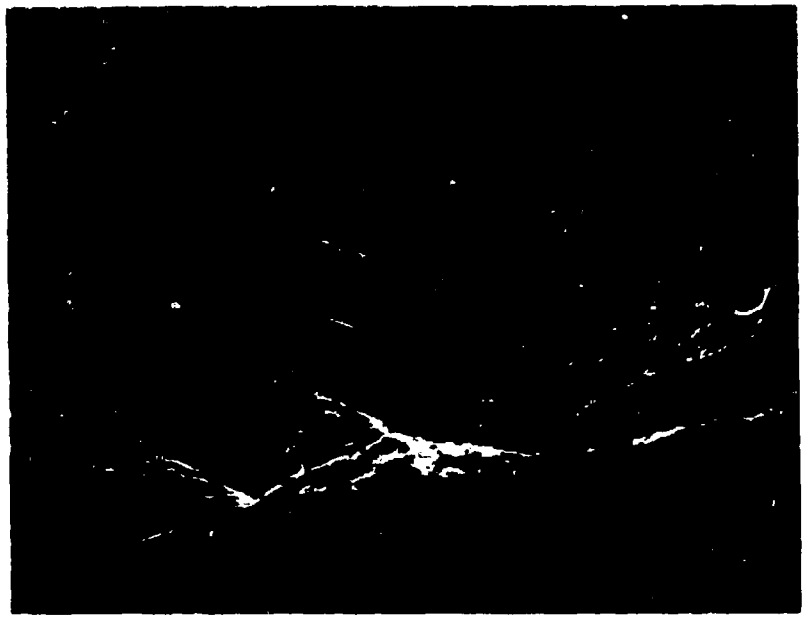

Figure 3-33c Same. SEM, 400×

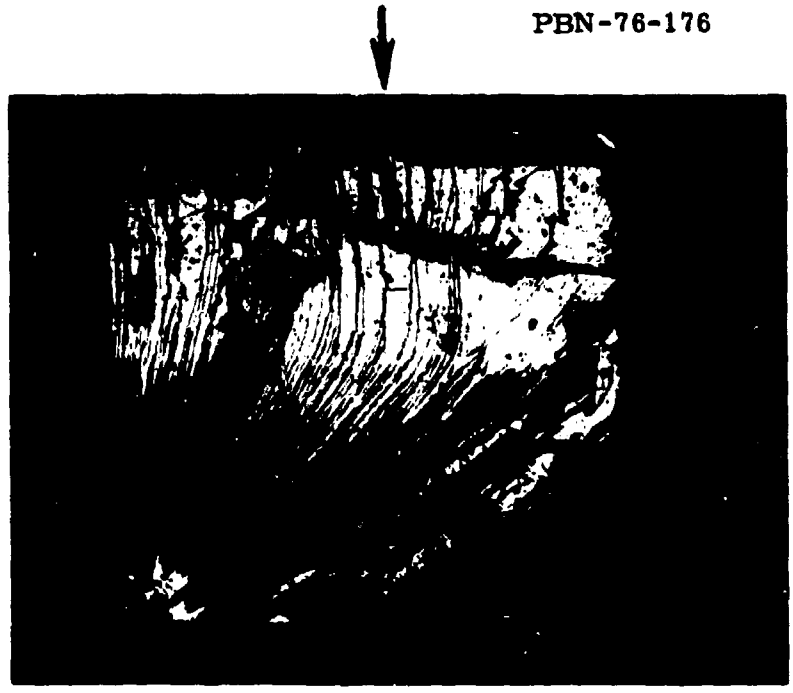

Figure 3-34 Fracture Surface of SrF_2 Sample That Failed at 4500 psi

3.2.6.3 Thermal Shock

A property of interest in the fluorides is the resistance to thermal shock. Qualitatively, it has been found that extreme care is necessary in the handling (cutting and polishing) of samples of CaF_2 and SrF_2 to avoid thermal shock fracture. Fig. 3-35 illustrates the problem. A five-centimeter-diameter, one-centimeter-thick sample of CaF_2 was plunged from room temperature (25°C) into an ice bath near 0°C and fractured. Clearly it is the degree of heat transfer to the sample that is important, since Fig. 3-36 shows a similar sample placed on edge in a freezer maintained at -14°C for one hour and removed to room temperature again with no fracture occurring. Subsequently, the sample was subjected to thermal shocks of up to $\Delta T = 150°C$ by placing it on edge into a lab oven maintained at temperatures up to 175°C and quenching it to room temperature with no fracture occurring. However, much more work must be performed on these materials to fully assess their thermal shock properties.

Figure 3-35 Sample of Cast CaF_2 Showing Thermal Shock Fracture. Plunged from room temperature into an ice bath at 0°C.

PRN-76-178

Figure 3-36 Sample of Cast CaF_2 Showing no Thermal Shock Fracture. Air quenched from 175°C to room Temperature.

4.0 SUMMARY AND CONCLUSIONS

4.1 Alkali Halides

4.1.1 TTT data

Time-temperature-transformation curves for precipitation and attendant hardness reduction in KCl-$SrCl_2$ alloys have been completed. The results indicate that for less than about 800 ppm $SrCl_2$ in solid solution, it should be possible to cool alloys to room temperature without precipitation.

4.1.2 Thermal conductivity

Thermal conductivity data at 93.5°C obtained on KCl-$SrCl_2$ alloys show that the thermal conductivity of KCl is little affected by the addition of up to 2 percent $SrCl_2$ (added to the melt).

4.1.3 Strain removal

Residual strain in KCl castings has been successfully removed by an appropriate annealing and cooling cycle.

4.1.4 Optical properties

4.1.4.1 RAP processing

Reactive atmosphere processing (RAP) of "reagent" grade starting material was successful in removing impurity bands in the infrared. However, the broad absorption band centered near 10 μm was not completely removed.

4.1.4.2 10.6 μm absorption and scattering

Many samples which do not exhibit the broad 10 μm absorption band still can have a high 10.6 μm absorption coefficient. Preliminary data indicated that this high apparent absorption coefficient can be correlated with scattering centers in the bulk.

4.2 Alkaline-Earth Fluorides

4.2.1 Casting

Consistently high quality castings of both CaF_2 and SrF_2 of up to six inches in diameter by one-half inch thick have been fabricated regardless of the starting materials. That is, either high-purity single-crystal chips or pre-treated (vacuum-baked and RAP-treated in teflon vapors) "reagent"-grade powder can be used as starting material to yield equivalent castings. Thicker samples have not been obtained without attendant problems of impurity precipitates and bubble inclusions.

Castings of CaF_2 were attempted in an inert atmosphere – partial pressures of argon and hydrogen from 1-50 torr. The advantage is that unidirectional solidification is better accomplished because of the better heat transfer provided by the gas. The procedure needs more refinement because the castings are typically discolored.

4.2.2 Hot forging

Hot forgings of both single-crystal and polycrystalline cast CaF_2 have been done at 1000°C. At this high temperature a large grain size results so that not much advantage in grain size reduction is gained.

4.2.3 Optical properties

5.25 μm calorimetric bulk absorption coefficients of high quality cast CaF_2 have been consistently obtained near $4.2 \times 10^{-4} cm^{-1}$ regardless of the starting material. Those castings of CaF_2 fabricated in an inert atmosphere of argon have 5.25 μm apparent absorption coefficients typically greater than $1.0 \times 10^{-3} cm^{-1}$, although one was as low as $4.1 \times 10^{-4} cm^{-1}$.

5.25 μm calorimetric bulk absorption coefficients of high quality cast SrF_2 have been obtained near $6.7 \times 10^{-5} cm^{-1}$ regardless of the starting material. Surface absorption for the SrF_2 samples lies near 3.7×10^{-5}

per surface, and may contribute substantially to total absorption values. For CaF_2, the surface absorption, compared with the bulk, is not so dominant with a value of 1.4×10^{-5} per surface.

4.2.4 Strain annealing

For highly strained ingots of cast CaF_2 strain annealing has been successful at 900°C either in vacuum or inert atmosphere furnaces. Highly strained ingots of cast CaF_2 and SrF_2 have been successfully strain-annealed at 1000°C in a high-vacuum furnace, as well as at 1000°C in a reactive atmosphere furnace. The reactive atmosphere is provided by the pyrolysis and vaporization of teflon.

Annealing at 1000°C in either low vacuum or an inert atmosphere furnace successfully removes residual stress in cast CaF_2 ingots. However, such annealing is accompanied by a large increase in the apparent 5.3 μm absorption coefficient and a significant increase in scatter center density.

4.2.5 Mechanical properties

Mechanical measurements (measured in three point bending) for cast CaF_2 show average fracture strengths ranging from a minimum near 6000 psi to near 24,000 psi, depending on both the quality of polished surfaces (and edges) and whether or not the polished test bars are subsequently vacuum-annealed. The results are equivalent to the values for single-crystal CaF_2 for which similar polishing and annealing procedures show average fracture strengths ranging from near 7000 psi to near 26,000 psi. The average fracture strengths for cast SrF_2 range from near 10,000 psi to near 24,000 psi for similarly treated samples. The dependence of fracture strength on both surface polish and annealing history is evidence that fracture for the fluorides is determined by surface and/or edge flaws. The results also show that SrF_2 is equivalent in strength to CaF_2 and that polycrystalline cast material is equivalent to single-crystal material.

Preliminary results of measurements taken in four-point bending tests show average values lower than three-point bend tests.

5.0 REFERENCES

1. P.A. Miles, D.W. Readey and R.T. Newberg, "Research on Halide Superalloy Windows," Rept. No. AFCRL-TR-73-0758 (October 1973).

2. D.W. Readey and P.A. Miles, "Polycrystalline Halides as Optical Materials," Proc. Conf. on High Power Laser Window Materials, (October 30 - November 1, 1972) p. 507, Report No. AFCRL-TR-73-0372 (19 June 1973).

3. D.W. Readey, R.T. Newberg and P.A. Miles, "The Properties of KCl-$SrCl_2$ Alloys and Their Fabrication by Casting," Proc. Third Conf. on High Power Laser Window Materials, (November 12 - 13, 1973), p. 555, Report No. AFCRL-TR-74-0085 (14 February 1974).

4. F.A. Horrigan, R.I. Rudko, Final Report, "Materials for High-Power CO_2 Lasers," Contract No. DAAH01-69-C-0038 (September 1969), AD693311.

5. F.A. Horrigan, T. Deutsch, Final Report, "Research in Optical Materials and Structures for High-Power Lasers," Contract No. DAAH01-70-C-1251 (September 1971) AD 888788L.

6. F.A. Horrigan and T.F. Deutsch, Prof. Conf. on High Power IR Laser Window Materials, AFCRL Special Report No. 127 (1972).

7. M. Sparks, The Rand Corporation, WN-7243-PR (April 1971).

8. M. Sparks, The Rand Corporation, WN-7296-PR, (April 1971).

9. C.C. Klick, "High Energy Laser Windows," ARPA Order No. 2031, Qtrly. Report No. 1 (NRL, Washington, D.C.) (April 1972).

10. W.L. Phillips, Jr., "Deformation and Fracture Processes in Calcium Fluoride Single Crystals," J. Am. Ceram. Soc. 44 (10) 499 (1961).

11. R.N. Katz and R.L. Coble, "Dislocation Etch Pits and Evidence of Room Temperature Microplasticity in SrF_2 Single Crystals," J. Appl. Phys. 41 (4) 1871 (1970).

12. T.S. Liu and C.H. Li, "Plasticity of Barium Fluoride Single Crystals," J. Appl. Phys. 35 (11) 3325 (1964).

13. G.W. Groves and A. Kelly, "Independent Slip Systems in Crystals," Phil. Mag. 8, 877 (1963).

14. A.G. Evans, C. Roy and P.L. Pratt, "The Rule of Grain Boundaries in the Plastic Deformation of Calcium Fluoride," Proc. Brit. Ceram. Soc. 6, 173 (1966).

15. J. Weertman and J.R. Weertman, "Mechanical Properties, Mildly Temperature-Dependent," Chap. 15 in Physical Metallury, (R.W. Cahn, ed., North Holland Publ. Co., Amsterdam), (1965).

16. J.R. Low, Jr., "The Fracture of Metals," Progress in Materials Science, 12, No. 1 (1963).

17. R.W. Rice, "Analysis of Tensile Strength-Grain Size Effects in Ceramics," Am. Ceram. Soc. Bull. 50, 374 (1971). (Abstract of paper presented at the 73rd Annual Meeting of the American Ceramic Society, April 24-29, 1971).

18. A.G. Evans, "Dislocation Interactions in Ceramic Materials," Proc. Brit. Ceram. Soc. 15, 113 (1970).

19. J.J. Gilman, "Mechanical Behavior of Ionic Crystals," Chap. 4 in Progress in Ceramic Science, 1, 146 (J.E. Burke, ed., Pergamon Press, N.Y.) (1961).

20. G.A. Keig and R.L. Coble, "Mobility of Edge Dislocation in Single-Crystal Calcium Fluoride," J. Appl. Phys. 39, 6090 (1968).

21. R.N. Katz and R.L. Coble, "Effect of Neodymium on Dislocation Velocity in CaF_2," J. Appl. Phys. 45, 2382 (1974).

22. R.L. Fleischer, "Solution Hardening by Tetragonal Distortions: Application to Irradiation Hardening in F.C.C. Crystals," Acta. Met. 10, 835 (1962).

23. J. Short and R. Roy, "Confirmation of Defect Character in Calcium Fluoride-Yttrium Fluoride Crystalline Solutions," J. Phys. Chem. 67 (9) 1861 (1963).

24. A.K. Cheetham, et al., "Defect Structure of Fluorite Compounds Containing Excess Anions," Solid State Comm. 8, 171 (1970).

25. W. D. Kingery, "Introduction to Ceramics," (John Wiley and Sons, New York, 628, 1960).

26. D. C. Stockbarger, "Artificial Fluorite," J. Opt. Soc. Am. 39, 731 (1949).

27. E. G. Chernevskaya and Z. N. Korneva, "The Production of Fluorite Crystals in an Atmosphere Containing Fluorine," Sov. J. of Optical Tech. 39, 213 (1972).

28. T. F. Deutsch, "Research in Optical Materials and Structures for High Power Lasers," Final Technical Report, Contract No. DAAH01-72-C-0194 (December 1973).

29. Private communication with G. Wong, TRW Systems, Redondo Beach, CA.

30. J. A. Harrington, K. V. Namjoshi, S. S. Mitra, and D. L. Stierwalt, "Low Loss Window Materials for Chemical and CO Lasers," Proc. 4th Annual Conf. on Infrared Laser Window Materials, Tucson, AZ., Nov. 1974 (Jan. 1975).

31. Private communication with J. Harrington, University of Alabama, Huntsville, AL.

32. Private communication with J. Larkin, Air Force Cambridge Research Labs., Hanscom Field, Bedford, Massachusetts.